JAERI-Research
96-022

SLUG FLOW TRANSITIONS IN HORIZONTAL GAS/LIQUID TWO-PHASE FLOWS (DEPENDENCE ON CHANNEL HEIGHT AND SYSTEM PRESSURE FOR AIR/WATER AND STEAM/WATER TWO-PHASE FLOWS)

May 1996

Hideo NAKAMURA

日本原子力研究所
Japan Atomic Energy Research Institute

本レポートは，日本原子力研究所が不定期に公刊している研究報告書です。
入手の問合わせは，日本原子力研究所技術情報部情報資料課（〒319-11 茨城県那珂郡東海村）あて，お申し越しください。なお，このほかに財団法人原子力弘済会資料センター（〒319-11 茨城県那珂郡東海村日本原子力研究所内）で複写による実費頒布をおこなっております。

This report is issued irregularly.
Inquiries about availability of the reports should be addressed to Information Division, Department of Technical Information, Japan Atomic Energy Research Institute, Tokai-mura, Naka-gun, Ibaraki-ken 319-11, Japan.

編集兼発行　日本原子力研究所
印　　刷　㈱原子力資料サービス

JAERI－Research 96－022

Slug Flow Transitions in Horizontal Gas/Liquid Two-phase Flows (Dependence on Channel Height and System Pressure for Air/Water and Steam/Water Two-phase Flows)

Hideo NAKAMURA

Department of Reactor Safety Research
Tokai Research Establishment
Japan Atomic Energy Research Institute
Tokai-mura, Naka-gun, Ibaraki-ken

(Received April 1, 1996)

The slug flow transitions and related phenomena for horizontal two-phase flows were studied for a better prediction of two-phase flows that typically appear during the reactor loss-of-coolant accidents (LOCAs). For better representation of the flow conditions experimentally, two large-scaled facility: TPTF for high-pressure steam/water two-phase flows and large duct test facility for air/water two-phase flows, were used. The visual observation of the flow using a video-probe was performed in the TPTF experiments for good understanding of the phenomena. The currently-used models and correlations based mostly on the small-scale low-pressure experiments were reviewed and improved based on these experimental results. The modified Taitel-Dukler model for prediction of transition into slug flow from wavy flow and the modified Steen-Wallis correlation for prediction of onset of liquid entrainment from the interfacial waves were obtained. An empirical correlation for the gas-liquid interfacial friction factor was obtained further for prediction of liquid levels at wavy flow. The region of slug flow regime that is generally under influences of the channel height and system pressure was predicted well when these models and correlations were applied together.

Keywords: Slug Flow, Wavy-dispersed Flow, Wavy Flow, Flow Regime Transition, High-pressure Steam/Water Two-phase Flow, Flow Visualization, Interfacial Friction Factor, Channel Height, System Pressure, Empirical Correlation

水平気液二相流におけるスラグ流遷移に関する研究
（空気／水及び蒸気／水二相流での流路高及び系圧力依存性）

日本原子力研究所東海研究所原子炉安全工学部
中村　秀夫

（1996年４月１日受理）

本研究は，軽水炉事故時の気液二相流挙動予測を高精度化するため，水平二相流でのスラグ流の発生条件と関連素過程に対し，従来の小規模，低圧力での実験に基づく予測モデルを改良，又は相関式を新たに作成し，実規模流動への拡張を試みたものである。このため，原研のＴＰＴＦ蒸気／水試験装置と水平矩形ダクト空気／水試験装置の２つの実規模装置を用い，流動の模擬と可視化観察を行なった。その結果，蒸気／水二相流でのスラグ流及び波状噴霧流への遷移境界を良く予測する為の，改良 Taitel-Duklerモデル，気液界面摩擦係数の相関式，改良Steen-Wallis相関式等を得た。さらに，これらの改良モデルや相関式を連係して用いると，本研究での実験条件範囲内ではあるが，スラグ流が生じる流量範囲を，発生条件の流路高と系圧力への依存性と共に良く予測できることを確認した。

東海研究所：〒319-11　茨城県那珂郡東海村白方白根２－４

Contents

目　　次

Nomenclature

a	Wave amplitude	(m)
A	Pipe cross section = $A_G + A_L$	(m^2)
A_k	Cross section of phase k	(m^2)
$A_G^{'}$	Cross section of gas phase at wave crest	(m^2)
α	Average void fraction (1 - α = Liquid holdup)	(-)
c	Celerity of interfacial waves on stationary liquid surface	(m/s)
c_w	Velocity of wave crest	(m/s)
C	Coefficient of **Equation (1-1)**	
C_d	Coefficient to account for non-uniformity of velocity distribution	(-)
D	Pipe diameter, or channel height for rectangular duct	(m)
D_k	Hydraulic diameter of phase k $D_L = 4A_L / S_L$, $D_G = 4A_G / (S_G + S_i)$	(m)
D_L^*	Hydraulic depth	(m)
d	Droplet diameter	(m)
δ	Film thickness	(m)
Δu	Average gas-liquid relative velocity = u_G - u_L	(m/s)
f_i	Gas/liquid interfacial friction factor	(-)
f_k	Wall friction factor of phase k	(-)
F	Function	
Fr	Froude number $Fr = u_L / \sqrt{g\ D_L^*}$	(-)
g	Gravity acceleration	(m/s^2)
h_k	Height of phase k	(m)
$h_G^{'}$	Gas phase height at wave crest	(m)
η	Displacement of interface from average liquid level	(m)
J_k	Superficial velocity of phase k	(m/s)
J_k^*	Density-modified Froude number, Non-dimensional superficial velocity of phase k $J_k^* = J_k \sqrt{\rho_k / [(\rho_L - \rho_G) g D]}$	(-)
J_{GL}^*	Non-dimensional gas-liquid relative velocity $J_{GL}^* = \alpha(u_G - u_L)\sqrt{\rho_G / [(\rho_L - \rho_G) g D]}$	(-)

K	Energy loss coefficient	(-)
Ku	Kutateladze number	(-)
k	Wave number = $2\pi/\lambda$	(1/m)
L	Length of pipe, Scale of length	(m)
λ	Wave length	(m)
μ	Dynamic viscosity	(Ns/m^2)
n	Exponent for coefficient of **Equation (3-16)**	(-)
ν	Kinematic viscosity (= μ/ρ)	(m^2/s)
P	Pressure	(Pa)
Q	Volumetric flow rate	(m^3/s)
θ	Inclination from horizontal	(degree)
Re_k	Reynolds number of phase k $Re_k = \frac{u_k D_k}{\nu_k}$	(-)
ρ_k	Density of phase k	(kg/m^3)
S_i	Width of gas/liquid interface	(m)
S_k	Perimeter on the pipe wall of phase k	(m)
σ	Standard deviation	(-)
T	Surface tension	(N/m)
τ_i	Gas/liquid interfacial shear stress	(Pa)
τ_k	Wall shear stress of phase k	(Pa)
u_k	Average velocity of phase k	(m/s)

Suffixes

c	Wave crest
d	Wave downstream
i	Interface
k	Phase k; G or L
G	Gas
L	Liquid
min	Minimum value
mod	Modified parameter
u	Wave upstream
0	Critical value

Acronyms

AN	Annular
AD	Annular-dispersed
i.d.	Inner diameter
IVO	Imatran Voima Oy (name of an electric power company in Finland)
JAERI	Japan Atomic Energy Research Institute
K-H	Kelvin-Helmholtz
l.h.s.	Left-hand side
o.d.	Outer diameter
LOCA	Loss-of-coolant accident
MT	Magnetic tape
PL	Plug
PWR	Pressurized Water Reactor
r.m.s.	Root mean square
SL	Slug
SS	Stratified-smooth
SW	Stratified-wavy
T-D	Taitel-Dukler
TPTF	Two-phase Flow Test Facility
UPTF	Upper Plenum Test Facility
WD	Wavy-dispersed
2(3)-D	Two (or three) dimensional

1. General Introduction

1.1 Backgrounds

In horizontal gas/liquid two-phase flows, various flow patterns appear depending on gas and liquid flow rates, channel geometry and fluid physical properties. The flow patterns with similar spatial and temporal phase distribution are usually classified into a single flow regime. **Figure 1-1** illustrates typical flow patterns that were observed in the flow regimes to be dealt with in this study. **Appendix-1** describes characteristics of these flow regimes. Primary flow characteristics of horizontal gas/liquid two-phase flow, such as the interfacial mass and heat transfer, the wall and interfacial friction, the wall heat transfer and the pressure drop along the channel, all depend on flow regime.

The prediction of flow regime to appear has been of major interest to many engineering applications, because the thermo-hydraulic performance of a two-phase flow system depends on the flow regime. The causes for the transition among flow regimes should be grasped for full-understanding of characteristics of two-phase flow [Wallis 1969, Akagawa 1974, Ueda 1981, Dukler et al. 1986] [1]. Of particular interest has been the transition into slug (SL) flow regime because it causes a significant increase in pressure drop along the channel and in interphase heat exchange. The slug flow causes large fluctuation in the flow rates and system pressure around the channel. Such flow intermittency is undesirable.

Many experimental studies have been performed to find the flow conditions for the flow regime transition. As a general approach, flow regime maps indicating the location of transition boundaries have been prepared to

1) Some early investigators tried to develop general correlations that would fit all flow regimes. Lockhart-Martinelli (1949), for example, achieved a great success in predicting pressure drop along channels in terms of simple parameters.

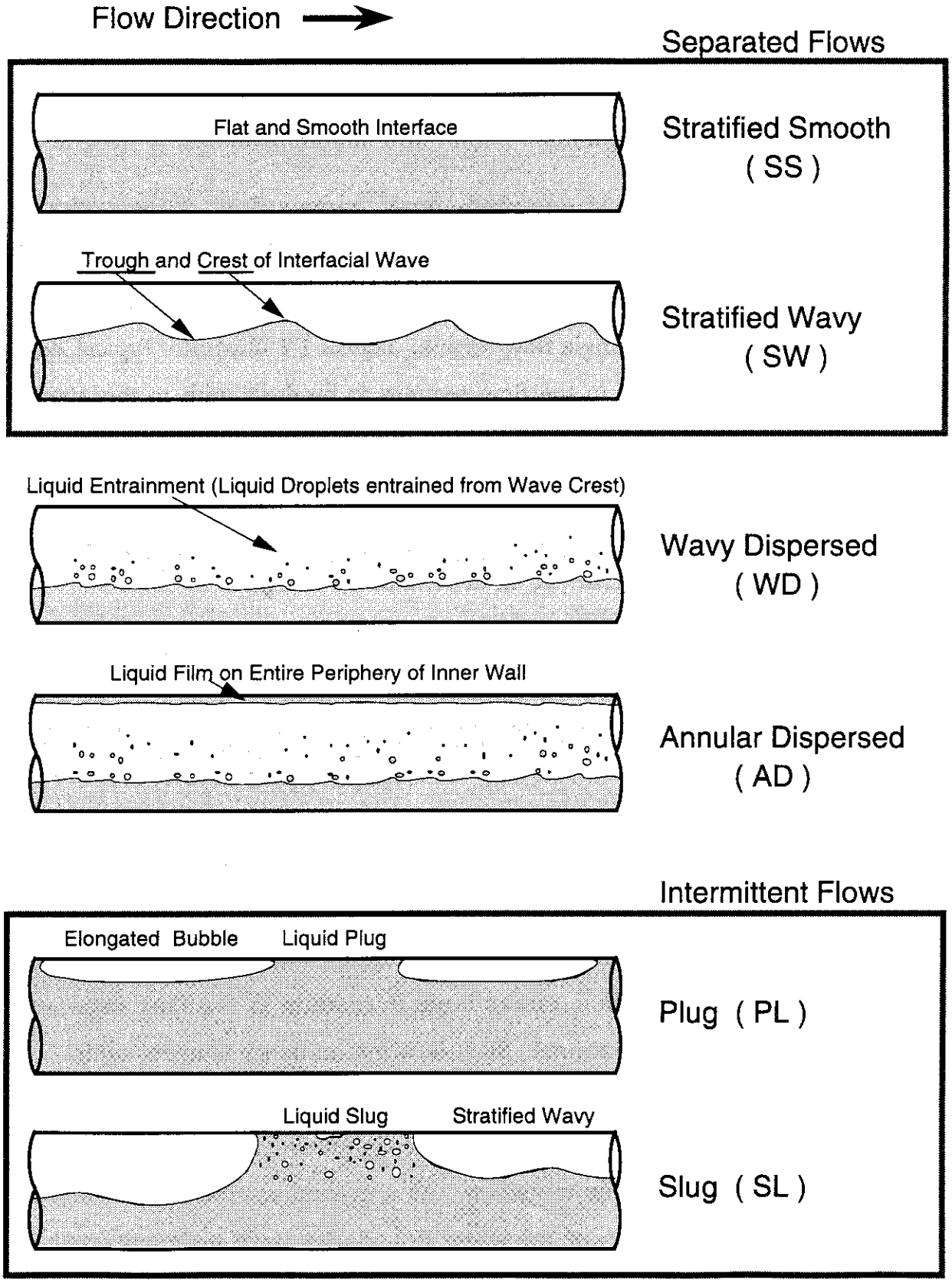

Fig. 1-1 Schematics of Flow Patterns

judge a flow regime to appear for a given combination of the flow parameters. Baker (1954) first obtained such a map for gas/oil (petroleum) two-phase flows, in a two-dimensional plot with coordinates presented as a function of flow rates, densities, viscosities and surface tension. Mandhane et al. (1974) presented their map simply taking gas and liquid superficial velocities as the coordinates for air/water two-phase flows. **Figure 1-2** presents a Mandhane-type map[2] for steam/water two-phase flows (Anoda et al. 1989) with the illustration of flow patterns presented in **Fig. 1-1**. Slug flow regime is bounded by stratified-wavy (SW) and wavy-dispersed (WD) flow regimes. The flow regime maps, however, apparently depend on the local flow conditions such as channel geometry and fluid properties specific to the experiments. Therefore, it is preferable to obtain models and correlations that cover a wide range of the two-phase flow conditions.

The flow regime transitions in horizontal legs of a pressurized water reactor (PWR) have an impact on the core cooling performance during a loss-of-coolant accident (LOCA) [Kukita et al. 1988]. In the PWR hot legs that connect the reactor vessel upper-plenum to the steam generator, for example, various flow regimes would appear depending on primary coolant inventory and steaming rate in the core. The occurrence of slug flow in particular is an important issue to reactor safety, because it would cause a significant decrease in the core coolant. Liquid slugs would convey reactor coolant away from the core through the hot legs. The correct prediction of the slug flow transition is thus indispensable for the nuclear safety analysis.

Current LOCA-analysis computer codes such as RELAP5/MOD3 and TRAC-PF1 [Ranson et al. 1987, Safety Code Development Group 1984] are furnished with models and correlations to represent flow regimes and transitions

---

2) The flow regime boundaries shown as lines in **Fig. 1-2** are, in reality, rather broad transition zones. The flow regime transition is invariably accompanied by some extent of fluctuation.

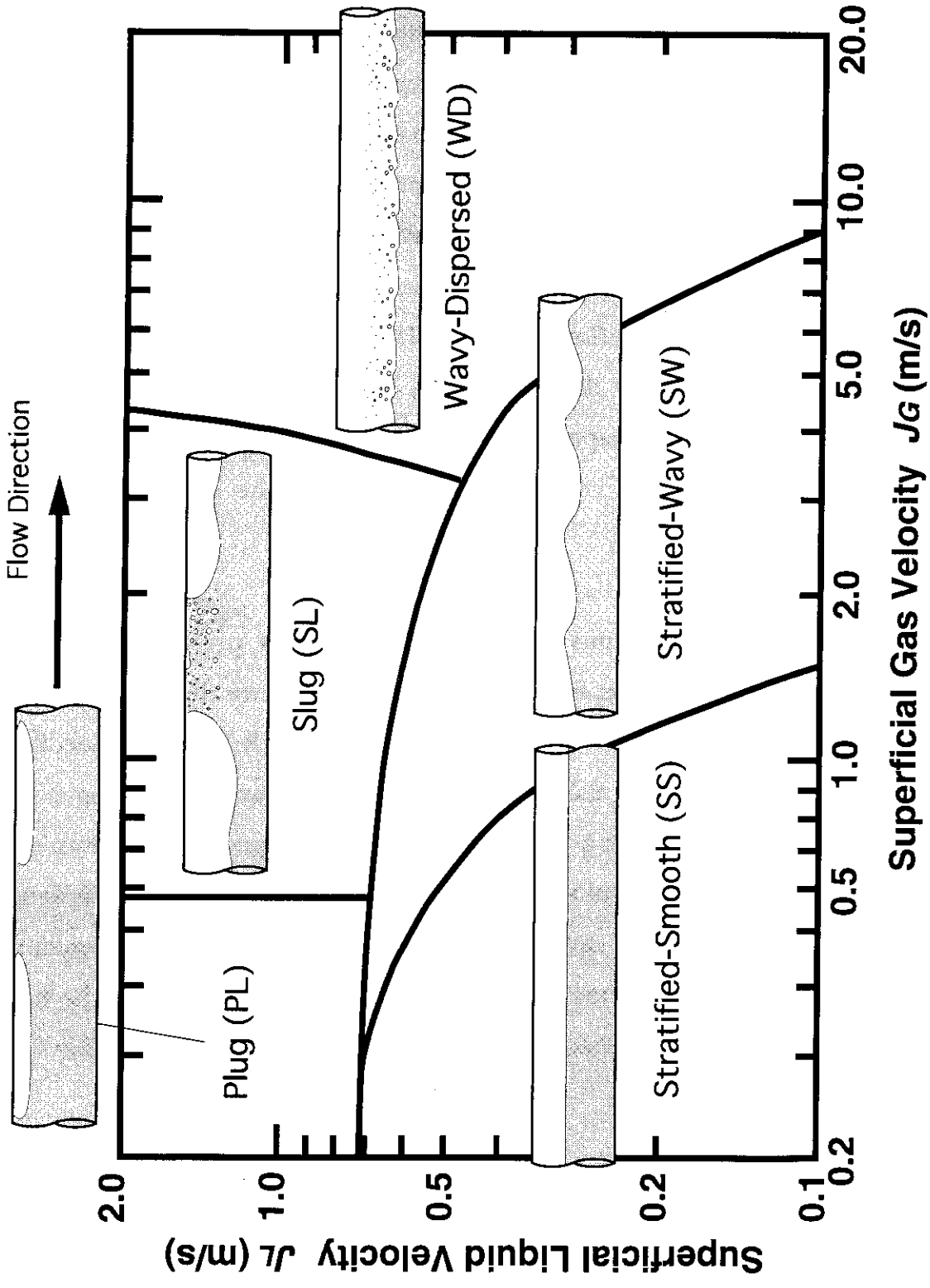

Fig. 1-2 Typical Flow Regime Map (TPTF 8-inch pipe, 3 MPa, Anoda et al. 1989)

among various flow regimes. These models and correlations, including those to predict slug flow transition, however, are based mostly on near-atmospheric-pressure experiments conducted in pipes with diameter much smaller than that of PWR hot legs. The high-pressure steam/water two-phase flows enclosed by opaque thick-metal wall of the facility are accompanied by considerable experimental difficulties in observing and measuring details of the flow. Absence of the experimental data taken under the conditions representative of a LOCA have resulted in the limitation in the current models and correlations. Therefore, there is a significant need for models and correlations applicable to high-pressure steam/water two-phase flows in a large-diameter pipe which are typical of PWR LOCAs and transients.

The present thesis describes a basic study on the mechanisms of the flow regime transition into slug (SL) flow and on the related phenomena. Efforts are made to extend the applicability of the current-available models and correlations to the reactor conditions. The influences of channel height (pipe diameter) and system pressure (that controls fluid physical properties) are taken into account. High-pressure (up to 12 MPa) steam/water two-phase flow experiments were conducted using the Two-Phase Flow Test Facility (TPTF) [Nakamura et al. 1983, Kawaji et al. 1987] to represent a prototypical pressure. Air/water two-phase flow experiments were also conducted using a large-height (0.7 m) duct test section [Nakamura et al. 1994] to represent a channel height that is prototypical to the PWR hot legs.

In the following, previous studies relating to the slug flow transition mechanisms are briefly reviewed in conjunction with the scope of the present study. The objectives and the structure of the present thesis are then summarized.

1.1.1 Models and Methods to Predict Flow Regime Transition from Stratified-Wavy to Slug Flow Regime

The transition from stratified-wavy (SW) to slug (SL) flow regime in a horizontal channel takes place when the growth of interfacial waves into a liquid slug comes to occur steadily. This wave growth process is termed "slugging". Liquid slugs are formed intermittently at a frequency depending on several parameters such as gas and liquid flow rates, and channel geometry. The instability of interfacial waves triggers slugging.

Many models have been proposed to predict the SW-to-SL flow regime transition by attributing the main mechanism of slugging to the classical Kelvin-Helmholtz (K-H) instability [Kordyban 1990, Andritsos et al. 1992]. As indicated in **Appendix-2**, the transition criterion based on the K-H instability for infinitesimal-amplitude long waves is presented by an equation

$$u_G - u_L \geq C \sqrt{\frac{(\rho_L - \rho_G) g h_G}{\rho_G}} \quad , \tag{1-1}$$

with a coefficient of C = 1.0 for two-dimensional flow condition. This criterion, however, overpredicts gas-liquid relative velocity $\Delta u = u_G - u_L$ by a factor of about two. Kordyban and Ranov (1970) first discussed that the instability is considerably enhanced by the decreased gas phase static pressure when the wave crest comes close to the channel upper wall. This destabilizing effect is often termed "Bernoulli" effect.

Many investigators have agreed this idea and proposed the various coefficient C experimentally and/or theoretically to apply the simple **Equation (1-1)** to the prediction of the SW-to-SL flow regime transition. Note that **Equation (1-1)** is in terms only of gas channel height of h_G as a local variable for given flow rates and system pressure.

Taitel and Dukler (1976) obtained $C = \left(1 - h_L/D\right)$ assuming that slugging takes place when the lift force by the gas-phase pressure drop at the wave crest overcomes the stabilizing force due to gravity. The expression $\left(1 - h_L/D\right)$ was finally obtained through an experimental observation for pipe flows [Taitel et al. 1977]. This model originally neglected the contribution of liquid velocity in l.h.s. of **Equation (1-1)**. Asaka et al. (1991) and Anoda et al. (1989), however, found that this model predicts the TPTF high-pressure steam/water two-phase flow data well, when the l.h.s. of **Equation (1-1)** is presented by the gas-liquid relative velocity Δu. This modified model has been used in the LOCA analysis code RELAP5/MOD2 and MOD3.

Mishima and Ishii (1980) obtained C = 0.487 by extending the stability theory of finite-amplitude interfacial waves by Kordyban and Ranov (1970) with an assumption that the wave with the largest growth rate develops into a slug. The Mishima-Ishii model predicts the transition to slug flow in a rectangular duct well, since this model is based on two-dimensional growth of waves. The value 0.487 of C is close to the empirical value of 0.5 obtained by Wallis and Dobson (1973) for a rectangular duct. The difference in C values between Taitel-Dukler and Mishima-Ishii models suggests that the wave growth process depends on the channel cross-sectional geometry. These models are discussed further in **Chapter 3**, in comparison with the experimental data obtained in this study.

Many other investigators have proposed models to predict the SW-to-SL flow regime transition as follows.

Hihara and Saito (1984) introduced a "pressure difference" term as a corrective in the balance between the gas lift force and the gravity restoring force for a slugging wave. The authors did not explain the physical meaning of this "pressure difference" term. However, they found that the "pressure difference"

term has a magnitude of the order of the water head corresponding to the wave height based on their air/water experiments.

Gardner (1979) assumed the "energy flux" of inviscid gas and liquid flows, and proposed that the transition takes place when the maximum difference in the "energy fluxes" is achieved between high and low liquid level sections in the flow. The high and low liquid levels correspond to the wave crest and trough shown in **Fig. 1-1**. This model therefore can predict the wave height when slugging takes place. However, the mass conservation law for a one-dimensional flow results in a significant decrease in the liquid velocity at the section for the wave crest. This flow condition does not represent the velocity profile of interfacial waves. Minato et al. (1986) proposed a mechanistic model, similar to Gardner's approach, assuming that change in the liquid kinematic energy due to the level change along interfacial waves contributes to wave growth.

Lin and Hanratty (1986) conducted linear stability analyses for both viscous and inviscid flows, by extending a method to predict the onset of roll waves in thin liquid film flows [Hanratty 1983] to low void fraction flows. The analysis expects that the instability occurs when the derived celerity for small interfacial disturbances becomes imaginary. The results showed that the liquid viscosity has an effect to enhance interfacial instability, and that the interfacial friction causes a decrease in the gas-liquid relative velocity for the slug flow transition. However, the same analysis showed that the inertia effects at large liquid viscosities become negligible. Consequently, both viscous and inviscid flows were controlled by the same stability criterion. Barnea et al. (1993) confirmed this results and found further that the wave amplification factors based on the viscous and inviscid flow analyses are almost the same.

Ferschneider et al. (1985) and Wu et al. (1987) incorporated a criterion into the above linear stability analyses that the instability occurs when the celerity of

continuity (kinematic) wave becomes larger than that of dynamic wave. These wave celerities are based on the one-dimensional wave theory [Wallis 1969]. Fukano et al. (1985) applied this criterion to predict generation of disturbance waves (roll waves) in horizontal duct liquid film flows, and Crowley et al. (1992) performed transient analyses for interaction of waves.

Ahmad and Banerjee (1985) performed a computational analysis on the instability of non-linear (finite-amplitude) Stokes waves for inviscid flows, using a perturbation technique based on the method of multiple scales. The stability of interfacial waves was shown to be determined by the derived non-linear Schrödinger equation that describes the modulation of the wave amplitude in terms of several parameters such as wave number. The instability is predicted to occur at a lower gas velocity with the consideration of non-linear effects than that obtained by the linear stability theory typically represented by **Equation (1-1)**.

In a brief review above, majority of investigators attributed the main mechanism to trigger slugging to the Kelvin-Helmholtz instability. The application of the variations of **Equation (1-1)**, such as the Taitel-Dukler model, requires to know the liquid level that depends on interfacial friction and gas/liquid velocities. The transitional conditions would depend on the wave height of interfacial waves, relative to the channel height. **Equation (1-1)** suggests further the influence of fluid properties that depend on system pressure for steam/water two-phase flows. These are all major subjects in the present study.

1. 1. 2 Interfacial Friction for Stratified-Wavy Flow Regime in the Vicinity of Transition Boundary to Slug Flow Regime

Majority of models and methods reviewed in **Section 1. 1. 1** require the knowledge of the liquid depth (or void fraction α) which depends on the gas and liquid flow rates as well as the wall and interfacial friction. The Taitel-Dukler

model (1976) modified by Anoda et al. (1989), for example, predicts the SW-to-SL flow regime transition to occur when the gas-liquid relative velocity $\Delta u = u_G - u_L$ exceeds a critical value of $\Delta u_{crit} \propto \alpha^n$, where $n \approx 5/2$ (cf. **Section 3. 2**). An increase in the interfacial friction has an effect to suppress the transition by lowering the liquid level and reducing the gas-liquid relative velocity. It is thus important to estimate the interfacial friction in the stratified-wavy (SW) flow regime to predict the SW-to-SL flow regime transition.

The interfacial friction depends on such parameters as the wave amplitude and the wave length of interfacial waves. The interfacial friction factor f_i for horizontal stratified two-phase flow, however, has been studied mostly for film flows where the amplitude and length of waves depend on the film thickness [Cohen et al. 1965, Cheremisinoff et al. 1979, Lee et al. 1983, Shoham et al. 1984, Kim et al. 1985, Kowalski 1987, Andritsos et al. 1987]. The film flows appear mostly in annular flow regime (**Fig. 1-1**), where the direction of channels has rather small influence on the flow characteristics. The SW-to-SL flow regime transition, on the other hand, takes place typically for rather deep-water flows (α < ~0.6). Koizumi et al. (1990) and Kawaji et al. (1993) pointed out that the profiles of interfacial waves in the SW flow regime are much different from those in film flows. However, the contribution of such interfacial waves to the interfacial friction have not been studied systematically for the SW flow. To calculate void fraction α at the SW-to-SL flow regime boundary, therefore, several investigators and LOCA computer codes assume simply that f_i is equal to the gas-phase wall friction factor f_G multiplied by an appropriate constant m around unity; $f_i = m \times f_G$ [Taitel et al. 1976, Lin et al. 1986, Ranson V. H. et al. 1987, Ohnuki et al. 1988, Crowley et al. 1992].

In this study, the applicability of current models and correlations to SW flow regime is assessed against the TPTF steam/water two-phase flow data for various system pressures and pipe diameters. The interfacial friction factor for

SW flow regime, particularly in the vicinity of the transition boundary to the SL flow regime, is investigated further based on the TPTF data.

1. 1. 3 Bernoulli Effect

The decrease in the gas-phase static pressure around the crest of slugging waves that results from the proximity of the channel top wall is considered to enhance the Kelvin-Helmholtz instability. This effect is often referred to as the "Bernoulli" effect. However, the significance of this effect has not yet been fully understood, partly because of lack in the detailed experimental data.

The measurement of the gas phase static pressure distribution over wave surface has been mostly limited to open-channel flow cases [Shemdin et al. 1967]. For closed channel flows, to the author's knowledge, Kordyban only [Kordyban 1974, Kordyban 1977, Kordyban et al. 1979 and Kordyban 1980] has measured the air static pressure on the water surface using a piezo-type pressure sensor which followed the vertical motion of the wavy interface. He reported that the pressure difference between the wave crest and trough was 1.81 times larger than that obtained from one-dimensional Bernoulli equation [Kordyban 1980], and that the decrease in static pressure at the crest was much smaller than the water static head corresponding to the wave height. His measurement, however, did not cover the final stage of wave growth into a slug, because of mechanical problems associated with the shape of the pressure measuring sensor.

In this study, the gas phase static pressure distribution was measured over the entire length of slugging waves in the large-height rectangular duct experiments. The liquid level was measured simultaneously at the same location to obtain the gas-phase cross-section. The measured data is evaluated in reference to the one-dimensional Bernoulli prediction of the local static pressure.

1. 1. 4 Onset of Liquid Entrainment

In the TPTF experiments, transition to wavy-dispersed (WD) flow regime (**Fig. 1-1**) from SL or SW flow regime occurred when the steam superficial velocity exceeded a certain critical value. This critical value which depends on the liquid flow rate decreased as the system pressure was raised. The SL flow regime finally became non-observable when the system pressure reached about 8.6 MPa [Anoda et al. 1989, Nakamura et al. 1991 a]. This finding is of major interest to reactor safety analysis of small-break (SB) LOCAs, because the occurrence of SL flow in hot legs would exert a significant influence on the coolant distribution during a SBLOCA [Kukita et al. 1988]. Visual observation has shown that the SL-to-WD flow regime transition is initiated by the onset of liquid entrainment in the stratified-flow part of the SL flow (**Fig. 1-1**). The liquid entrainment have an effect to suppress the wave growth into slugs.

In the air/water large-height duct experiments, the liquid entrainment was observed to occur at the wave crest in the final stage of slugging [Nakamura et al. 1994]. It suppressed the wave growth by cutting-off the wave crests. For high-pressure steam/water flows, the onset of liquid entrainment in the stratified flow part of SL flow regime is considered to suppress the wave growth into slugs in the early stage of slugging.

Ishii et al. (1975) reviewed several mechanisms that initiate liquid entrainment at the gas/liquid interface for horizontal co- and counter-current flows based on the results by various investigators. The mechanisms include shearing-off of crests of roll waves by the turbulent gas flows, undercutting liquid films by a gas flow, the bursting of gas bubbles and the impingement of liquid droplets. The liquid entrainment in a co-current two-phase flow, however, has been studied mostly for thin liquid-film flows, in conjunction with the interfacial friction, in annular flow regime in both vertical and horizontal channels.

In thin liquid-film flows, the entrainment is dominated by shearing-off of roll waves with amplitudes comparable to the film thickness δ, and is greatly influenced by liquid viscosity. Ishii et al. (1975), however, showed that the gas velocity at the onset of entrainment becomes independent of the liquid Reynolds number when the liquid film Reynolds number = $4 u_L \delta / \nu_L$ > 1500 to 2000. Steen et al. (1964) also reached a similar conclusion based on their air/water experiments. As noted in **Section 1.1. 2** for the interfacial friction, the phenomena should be greatly influenced by the gas/liquid interfacial wave forms. For SW flow regime, the amplitude of interfacial waves are smaller than the liquid depth and the dominant entrainment mechanism are expected to be different from those for thin liquid-film flows.

Ishii et al. (1975) obtained a model to predict onset of entrainment based on the mechanism of shearing-off of roll waves. However, recent study for the entrainment has been limited to the prediction of the diameter and amount of liquid droplets (entrainment) flowing in gas core [Kocamustafaogullari et al. 1994, Ishii et al. 1989, Kataoka et al. 1983]. Furthermore, previous studies are limited to pressures much lower than those in the present study which represented reactor pressures typical of a small-break LOCA [Ishii et al. 1975].

In this study, therefore, attempts are made to modify major correlation and models to take into account properly the predominant entrainment mechanisms and to better represent the influences of system pressure for steam/water flows.

1.2 Objectives of Thesis

The general objective of this study is to clarify the conditions for the flow regime transition into slug (SL) flow in horizontal gas/liquid two-phase flows. A wide range of flow conditions is covered particularly in channel height and system pressure to represent reactor accidental conditions more rigorously than the previously-available data, models and correlations. Specific objectives are;

1) To clarify the dependence of the conditions for the SW-to-SL flow regime transition on channel height (pipe diameter) and system pressure which controls fluid physical properties for steam/water two-phase flows,

2) To obtain interfacial friction factor for SW flow regime, in the vicinity of the flow regime transition to SL flow regime, in order to predict the SW-to-SL flow regime transition,

3) To clarify the influence of the "Bernoulli" gas-phase pressure drop on the growth of interfacial waves in a slugging process, and

4) To examine the pressure dependence of the conditions for the onset of entrainment in high-pressure steam/water two-phase flows, as a mechanism to cause the transition into WD flow regime.

The subjects based on the above objectives are noted on the flow regime map in **Fig. 1-3**.

For these purposes, the TPTF steam/water experiments (for pipe i.d.s of 180 and 87 mm, and system pressures up to 12 MPa), and the air/water experiments using a large-height (0.7 m) duct have been performed. The data obtained from these experiments are unique in covering the system pressure and the channel height typical of reactor accidents.

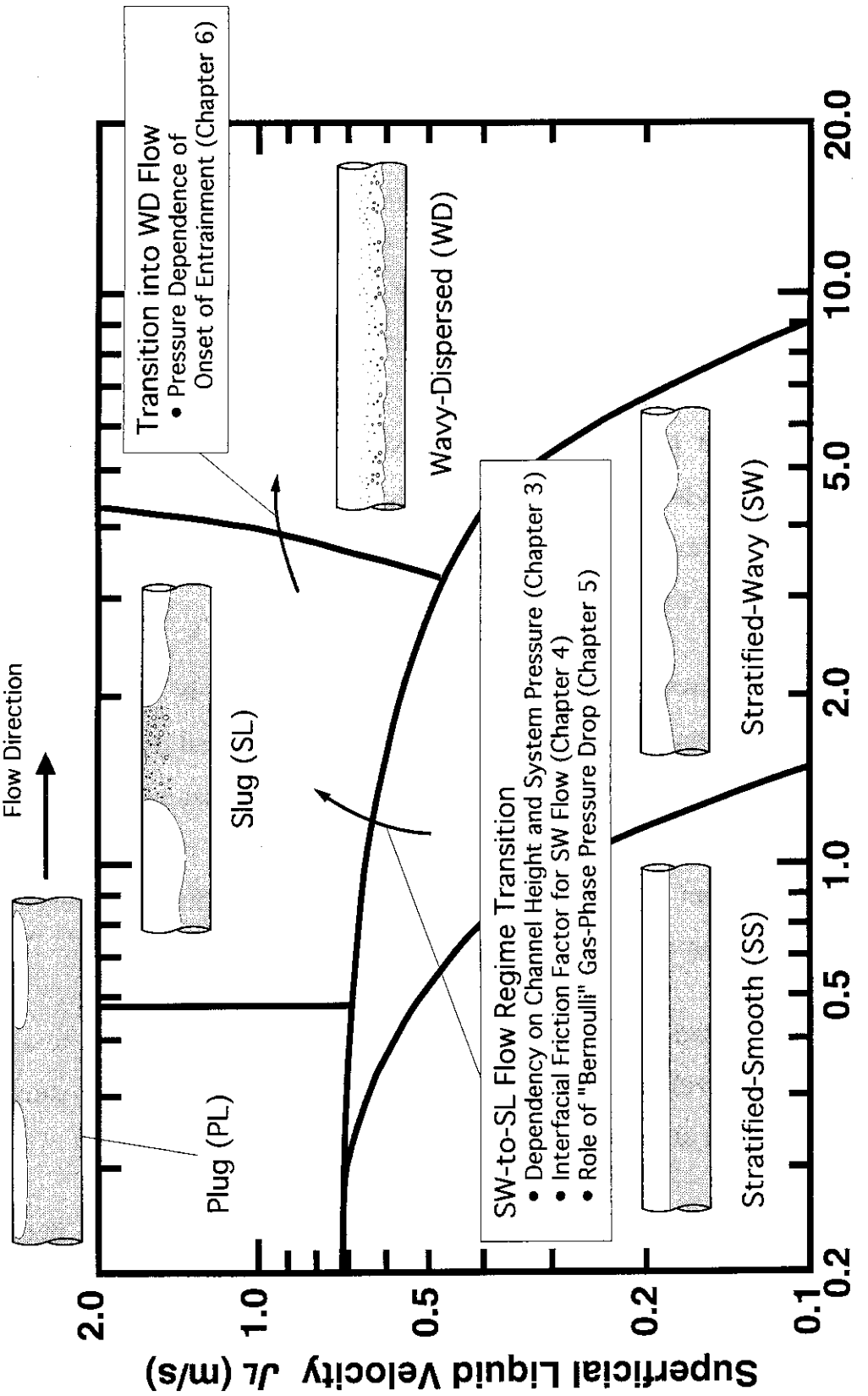

Fig. 1-3 Subjects Dealt With in This Study

1. 3 Structure of Thesis

Chapter 2 describes details of two experimental facilities; the TPTF for steam/water two-phase flows and the air/water two-phase flow loop with a large-height duct test section.

In **Chapter 3**, the results on SW-to-SL flow regime transition in both the TPTF and large-height duct experiments are summarized. The dependence of the flow regime transition on the channel height (pipe diameter) and system pressure are investigated [Anoda et al. 1989, Nakamura et al. 1991 a]. An applicability of an extended Taitel-Dukler model to large diameter pipes is demonstrated in conjunction with the discussion on the influence of the wave height on the flow regime transition.

In **Chapter 4**, the interfacial friction in SW flow regime is investigated using the TPTF steam/water two-phase flow data. A new empirical correlation is obtained to predict the interfacial friction factor f_i, employing parameters based on the Kelvin-Helmholtz instability theory. This correlation represents the dependence of f_i on system pressure and pipe diameter well within the present experimental ranges [Nakamura et al. 1995 b].

In **Chapter 5**, the static pressure drop over a slugging wave, referred to as the Bernoulli effect, is evaluated from measurement in the large-height duct experiments [Nakamura et al. 1994].

In **Chapter 6**, the conditions for the onset of entrainment in the SL flow regime is investigated for the TPTF experiments. The entrainment suppresses the growth of interfacial waves in high-pressure steam/water flows. The previous models and correlations to predict the onset of entrainment are examined and extended for the high-pressure steam/water conditions [Nakamura et al. 1995 a].

Chapter 7 gives the summary of this thesis.

2. Experimental Facilities with Typical Observed Flows

2.1 Introduction

Two test facilities: the Two-Phase Test Facility (TPTF) [Nakamura et al. 1983, Kawaji et al. 1987] for high-pressure steam/water two-phase flows and the air/water two-phase flow loop, were used for the present study. In the TPTF experiments, the influences of both channel height (pipe diameter) and system pressure were examined. Two horizontal pipe test sections with different diameters of 180 and 87 mm, to be shown schematically in **Fig. 2-1**, were used under system pressures ranging from 3 to 12 MPa. The air/water two-phase flow loop with a large-height (0.7 m) rectangular duct test section, to be shown schematically in **Fig. 2-5**, was used to examine the influences of the channel height on the transition and basic phenomena in wave growth. This chapter describes these facilities, and summarizes the flows observed in their experiments.

2.2 Two-Phase Flow Test Facility (TPTF)

2.2.1 Outline of TPTF

The Japan Atomic Energy Research Institute (JAERI) initiated the Rig of Safety Assessment Number 4 (ROSA-IV) program [Tasaka 1982, ROSA-IV Group 1984] in 1980, one year after the Three-Mile Island Unit-2 (TMI-2) accident [Rogovin et al. 1980], to study thermal-hydraulic responses during small-break LOCAs and anticipated transients of a PWR. The ROSA-IV program comprised three major tasks; (1) the integral-system-effect tests using the large scale test facility (LSTF) [ROSA-IV Group 1990] simulating a Westinghouse-type PWR, (2) the separate-effect tests using the TPTF facility and (3) the development of advanced LOCA analysis code. The operation of the TPTF was initiated in 1982.

The ROSA-IV program ended in 1992, but was succeeded by the ROSA-V program in 1991.

The primary objectives of the TPTF experiments were to obtain the fundamental data on the thermal-hydraulic responses in the primary components of LWRs such as the core, the steam generator of a PWR and the horizontal and vertical pipes, and to calibrate and develop the two-phase flow instruments to be used in the LSTF. For these purposes, the facility was designed to achieve the saturated steam/water two-phase flow condition under a PWR nominal saturation pressure of 12 MPa for steady-state experiments. The TPTF had two test sections; (1) a heat transfer test section to study heat transfer and void distribution in a core rod bundle, and (2) a horizontal pipe test section to study flow regime transition, interfacial friction and interphase heat transfer. In the present study, the horizontal pipe test section was used.

2. 2. 2 Test Facility and Test Sections

Figures 2-1 (a) and (b) show the overall test facility and test sections used for the present study. Saturated steam and water at pressures of 3 to 12 MPa were produced in an electrically heated boiler from demineralized water and delivered separately to a mixer by steam and water pumps, respectively. Steam/water two-phase flow was produced in the mixer and flowed through the horizontal test section, returning to the boiler. The steam and water flow rates were controlled by the pump rotational speed and/or flow control valve opening. The maximum flow rates were decided to be 0.222 and 0.0556 m^3/s for steam and liquid phases, respectively, to fulfill the low flow rate conditions in a horizontal pipe and core of a PWR during a small-break LOCA. The facility including the test section was thermally insulated to minimize the heat loss.

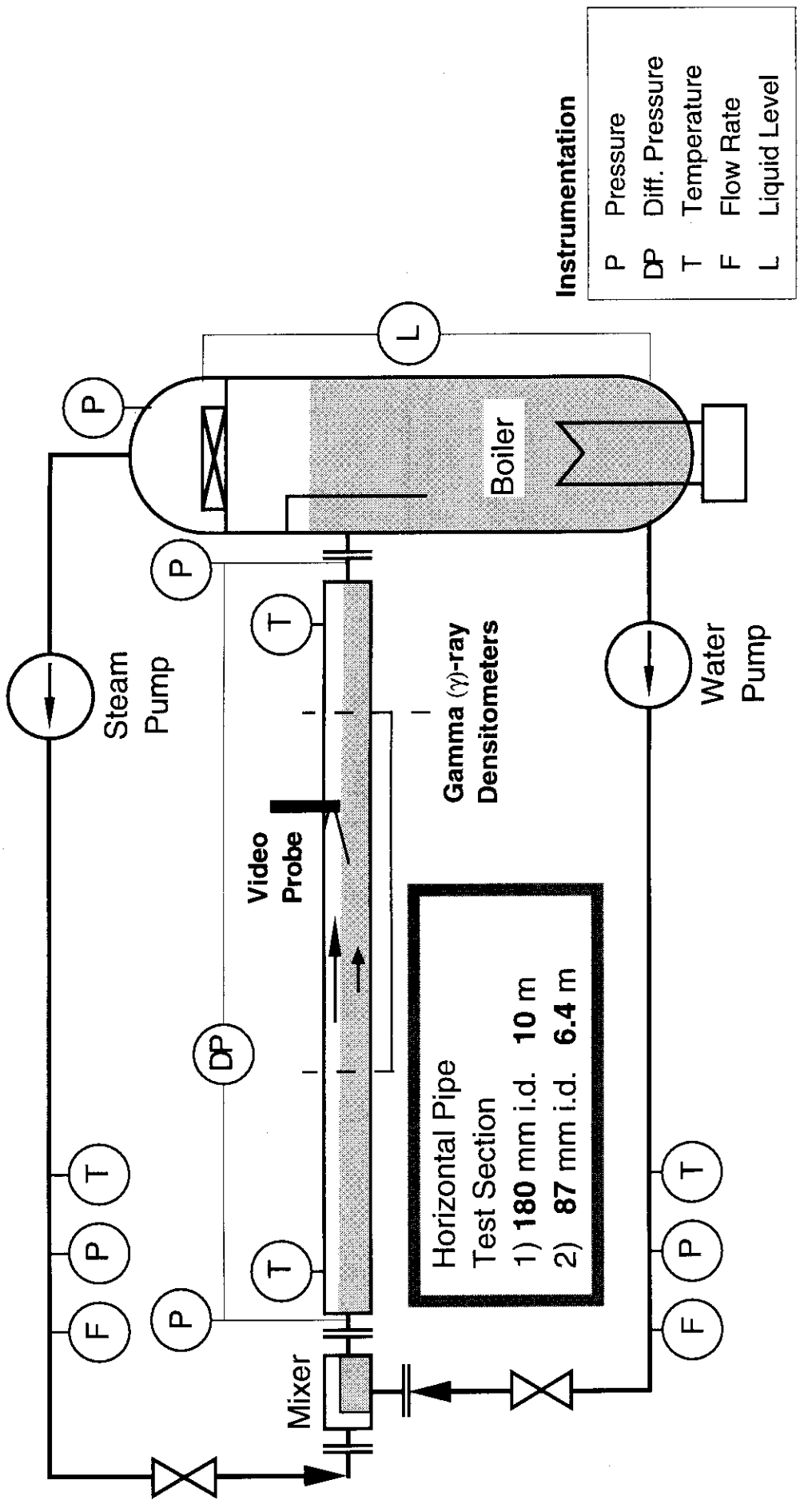

Fig. 2-1 Schematic of Two-Phase Flow Test Facility (TPTF)
(a) Facility Overview

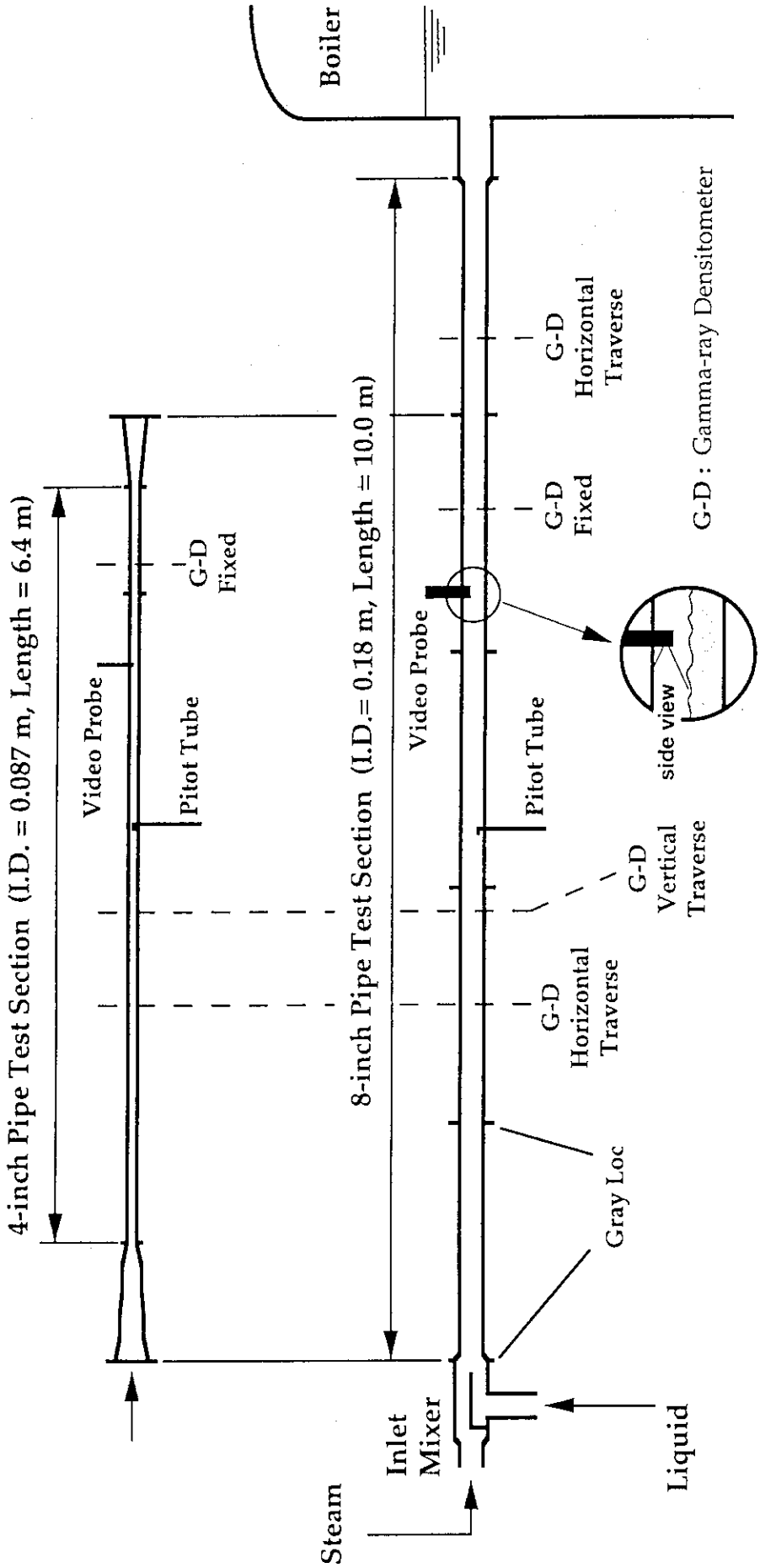

Fig. 2-1 Schematic of Two-Phase Flow Test Facility (TPTF)
(b) Horizontal Pipe Test Sections

Two test sections having different inner diameters (I.D.s), shown schematically in **Fig. 2-1 (b)**, were horizontally leveled. The 8-inch (180 mm I.D.) pipe test section was 10 m in length and consisted of five 2-m-long segments. The inner diameter of the 8-inch pipe test section was almost the same as that of the hot legs of the LSTF, and was about one third of that of a PWR. The 4-inch (87.3 mm I.D.) pipe test section consisted of 5.5-m and 0.9-m-long segments. Each test section was connected to the 12-inch (268 mm I.D.) mixer and boiler. The pipe diameter was smoothly decreased from 268 to 87 mm in a 1-m long inlet reducer and was expanded from 87 to 180 mm in a 0.6-m long outlet diffuser for the 4-inch pipe test section. Gray-Loc® flange coupler was used to connect the mixer, reducer, test section segments, diffuser and boiler. The 12-inch mixer was tee-shaped with a horizontally-flat inner baffle plate that led steam and water flows horizontally but separately to prepare the horizontal stratified flow at the mixer exit. In the experiments, the mixture level in the boiler at the test section exit was kept above the pipe center line by about 0.5 m to have a flow situation similar to that in PWR hot legs.

2. 2. 3 Instrumentation

The test facility and the test sections were equipped with various instruments as shown in **Figs. 2-1 (a) and (b)**. The system pressure was measured by a diaphragm-type differential pressure cell with an uncertainty of 0.090 MPa (0.61% of the total range). Flow rates were measured by orifice meters with a measurement uncertainty of less than ~1.5% of the total range. Each of gas and liquid measurement lines had two lines with different orifice capacities to have a wide flow rate range. The liquid temperature drop from the saturation at the mixer inlet was less than the measurement uncertainty of 0.48% of the total range, which corresponded to ~2.3 deg K.

The liquid level and flow regimes in the test section were measured by four current-integration type gamma(γ)-ray densitometers with a ^{137}Cs source; two with vertical-shot beam(s) traversed horizontally, one with horizontal-shot beam traversed vertically and one fixed with vertical-shot beam. The γ-ray beam was collimated through a 13 mm i.d. beam hole in a lead cask, and was shot along the pipe diameter. The reference single-phase steam and liquid flow data were taken for every five to six two-phase flow measurements to minimize the data uncertainty, which was less than 2% of the measured void fraction. For stratified-smooth flow, flatness of the interface across the pipe cross-section was confirmed by using two γ-ray densitometers (vertical-shot three beams and horizontal-traverse) [Kawaji et al. 1987]. The increase in the liquid level near the wall, which may occur in a small-diameter pipe, was not observed, because of the large diameter and low surface tension under high-pressure condition. The chordal void fraction was obtained as the liquid level using the single vertical-shot beams through the pipe axis, and was converted into the area-averaged void fraction assuming a flat interface. To detect the mixture level and liquid slug passage, conductivity probes and vertical-traverse pitot tube were also used in several experiments. The conductivity probes were installed flush inner-wall of the test section at L/D = 28, and the pitot tubes were installed at L/D = 25.

The instrument signals were recorded on a magnetic tape by the data logger (Iwatsu Inc. DA-8500), generally 8000 data points in each experimental run, at a maximum rate of 100 Hz. Every measurement for parameters such as pressure, differential pressure, flow rate, liquid level, fluid temperature, and fluid density was taken into the memory simultaneously, and was recorded on a magnetic tape (MT). Selected instrument signals were monitored by chart recorders during the experiments for the detection of flow regime transition; especially the transition to slug flow. The data recording was started when the monitored signals reached steady-state. The obtained data on MTs were off-line transferred to the JAERI main-frame computer (FACOM) after each experiment and were post-processed.

A video probe [Nakamura et al. 1992]: a periscope designed to withstand high-pressure steam/water two-phase flow condition, was employed further for the visual observation of the gas-liquid interface upstream the probe. The video probe was composed of a SUS casing containing a optical bore-scope and optical fibers for lighting, sapphire windows, lenses and a high-sensitivity video camera. The video probe (~70 mm O.D.) with a side view was inserted vertically into the test section, by ~5 cm from the top ceiling at L/D = 39.

2. 3 Flows in TPTF

2. 3. 1 Flow Regimes

In **Fig. 2-2**, the flow regime map obtained from the TPTF 8-inch pipe experiments [Anoda et al. 1989] at 3 MPa is compared with the Mandhane map [Mandhane 1974]. The observed flow regimes in the TPTF experiments were separated flows including stratified-smooth (SS) and stratified-wavy (SW) flows, intermittent flows including slug (SL) and plug (PL) flows, and wavy-dispersed (WD) flow. Typical flow patterns that are sketched in **Fig. 1-1** appear in these flow regimes.

The threshold flow rates for flow regime transition were searched for by changing slowly the flow rate of one phase, while the flow rate of the another phase was kept constant. Flow regimes were identified mainly by the video probe observation. The γ-ray densitometer and conductivity probe signals were used to confirm the judgment. The pitot tube signals were also referred in several experiments in judging the transition to SL flow regime. The criterion for the judgment for the SW-to-SL flow regime transition, for example, was whether the liquid slugs dragged their top along the pipe inner ceiling wall or not.

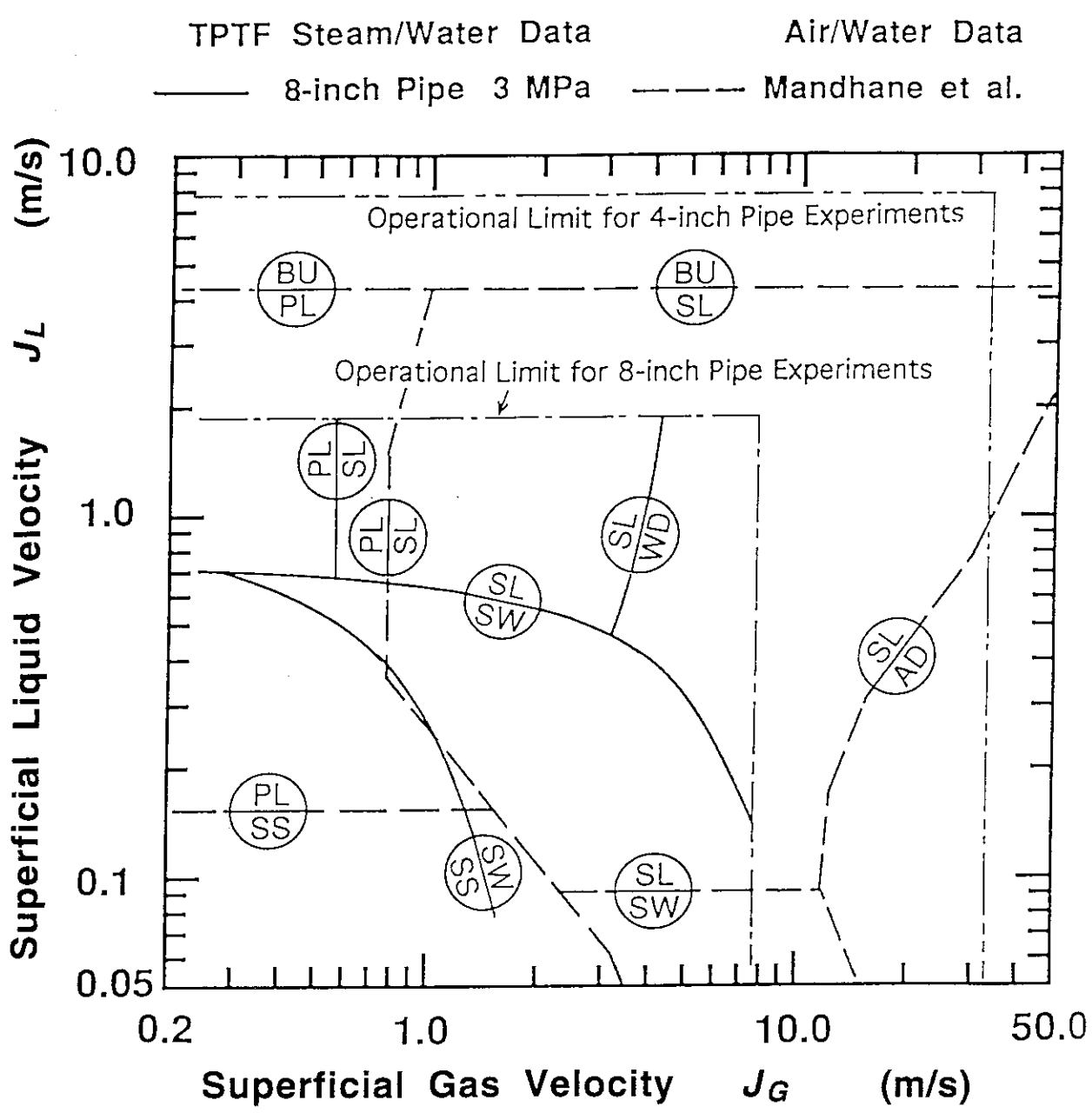

SS: Stratified Smooth, SW: Stratified Wavy
PL: Plug, SL: Slug
WD: Wavy Dispersed, AD: Annular Dispersed
BU: Bubbly

Fig. 2-2 Flow Regime Map for TPTF Experiments

2. 3. 2 Influence of Inlet Mixer Internal Structure

The flow in the test section was found to be influenced by the internal structure in the tee-shaped 12-inch mixer. Two different internal structures were prepared to change the inlet mixture condition: a "bubbly flow" type mixer consisting of a bundle of horizontal perforated pipes and a "separated flow" type mixer containing one horizontal flat plate. For both types of mixer, steam was introduced horizontally and liquid was introduced from bottom of the mixer.

A significant influence of mixer configuration was observed on flow regime transition in 8-inch pipe experiments. Intermittent flow (slug or plug flows) was not well established when the "bubbly flow" type mixer was used, introducing a two-phase mixture into the test section. In high-pressure steam/water two-phase flows, difference in fluid densities between steam and water becomes small. Therefore, phase separation takes place gradually. The gas-liquid relative velocity did not sufficiently develop in the test section to cause the transition. On the other hand, when the "separated flow" type mixer was used, steam and liquid were introduced parallel to the channel axis, with a relative velocity, and the transition to intermittent flow took place in the test section. In 4-inch pipe experiments, however, the SW-to-SL flow regime transition occurred irrespective of the mixer internal geometry, probably because a low flow velocities in the inlet reducer enhanced a good phase separation.

2. 3. 3 Dependence of Liquid Level Gradient on Pipe Exit Level

The liquid level gradient along the length of the test section becomes independent of the downstream level when the liquid flow is supercritical where the liquid velocity exceeds the celerity of interfacial gravity waves. For an open channel flow, the criticality criterion is given by the Froude number [Chow 1959],

$$Fr = u_L / \sqrt{g\ D_L^*} = 1.0, \qquad (2\text{-}1)$$

where $D_L^* = A_L/S_L$ is the hydraulic liquid depth, A_L is the cross section of liquid flow and S_L is the wet perimeter on the channel wall. Gardner (1988) derived the criticality criterion for a separated flow in a horizontal pipe

$$\frac{J_L^{*2}}{(1-\alpha)^3} + \frac{J_G^{*2}}{\alpha^3} = \frac{\pi D}{S_i} \quad , \tag{2-2}$$

where, $J_k^* = J_k \sqrt{\rho_k / \left[(\rho_L - \rho_G) g D\right]}$ is the non-dimensional superficial velocities and S_i is the interface width.

For the TPTF experiments conducted with the "separated flow" type mixer, the flow at the SW-to-SL flow regime transition boundary and a large part of the SW flow regime was supercritical. The liquid level in the test section was thus independent of the downstream level of the test section outlet. **Figures 2-3 (a)** and **(b)** compare the TPTF 4 and 8-inch pipe data at the SW-to-SL flow regime transition boundary with the Gardner flow criticality criterion. All the data points used for the present study, including those presented in **Fig. 2-3**, are in the supercritical region. As the gas flow rate was decreased in the SW flow regime, the flow became to be subcritical and the void fraction decreased stepwise as shown in **Table 2-1** for 8-inch pipe, 3 MPa experiments. For the low-pressure air-water experiments, the SW-to-SL transition usually takes place under subcritical flow condition. The observed supercritical flow may be particular to high-pressure steam/water experiments where gas density is high. However, the supercritical flow condition is advantageous in obtaining a well-developed flow in a relatively small L/D. Furthermore, this flow condition is good in observing the wave growth, since there is no influences of waves that go up the test section. It is not known whether the flow criticality has a direct influence on the flow regime transition mechanisms or not. The good agreement of the SW-to-SL transition in the TPTF experiments with the Taitel-Dukler model (1976), to be shown in **Chapter 3**, suggests that the influence is small.

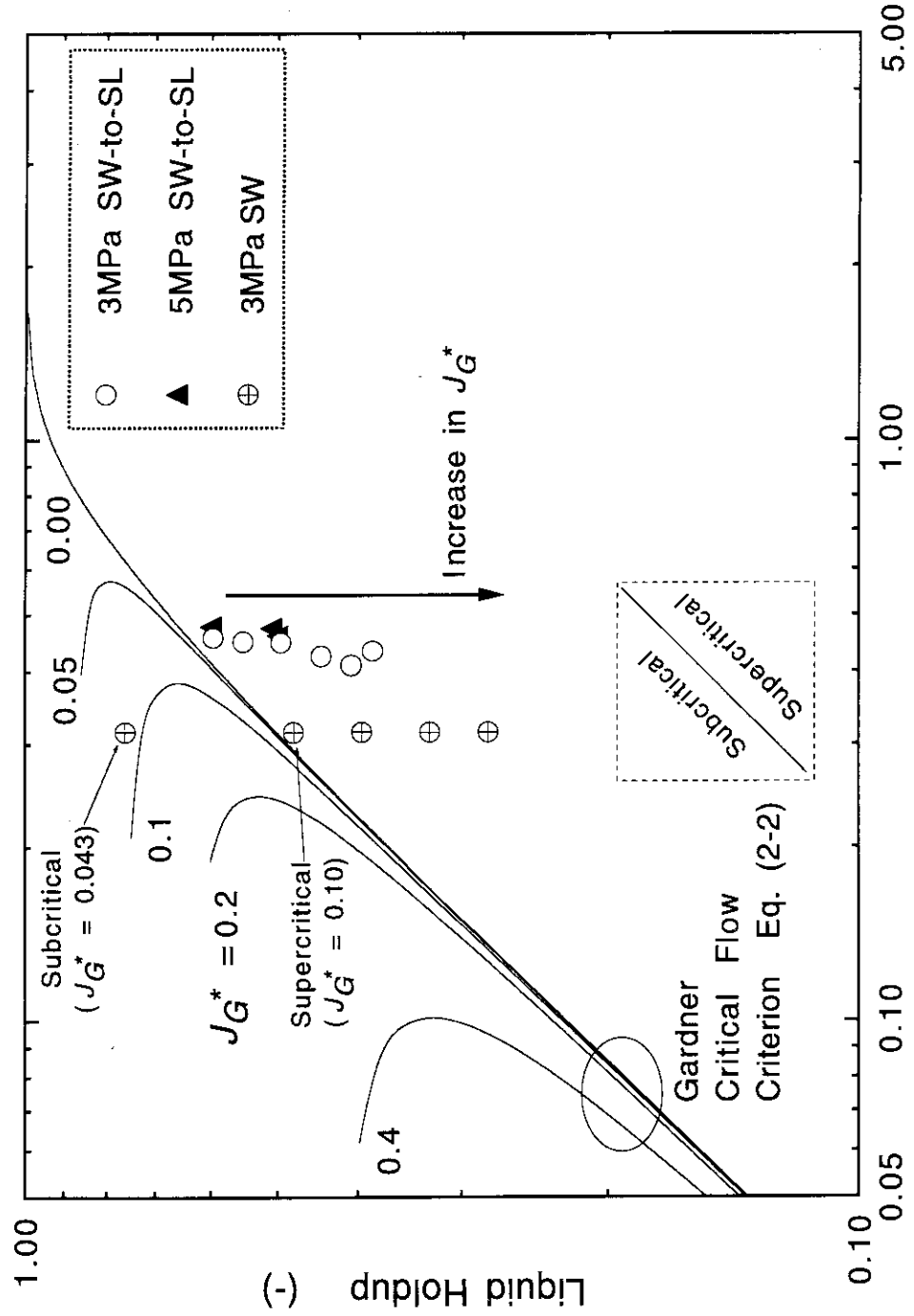

Fig. 2-3 (a) Criticality of Stratified-Wavy-to-Slug Transition Boundary Data (8-inch Pipe)

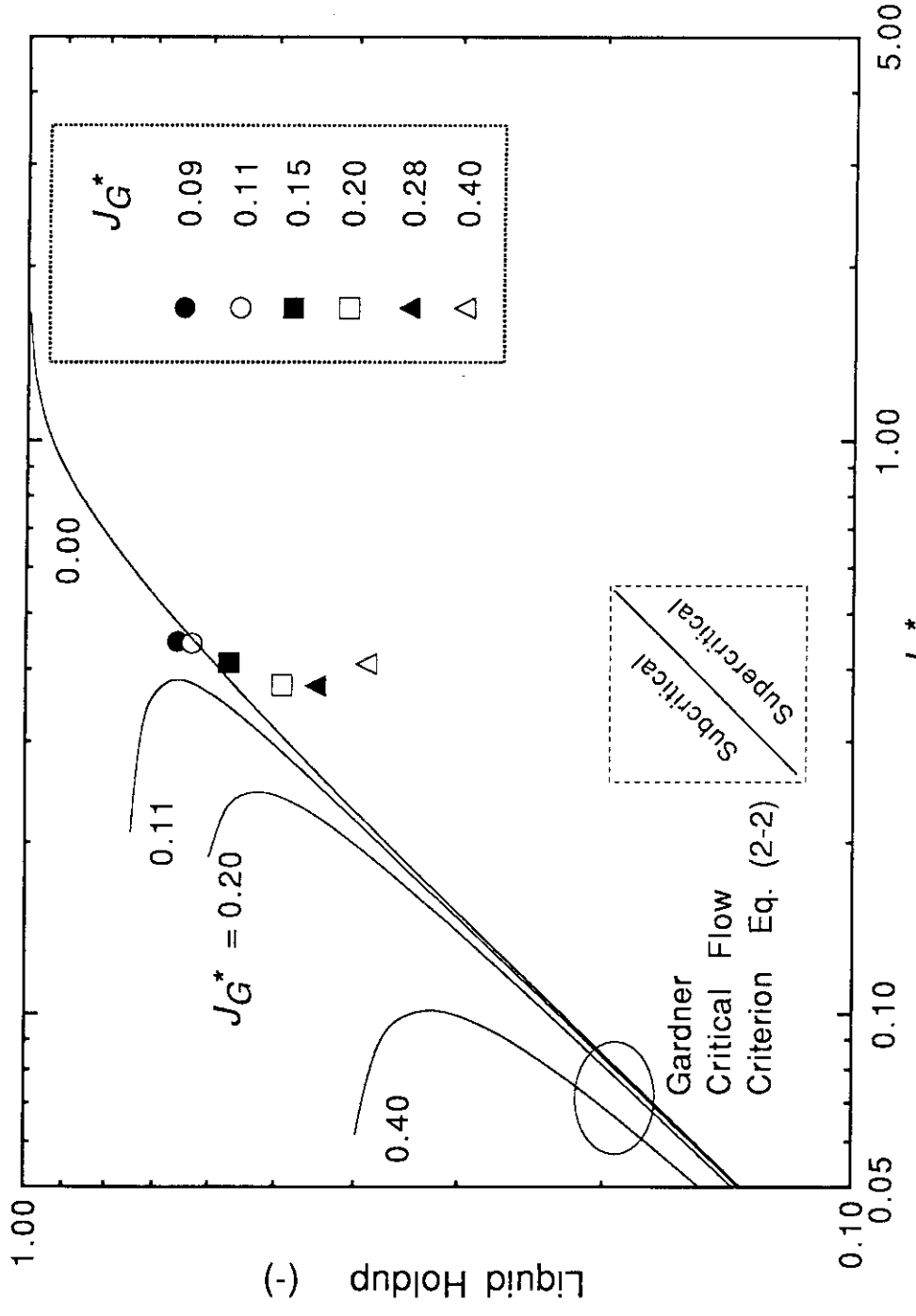

Fig. 2-3 (b) Criticality of Stratified-Wavy-to-Slug Transition Boundary Data (4-inch Pipe, 3 MPa)

Table 2-1 Primary Parameters for TPTF Horizontal Pipe Experiments (1/3)

180 mm i.d. pipe

(1) Pressure = 3 MPa, $\Delta U_{min} \approx 1.43$

RUN	J_L	J_G	Flow Regime	σ x 10^2	α	J_{GL}^* x 10^2	Re_L x 10^{-5}	Re_G x 10^{-5}	f_L x 10^3	f_G x 10^3	f_i x 10^2	XX *)
475	1.01	1.01	SL	13.7	0.402	3.40	23.9	2.15	2.01	3.67	29.9	0.127
476	0.724	1.01	SL	11.4	0.429	4.85	17.5	2.11	2.17	3.69	9.97	0.163
479	1.01	1.74	SL	13.4	0.538	5.77	27.3	3.38	1.94	3.28	35.9	0.132
480	0.672	1.70	SL	12.0	0.579	8.06	18.9	3.24	2.13	3.31	12.5	0.163
483	1.01	2.58	SL	9.85	0.547	14.1	27.5	4.98	1.94	2.97	6.13	0.313
484	0.646	2.58	SL	10.1	0.604	16.4	18.7	4.82	2.14	3.00	3.29	0.308
493	0.607	2.39	SL	9.54	0.606	14.9	17.6	4.40	2.17	3.07	3.68	0.279
494	0.631	1.58	SL	10.5	0.511	9.46	16.5	3.08	2.20	3.35	4.15	0.236
486	0.414	4.08	SW(spr)	3.60	0.730	30.6	14.1	7.20	2.29	2.71	1.37	0.416
478	0.414	1.71	SW(spr)	3.94	0.606	11.1	12.0	3.21	2.39	3.32	3.33	0.207
482	0.414	2.57	SW(spr)	3.65	0.683	17.3	13.2	4.63	2.33	3.03	2.82	0.264
473	0.414	0.411	SW(sub)	2.40	0.223	3.03	8.28	1.05	2.62	4.39	0.357	0.305
474	0.413	1.01	SW(sub)	3.42	0.429	7.21	10.0	2.10	2.50	3.69	1.29	0.242
477	0.616	1.01	SW-SL	9.08	0.448	5.29	15.2	2.07	2.25	3.70	7.40	0.165
481	0.559	1.70	SW-SL	8.84	0.565	10.0	15.5	3.24	2.24	3.31	4.91	0.211
485	0.539	2.56	SW-SL	7.89	0.608	17.9	15.7	4.79	2.23	3.00	1.97	0.333
495	0.592	1.35	SW-SL	7.76	0.452	8.85	14.6	2.73	2.27	3.46	2.28	0.272
2473	0.601	1.01	SW-SL	7.04	0.398	6.30	14.1	2.14	2.29	3.67	2.82	0.240
2474	0.590	1.82	SW-SL	8.76	0.519	12.2	15.6	3.55	2.24	3.24	2.23	0.296
2475	0.571	2.78	SW-SL	8.18	0.628	18.8	17.0	5.14	2.19	2.95	2.45	0.330
492	0.679	3.44	SL-WD	8.44	0.659	21.8	21.0	6.18	2.08	2.82	3.41	0.354
487	1.01	4.09	WD	9.69	0.649	22.8	31.0	7.43	1.88	2.69	5.97	0.379
488	0.583	4.09	WD	7.79	0.704	27.8	19.2	7.26	2.12	2.71	2.45	0.403
489	0.473	4.09	WD	6.07	0.717	29.8	15.8	7.22	2.23	2.71	1.63	0.417
490	0.415	7.76	WD	3.66	0.840	57.4	17.5	13.1	2.17	2.34	1.61	0.614
491	1.01	7.74	WD	6.59	0.779	43.1	37.5	13.4	1.80	2.32	6.42	0.525
2476	0.547	4.09	WD	7.15	0.709	28.6	18.1	7.31	2.15	2.70	2.16	0.408
2477	0.496	6.74	WD	5.39	0.811	47.7	19.5	11.6	2.11	2.41	2.12	0.543

Table 2-1 Primary Parameters for TPTF Horizontal Pipe Experiments (2/3)

180 mm i.d. pipe

(2) Pressure = 5 MPa, $\Delta U_{min} \approx 1.04$

RUN	J_L	J_G	Flow Regime	σ x 10^2	α	J_{GL}^* x 10^2	Re_L x 10^{-5}	Re_G x 10^{-5}	f_L x 10^3	f_G x 10^3	f_i x 10^2	XX *)
515	0.412	1.667	SW(SPR)	3.36	0.555	15.9	12.0	4.99	2.39	2.97	0.747	0.327
519	0.412	2.548	SW(SPR)	2.88	0.669	23.7	13.7	7.20	2.31	2.71	1.13	0.353
523	0.413	4.054	SW(SPR)	3.04	0.753	38.4	15.5	11.0	2.24	2.44	1.06	0.470
513	0.624	1.000	SW-SL	5.42	0.386	8.37	15.4	3.33	2.24	3.29	1.21	0.318
518	0.602	1.666	SW-SL	6.38	0.516	14.1	16.8	5.09	2.19	2.96	1.51	0.329
2480	0.623	0.992	SW-SL	5.01	0.391	8.09	15.4	3.26	2.24	3.31	1.42	0.301
2481	0.620	1.694	SW-SL	6.43	0.507	14.4	17.2	5.12	2.18	2.95	1.40	0.345
522	0.600	2.562	SW-WD	5.87	0.611	22.3	18.6	7.41	2.14	2.69	1.48	0.388
527	0.578	4.037	SW-WD	5.35	0.708	36.1	20.3	11.1	2.09	2.43	1.38	0.490
2482	0.579	2.457	SW-WD	5.97	0.609	21.3	17.9	7.04	2.16	2.73	1.49	0.374
2483	0.527	3.976	SW-WD	4.81	0.719	35.9	18.8	10.9	2.13	2.45	1.32	0.475
2484	0.463	5.954	SW-WD	3.83	0.814	53.6	19.5	15.7	2.12	2.23	1.50	0.574
524	1.011	4.049	WD	7.49	0.644	30.6	32.6	11.5	1.86	2.41	2.92	0.488
525	1.011	7.702	WD	4.51	0.794	52.5	40.9	20.6	1.76	2.09	5.06	0.586
526	0.414	7.674	WD	2.43	0.864	69.4	19.6	20.0	2.11	2.10	1.58	0.670

(3) Pressure = 7.3 MPa, $\Delta U_{min} \approx 0.771$

RUN	J_L	J_G	Flow Regime	σ x 10^2	α	J_{GL}^* x 10^2	Re_L x 10^{-5}	Re_G x 10^{-5}	f_L x 10^3	f_G x 10^3	f_i x 10^2	XX *)
542	0.414	2.53	SW(SPR)	2.62	0.690	28.3	14.6	10.0	2.27	2.50	0.943	0.377
546	0.412	4.03	SW(SPR)	2.35	0.778	45.6	16.6	15.4	2.20	2.24	0.989	0.494
2527	0.488	2.30	SW(SPR)	2.08	0.642	25.3	16.2	9.44	2.22	2.53	0.973	0.379
2528	0.493	2.29	SW(SPR)	2.03	0.640	25.2	16.3	9.42	2.21	2.54	0.974	0.380
541	1.01	2.56	WD	6.52	0.549	23.4	30.1	10.9	1.90	2.45	1.89	0.461
543	1.86	2.55	WD	5.22	0.468	16.1	51.1	11.4	1.66	2.42	6.28	0.415
544	1.86	4.04	WD	5.34	0.581	25.7	57.4	16.9	1.61	2.19	7.03	0.459
545	1.01	4.04	WD	5.29	0.656	37.2	34.0	16.3	1.84	2.21	2.11	0.540
547	0.415	7.67	WD	1.77	0.895	72.9	22.3	28.2	2.05	1.93	2.66	0.622

(4) Pressure = 8.6 MPa, $\Delta U_{min} \approx 0.665$

RUN	J_L	J_G	Flow Regime	σ x 10^2	α	J_{GL}^* x 10^2	Re_L x 10^{-5}	Re_G x 10^{-5}	f_L x 10^3	f_G x 10^3	f_i x 10^2	XX *)
2487	0.668	0.827	SW(SPR)	3.63	0.370	8.71	17.6	4.73	2.17	3.01	0.831	0.321
2489	0.635	1.31	SW(SPR)	3.96	0.466	15.0	18.3	6.90	2.15	2.74	0.679	0.374
2490	0.580	2.10	SW(SPR)	3.63	0.606	23.9	19.4	10.2	2.12	2.49	1.02	0.382
2458	1.864	1.00	WD	4.22	0.268	6.36	44.8	6.31	1.72	2.80	4.19	0.403
2459	1.009	1.01	WD	6.27	0.358	8.86	26.3	5.78	1.96	2.87	1.86	0.345
2462	1.011	1.67	WD	5.46	0.441	17.4	28.5	9.00	1.92	2.57	1.02	0.477
2463	1.862	1.67	WD	4.39	0.349	13.4	48.2	9.68	1.69	2.52	2.33	0.542
2464	1.860	2.58	WD	4.94	0.479	17.4	54.4	13.5	1.64	2.32	5.72	0.415
2465	1.010	2.56	WD	4.94	0.557	25.7	32.0	12.8	1.87	2.35	1.61	0.474
2467	0.412	4.06	WD	2.36	0.798	48.6	18.2	18.3	2.15	2.15	1.12	0.485
2468	1.01	4.08	WD	4.14	0.676	39.1	36.8	19.2	1.80	2.12	2.31	0.518
2492	0.440	4.14	WD	2.36	0.800	47.5	19.5	18.6	2.11	2.14	1.40	0.472

Table 2-1 Primary Parameters for TPTF Horizontal Pipe Experiments (3/3)

87 mm i.d. pipe

(1) Pressure = 3.0 MPa, $\Delta U_{min} \approx 1.43$ m/s

RUN	J_L	J_G	Flow Regime	σ x 10^2	α	J_{GL}^* x 10^2	Re_L x 10^{-5}	Re_G x 10^{-5}	f_L x 10^3	f_G x 10^3	f_i x 10^2	XX *)
4304	0.342	1.90	SW-SL	3.53	0.552	22.1	4.55	1.79	3.40	4.09	0.709	0.695
4305	0.343	1.36	SW-SL	3.39	0.508	15.1	4.36	1.32	3.43	4.35	1.17	0.544
4306	0.375	0.994	SW-SL	3.00	0.430	10.6	4.42	1.01	3.42	4.59	1.34	0.510
4307	0.406	0.718	SW-SL	2.87	0.368	7.21	4.51	0.768	3.40	4.85	1.98	0.449
4308	0.373	2.66	SW-SL	3.97	0.611	31.0	5.30	2.437	3.30	3.85	0.774	0.820
4309	0.409	0.578	SW-SL	2.78	0.342	5.46	4.44	0.633	3.41	5.04	2.83	0.386
2172	0.254	0.760	SW(SPR)	2.95	0.530	46.2	3.07	0.729	3.68	4.90	1.73	0.337
2173	0.245	1.36	SW(SPR)	2.53	0.425	59.5	3.40	1.21	3.60	4.43	1.66	0.405
2174	0.244	2.69	SW(SPR)	3.06	0.370	66.4	3.68	2.31	3.55	3.89	0.483	0.741

(2) Pressure = 7.3 MPa, $\Delta U_{min} \approx 0.771$

RUN	J_L	J_G	Flow Regime	σ x 10^2	α	J_{GL}^* x 10^2	Re_L x 10^{-5}	Re_G x 10^{-5}	f_L x 10^3	f_G x 10^3	f_i x 10^2	XX *)
542	0.414	2.53	SW(SPR)	2.62	0.690	28.3	14.6	10.0	2.27	2.50	0.943	0.377
546	0.412	4.03	SW(SPR)	2.35	0.778	45.6	16.6	15.4	2.20	2.24	0.989	0.494
2527	0.488	2.30	SW(SPR)	2.08	0.642	25.3	16.2	9.44	2.22	2.53	0.973	0.379
2528	0.493	2.29	SW(SPR)	2.03	0.640	25.2	16.3	9.42	2.21	2.54	0.974	0.380
537	1.01	1.00	SW-SL	8.45	0.364	7.37	25.2	4.79	1.98	3.00	3.36	0.291
541	1.01	2.56	WD	6.52	0.549	23.4	30.1	10.9	1.90	2.45	1.89	0.461
543	1.86	2.55	WD	5.22	0.468	16.1	51.1	11.4	1.66	2.42	6.28	0.415
544	1.86	4.04	WD	5.34	0.581	25.7	57.4	16.9	1.61	2.19	7.03	0.459
545	1.01	4.04	WD	5.29	0.656	37.2	34.0	16.3	1.84	2.21	2.11	0.540
547	0.415	7.67	WD	1.77	0.895	72.9	22.3	28.2	2.05	1.93	2.66	0.622

*) Note: $XX = \dfrac{\sqrt{3}\,\lambda_0}{D_G} \cdot \dfrac{u_G - u_L}{\Delta u_{\min}}$ in **Equation (4-6)**

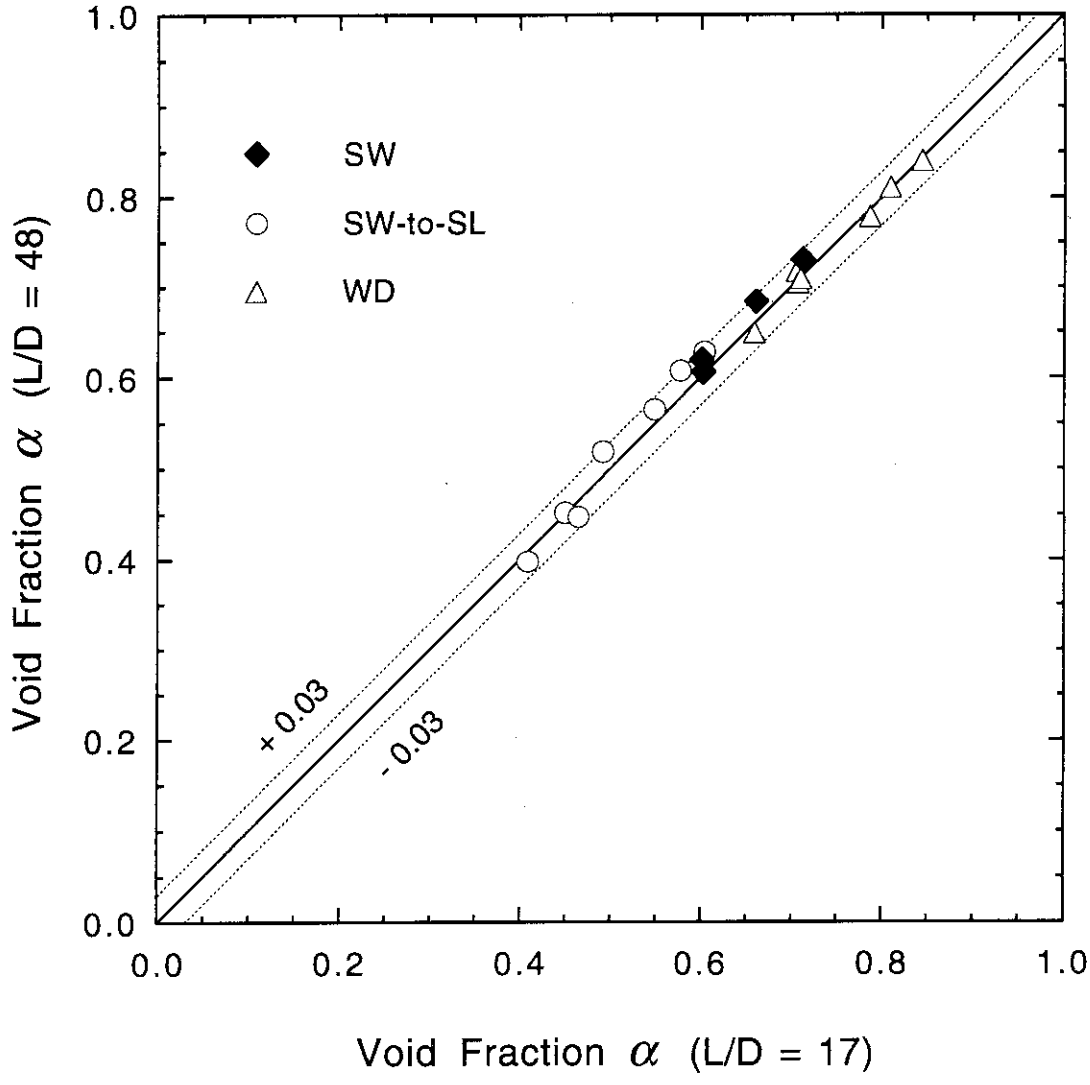

Fig. 2-4 Cross-Plot of Void Fractions at L/D = 17 and 48 (8-inch Pipe, 3 MPa)

In **Fig. 2-4**, time-averaged void fraction data at L/D = 17 and 48 are cross-plotted for the 8-inch pipe 3 MPa data. The liquid level decreased only slightly toward the downstream end with a level gradient ≤ 1/1033 between these two measurement stations. However, since the flow condition was supercritical and thus the liquid level gradient decreased along the test section, the flow at L/D = 48 was taken as a well-developed flow.

2. 4 Air/Water Two-Phase Flow Loop

2. 4. 1 Outline of Test Apparatus

The air/water two-phase flow loop schematically shown in **Fig. 2.5 (a)** was constructed in 1985. The objective of the facility was to obtain a calibration data of the drag-disc flow meters used in the LSTF with a detailed observation of two-phase flow behavior, being supplemental to the TPTF high-pressure steam/water two-phase flow experiments. Basic air/water two-phase flow experiments were performed first with a horizontal pipe test section with the inner diameter of 210 mm and the length of 30.5 m, made of transparent acrylic resin [Koizumi et al. 1989, Koizumi et al. 1990 a, Koizumi et al. 1990 b]. A large-height duct test section with the height of 0.7 m being equal to that of PWR hot leg was added to the loop later. The shape of the duct test section was decided to clearly observe the two-dimensional behavior of interfacial waves and their growth along the length of the test section. The width of the duct test section, however, was limited to 0.1 m, because of the maximum capacity of the large water pump of 500 m^3/h. In the present study, this duct test section was used to investigate the influence of the channel height on the slug flow transitions and the role of interfacial waves in the transition mechanisms.

2. 4. 2 Test Apparatus and Test Section

Figures 2-5 (a) and **(b)** show the test apparatus. Demineralized water and filtered air entered the test section through a 2.4-m^3 inlet tank, where the liquid level was stationary because of a large cross section of 0.8 m^2. At the test section inlet, a co-current stratified flow was formed. The test section discharged into a 10-m^3 exit tank which was open to atmosphere.

The horizontally leveled rectangular duct test section, 0.7-m-high, 0.1-m-wide and 28.3-m-long, was composed of 0.3, 1 and 2-m-long transparent acrylic resin segments and 2-m-long (opaque) stainless-steel segments. The transparent segments were used for visual observation and measurement of the local liquid level and pressure, and were arranged to best observe the wave growth into liquid slug.

2. 4. 3 Instrumentation

The inlet tank pressure and the flow rates and temperatures of air and water were measured in the air/water loop. Air and water flow rates were measured using orifice flow meter located upstream the flow control valves. Measurement uncertainty for the air and water flow rates was ±1.0% of the total range. Differential pressure cells used for the flow rate measurements were calibrated before initiating experiments. Air pressure upstream the flow control valve was kept constant at 0.30 MPa by adjusting a pressure regulator. Since the fluctuations in the test section static pressure was lower than 6.0 kPa, even at formation of a liquid slug, the inlet air flow rate change was no more than 1.0% of the total flow range. Similarly, inlet water flow rate was kept constant within 1.0% because of high pump head of 0.29 MPa and a large water inertia in the loop.

In the test section, the local water levels and gas phase pressures were

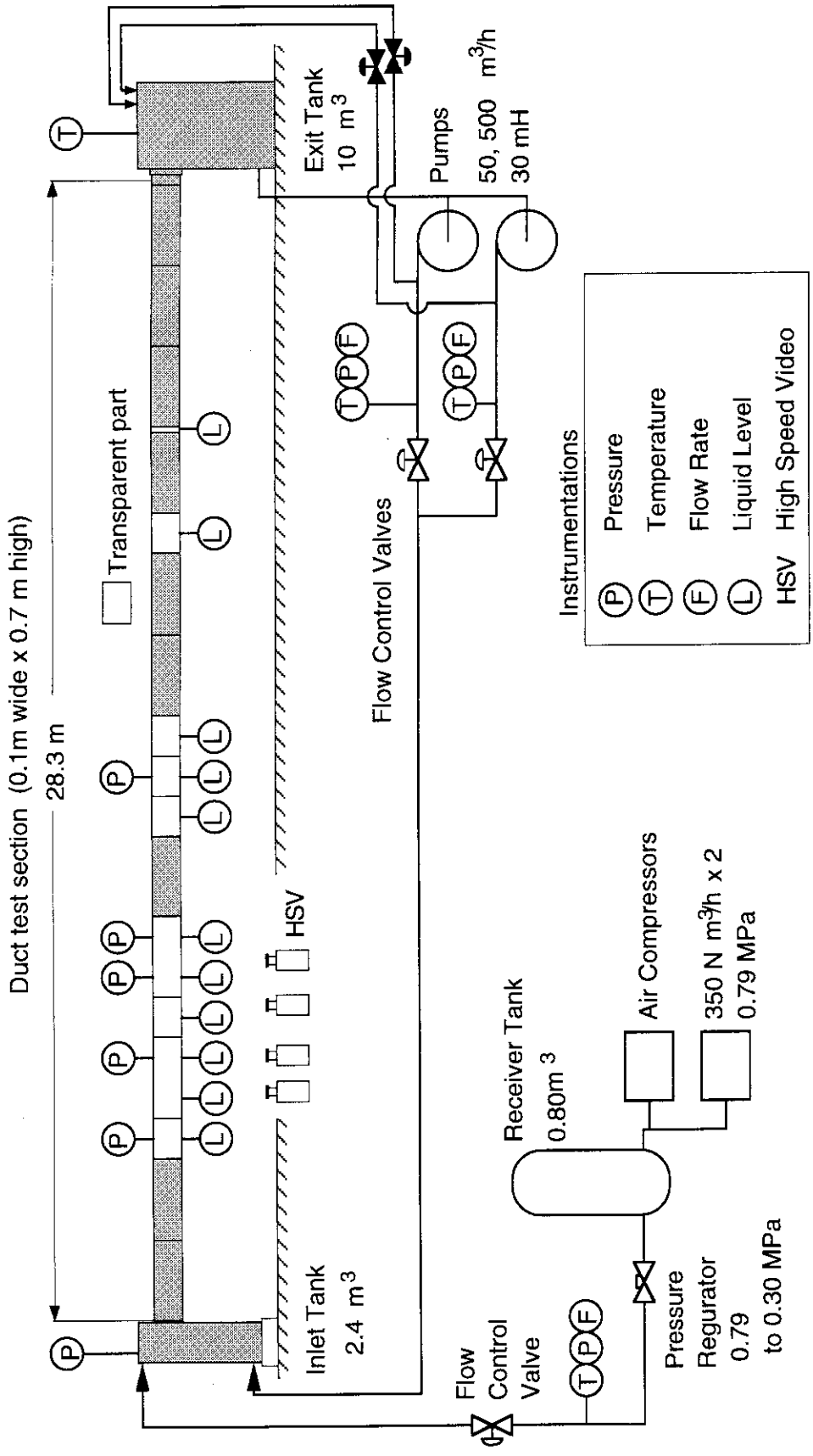

Fig. 2-5 Schematic of Test Facility
(a) Facility Overview

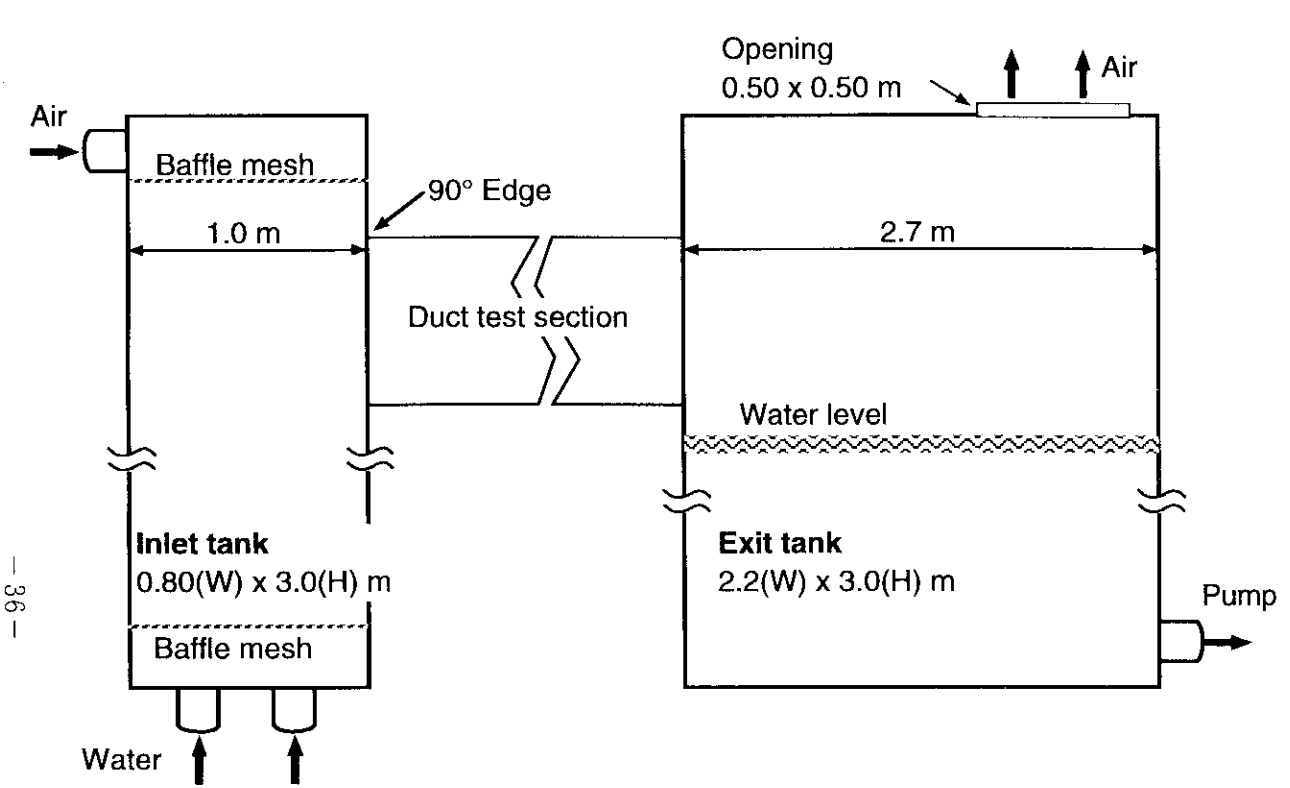

(b) Geometry of Test Section Inlet and Exit

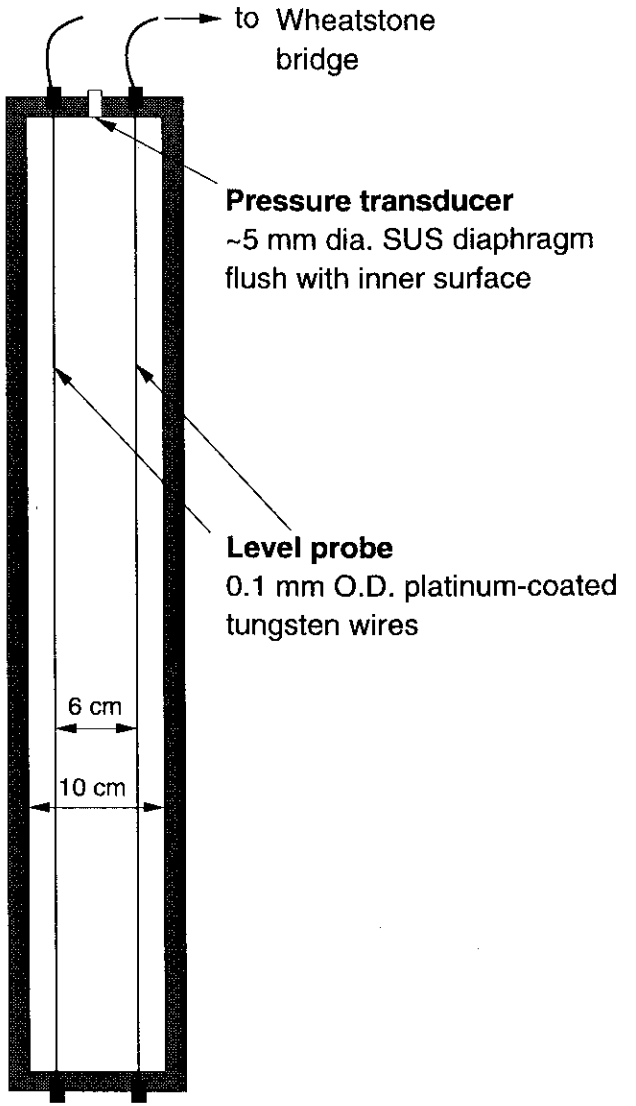

(c) Water Level and Pressure Measurement Setup

Fig. 2-5 Schematic of Test Facility

measured. Water levels were measured using probes composed of two wires (parallel, 60 mm apart) mounted vertically on a plane normal to the flow as shown in **Fig. 2-5 (c)**. The very thin wire was employed because a cocktail-like wake and/or small gas bubble entrainment was found to form in the wire downstream at water surface when a rather thick wire was used. The probe output was found to be very sensitive to pH and temperature of water. In a number of test runs, the sensitivity to the water pH was found to be weaker for platinum than for tungsten or Inconel X-750. Since platinum wire was cut only by several impacts from slug passage, a platinum-coated tungsten wire with outer diameter of 0.09 mm was specially manufactured. Water temperature was nearly constant but increased gradually at a rate of about 1 K/h because of a pump operation. Therefore, calibration data were obtained for every 1 or 2 experimental runs. The probe wire was connected to a Wheatstone bridge with four 120 Ω resistances. Eleven probes were installed along the duct test section as shown in **Fig. 2-5 (a)**.

Gas phase static pressures were measured on the channel top wall using strain-gauge type pressure transducers (Kyowa Electronic Instruments Inc. PGM-02KG). The transducer was mounted so that the thin stainless-steel diaphragm (about 5 mm dia.) was flush with the channel ceiling inner surface as shown in **Fig. 2-5 (c)**. The measuring pressure capacity and natural frequency of the transducer were 19.6 kPa and 2 kHz, respectively. The pressure transducers were factory-calibrated and installed at five locations, between the two wires of the water level measurement probe.

The signals from both the pressure transducers and the level probes were converted to voltage signals by the same type of dynamic strain amplifiers (Kyowa Electronic Instruments Inc. DPM-13A) with maximum response frequency of 10 kHz, which were electrically insulated each other. Then, care was

taken for the ground which was connected to a common terminal of the facility building.

The instrument signals were recorded at 200 Hz, typically for 5 minutes by the data logger (Iwatsu Inc. DA-8503), for every parameter when the flow in the test section reached a steady-state. The recorded data were copied to the floppy disks after several experimental runs, and were transferred to the JAERI main-frame computer (FACOM) for the data post-processing.

The two high-speed video cameras (nac Inc. HSV-200 and HSV-400) were employed further to record video pictures of the wave growth behavior in the transparent segments of the duct test section at a frame rate of 200 frame/s. The data recording of the high-speed video was performed simultaneously with the data logger. A typical picture taken by the high-speed video cameras will be presented in **Chapter 5**.

2. 5 Flows in Air/Water Two-Phase Flow Loop

The exit tank water level was always kept to be lower than the test section bottom. The time-averaged water level in the test section thus decreased gradually towards the downstream end where the water level was close to the critical depth.

Figure 2-6 summarizes flow regimes observed in the large-height duct test section in a Mandhane-type flow regime map. Appearances of the flow regimes, visually observed in the transparent segments, were the same as those sketched in **Fig. 1-1**. The SW-to-SL flow regime transition boundary was searched for following the same procedure taken in the TPTF experiments. The SW-to-SL transition boundary in the present experiment spanned a wide range in air flow

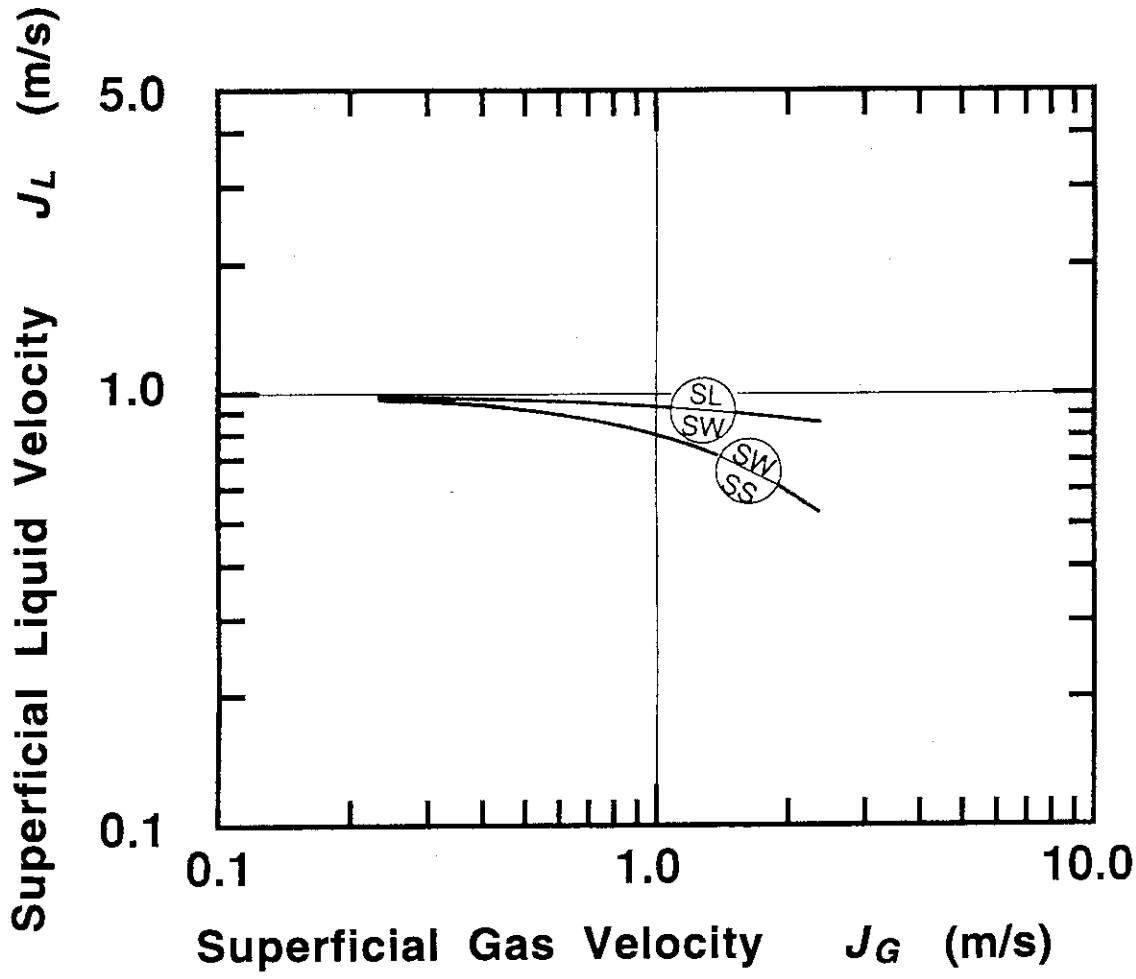

Fig. 2-6 Flow Regime Map for Large-Height Duct Experiments

rates up to the facility maximum capacity of 0.19 Nm^3/s, while it lay near a constant value of 0.06 m^3/s in water flow rate.

Stratified-wavy (SW) flows were always subcritical, making a contrast to the flow observed in the TPTF steam/water experiments. The WD flow regime was not observed because of limitation in the air and water flow rates. In the SL flow regime, however, the liquid entrainment was observed to occur at the crests of the large amplitude waves which grew into a liquid slug.

For this large-height duct experiments, a 90° angle rectangular-edged inlet was used as a standard boundary condition. In several experiments, however, the influence of the inlet geometry on the SW-to-SL flow regime transition was investigated by employing a bell-mouth type inlet nozzle at the test section inlet. When the inlet geometry was 90° angle rectangular-edged, the liquid level fell down once from the inlet tank and recovered gradually to the equilibrium level. On the liquid surface where the liquid level almost reached the equilibrium level, small interfacial waves were continuously generated because the liquid level, thus the air velocity, was highest in the test section. The interfacial waves sometimes grew very fast and block the gas-phase channel there. However, no liquid slugs evolved from such temporarily-grown waves, because these waves were readily shattered by the high-velocity air flow. When the bell-mouth type inlet nozzle was used, the liquid level smoothly decreased from the inlet tank to the equilibrium level in the test section. The air velocity was thus largest in the inlet nozzle where small waves were generated. In spite of these differences in the flow conditions, difference in the flow rates for the SW-to-SL flow regime transition was negligible between these cases with and without the smooth inlet nozzle.

3. Influences of Channel Height and System Pressure on Slugging

3.1 Introduction

The stratified-wavy to slug (SW-to-SL) flow regime transition for horizontal steam/water two-phase flow is under influences of channel height (pipe diameter) and system pressure. The influences of these parameters on the transition were studied experimentally. The TPTF steam/water two-phase flow experiments were conducted to investigate the influences of both pipe diameter and system pressure, changing the system pressure up to 12 MPa for the 8- and 4-inch pipe horizontal test sections with 180 and 87 mm i.d., respectively. The air/water two-phase flow loop experiments were performed to investigate the influences of the channel height with a high (0.7 m) rectangular duct test section.

This chapter summarizes the experimental results regarding the influences of the channel height and system pressure on the SW-to-SL flow regime transition, and discusses the mechanisms of slugging.

3.2 Influence of Channel Height

3.2.1 Air/Water Slugging Experiments in Large-Height Duct

Figure 3-1 shows typical liquid level signals measured at eight stations along the duct test section, indicating evolution of an interfacial wave into a liquid slug (slugging) between liquid level sensors Nos. 3 and 6. This experiment was conducted with air and water superficial velocities, J_G and J_L, of 0.89 and 1.49 m/s, respectively. The similar data were obtained in ten experimental runs performed with J_G between 1.12 and 2.18 m/s along the SW-to-SL flow regime transition boundary shown in the flow regime map (**Fig. 2-6**).

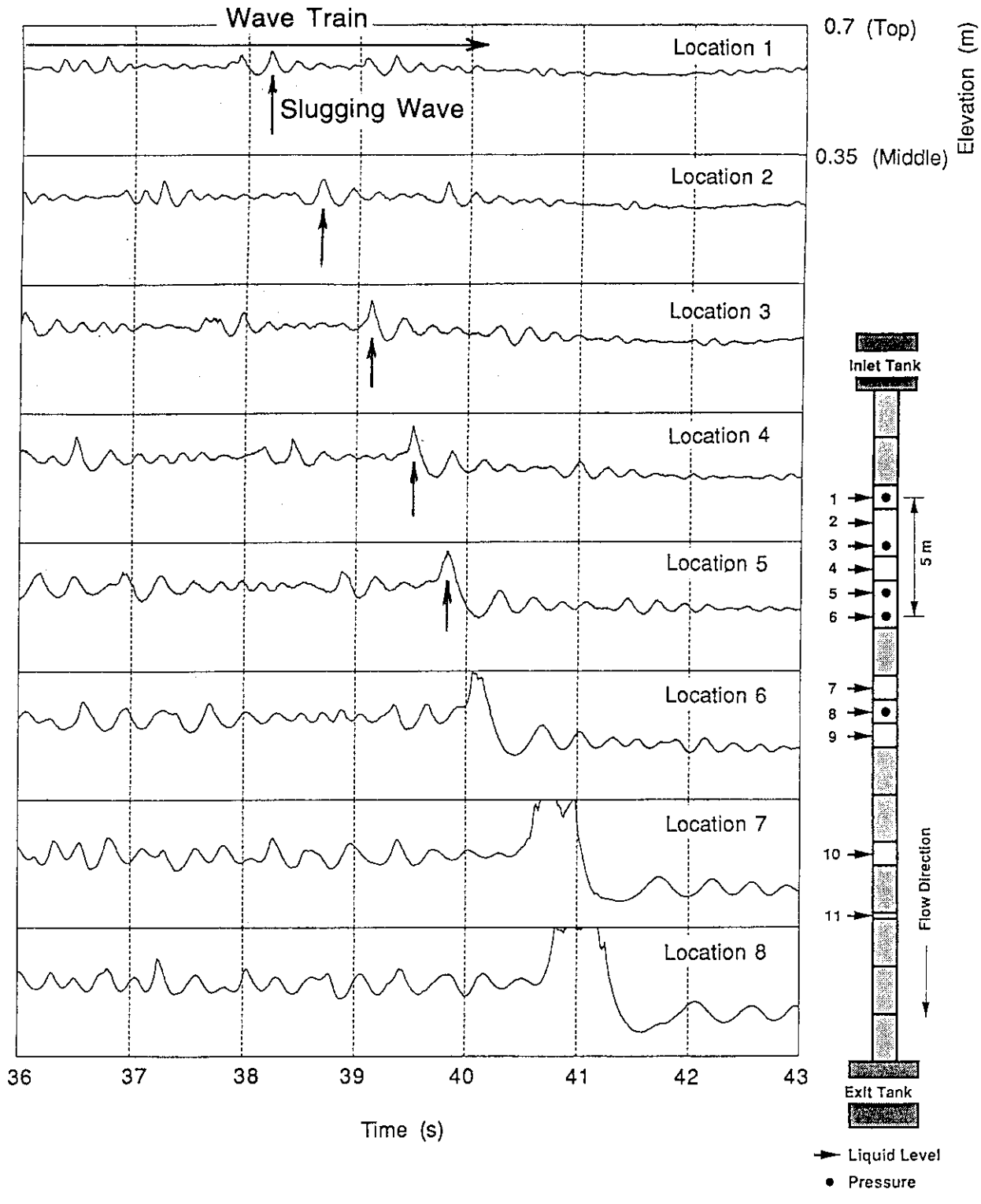

Fig. 3-1 Typical Liquid Level Transient at Slugging in Large-Height Duct (J_G = 1.49 m/s, J_L = 0.89 m/s)

When the liquid flow rate was at or slightly larger than that for the SW-to-SL flow regime transition boundary, slugging was usually preceded by formation of trains of two-dimensional interfacial waves, as shown in **Fig. 3-1**. These wave trains appeared somewhat periodically. All the waves in wave trains grew as they traveled along the channel. Size of these waves was rather random, and one of the waves that appeared occasionally grew faster than the other waves into a liquid slug. Such waves, termed "slugging waves" hereafter, had an amplitude larger than that of the other waves soon after the formation of a wave train as shown in **Fig. 3-1**. In the SW flow regime also, such relatively-large waves appeared, though infrequently, and they failed to grow enough to block the whole channel. Anyhow, slugging is resulted from the growth of interfacial (wind) waves bearing random process by nature.

The slugging in the present large-height duct experiments, in particular at higher air flow rates, was characterized by much slower growth of waves along the channel than in smaller scale experiments. It took about one second for a slugging wave to grow and block the air flow path completely. The location of slug formation depended on the gas flow rate at conditions close to the transition boundary, and shifted downstream largely as the gas flow rate was increased.

After a liquid slug had been formed, the complete blockage of the gas flow channel caused an increase in the gas phase pressure and a depression of the liquid level upstream of the slug. The axial pressure difference across the slug accelerated the slug. Generally, the liquid slug was aerated and the upstream slope of it looked like a "Benjamin bubble" [Benjamin 1968] followed by a wake-like large amplitude wave. As the liquid level decreased further, the liquid surface became smooth without interfacial waves, forming a stratified-smooth flow shown in **Fig. 1-1**. When a liquid slug exited the duct test section, the air velocity through the duct increased temporarily, and the gas pressure decreased to the atmospheric pressure.

From this time on, the liquid level recovered gradually to the equilibrium level, and wave trains appeared again on the water surface.

When the liquid flow rate was increased in the SL flow regime while keeping the air flow rate unchanged, the time for the liquid level to recover to the equilibrium level decreased. Then, the location of slug formation shifted towards the duct inlet where the liquid level recovered first. When the liquid flow rate was large enough to cause slugging successively, a large-amplitude wake-like wave following the slug sometimes grew into another slug. Thus, more than two liquid slugs became to coexist at higher liquid flow rates, while only one slug existed in the test section at conditions close to the SW-to-SL flow regime boundary.

At higher air flow rates, the length of liquid slugs increased as it traveled along the channel. This occurred because the velocity increased for slugs that scooped up water flowing rather slowly ahead of the slug. At lower air flow rates, on the other hand, top of slugs detached from the duct ceiling before exiting the test section, since the equilibrium liquid level gradually decreased towards the test section exit as noted in **Chapter 2**. The detached liquid slug looked like a surge [Chow 1959].

3. 2. 2 Analysis of Air/Water Duct Experiments

The data obtained from the present duct experiments are compared with the results of the other investigators; first in a Mandhane-type flow regime map presented in terms of superficial velocities J_k, and next in terms of non-dimensional gas-liquid relative velocity J_{GL}^* and time-averaged void fraction α.

Figure 3-2 compares the flow regime map obtained from the present duct experiments with those of Simpson et al. (1981) and Mandhane et al. (1974). These investigators conducted air/water experiments in horizontal pipes with diameters

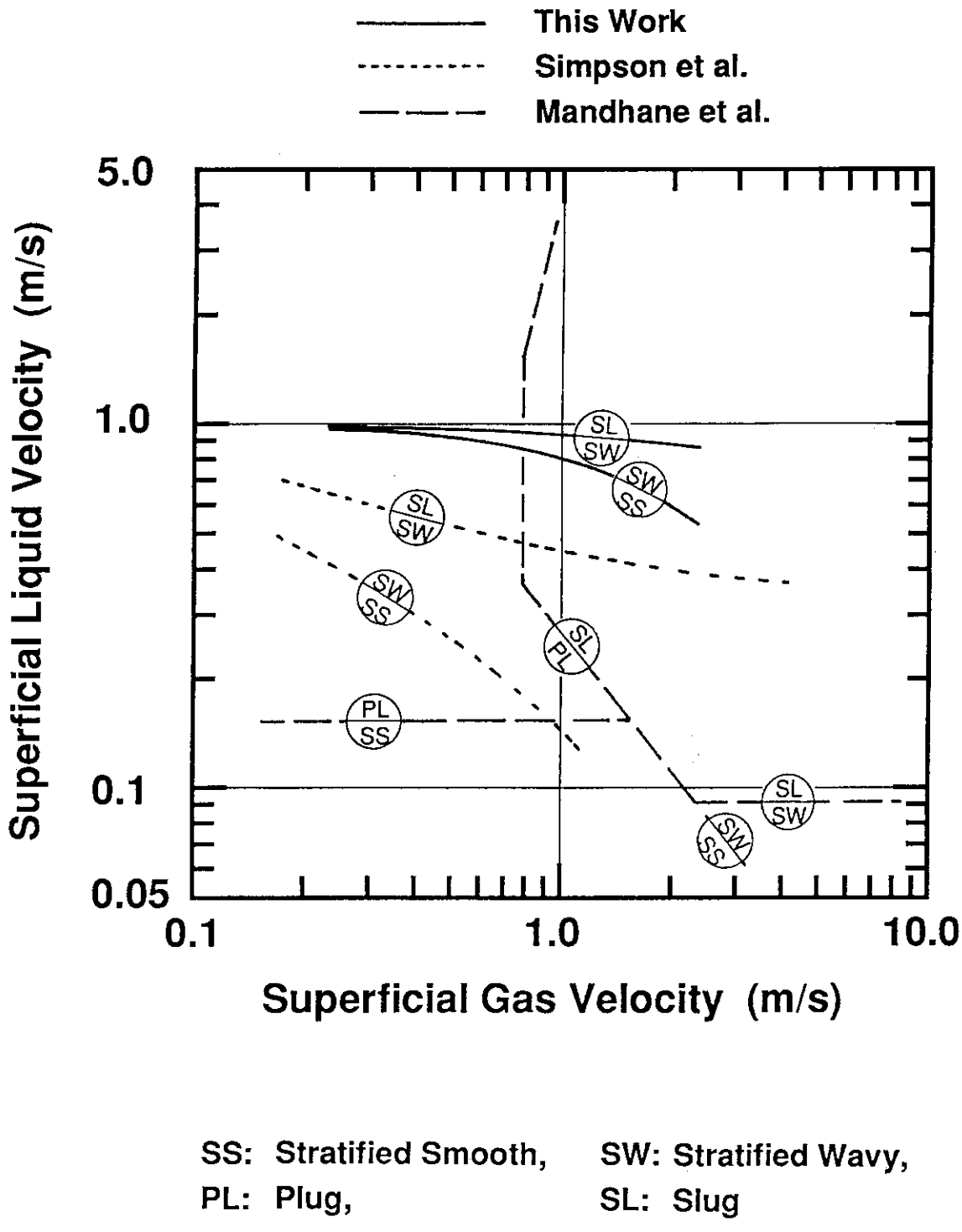

Fig. 3-2 Comparison of Flow Regime Map of Large-Height Duct with Those of Air-Water Experiments using Pipes

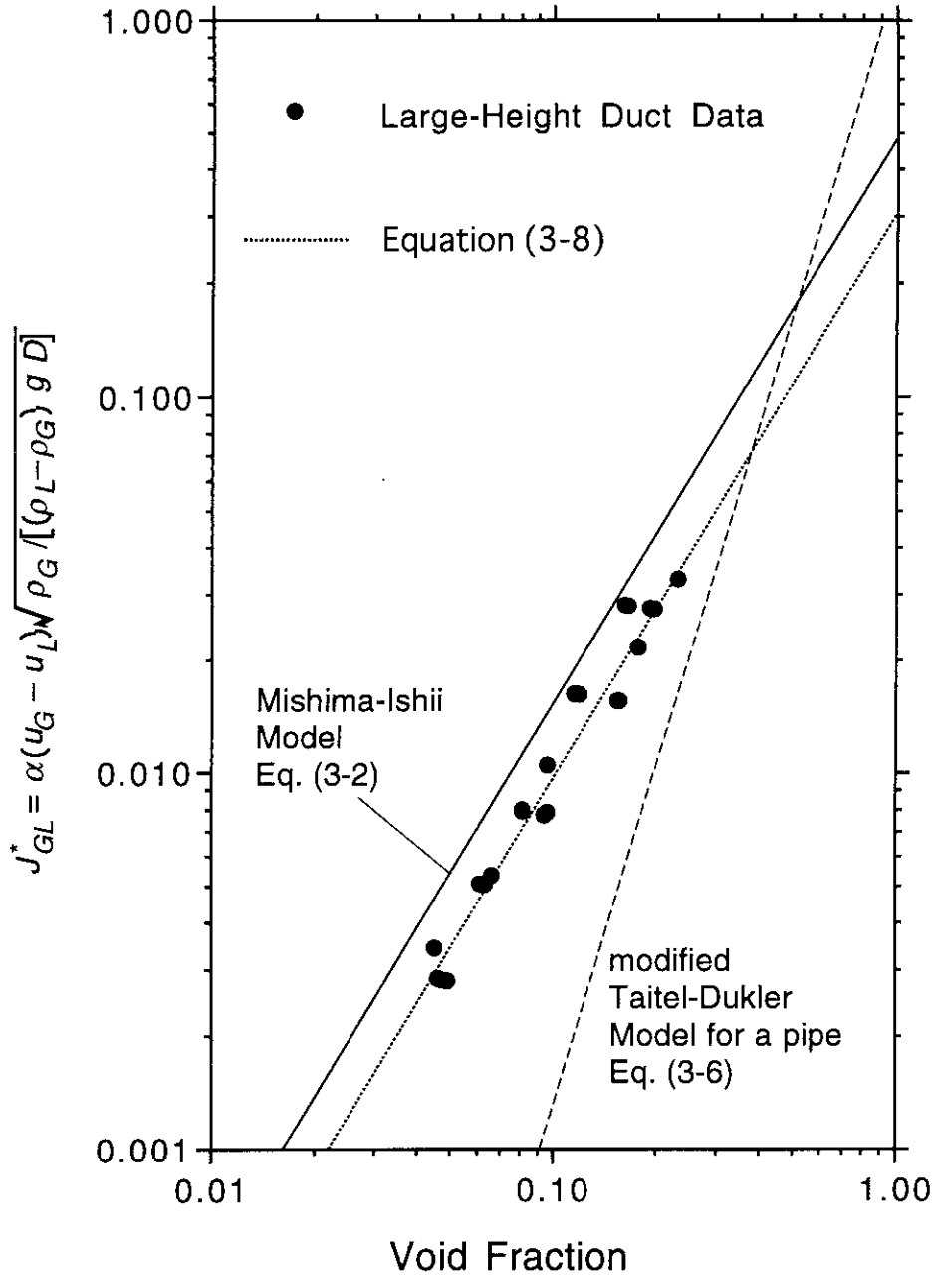

Fig. 3-3 Comparison of Large-Height Duct Data with Models

of 0.2 and about 0.05 m, respectively. In pipes, the decrease in gas-phase flow area by amplitudes of interfacial waves is more significant than in ducts. Slugging in pipes thus tends to occur at lower gas-liquid relative velocity compared with duct cases. This comparison in **Fig. 3-2**, however, clearly shows that the superficial liquid velocity J_L , to occur the transition at the same superficial gas velocity J_G , increases with the channel height (pipe vertical diameter).

Figure 3-3 compares the present data with the models and correlations in terms of time-averaged void fraction α and non-dimensional gas-liquid relative velocity J^*_{GL} ,

$$J^*_{GL} = \alpha(u_G - u_L)\sqrt{\frac{\rho_G}{(\rho_L - \rho_G)\,g\,D}} \quad , \tag{3-1}$$

where D is the channel height for a rectangular duct and the diameter for a pipe. The experimental data are the local time-averaged void fraction α where, but just before, the liquid slug was formed. The local averaged gas and liquid velocities, u_G and u_L, are based on this α.

The Mishima-Ishii model [Mishima and Ishii 1980] is given by

$$u_G - u_L \geq 0.478\sqrt{\frac{(\rho_L - \rho_G)\,g\,h_G}{\rho_G}} \tag{3-2}$$

for flows with two-dimensional interfacial waves that typically appear in a rectangular duct. The form of this model is identical to that of **Equation (1-1)**, but with the coefficient C = 0.478. This value of 0.487 is close to 0.5 of the empirical correlation by Wallis and Dobson (1973)

$$u_G - u_L \geq 0.5\sqrt{\frac{(\rho_L - \rho_G)\,g\,h_G}{\rho_G}} \quad . \tag{3-3}$$

This correlation was obtained from the co- and counter-current air/water flow experiments in a rectangular duct with the maximum height of 305 mm.

Compared also in **Fig. 3-3** is the Taitel and Dukler model (1976) for pipe flows

$$u_G - u_L \geq \left(1 - \frac{h_L}{D}\right)\sqrt{\frac{\left(\rho_L - \rho_G\right) g \cos\theta A_G}{\rho_G dA_L / dh_L}} \quad . \tag{3-4}$$

in the form as modified by Anoda et al. (1989) to take an influence of liquid velocity u_L into account. The original form of this model is

$$u_G \geq \left(1 - \frac{h_L}{D}\right)\sqrt{\frac{\left(\rho_L - \rho_G\right) g \cos\theta A_G}{\rho_G dA_L / dh_L}} \quad . \tag{3-5}$$

For flows in a horizontal rectangular duct, the modified Taitel-Dukler model can be presented as

$$u_G - u_L \geq \left(1 - \frac{h_L}{D}\right)\sqrt{\frac{\left(\rho_L - \rho_G\right) g \, h_G}{\rho_G}} \quad . \tag{3-6}$$

The form of this equation is also identical to that of **Equation (1-1)**, but with the coefficient $C = \left(1 - h_L / D\right)$, and can be approximated to be

$$J_{GL}^{*} \geq \alpha^{5/2} . \tag{3-7}$$

The present data lay between these two models as shown in **Fig. 3-3**, but with systematic deviations from the Taitel-Dukler model, and can be correlated by

$$u_G - u_L \geq 0.3\sqrt{\frac{\left(\rho_L - \rho_G\right) g \, h_G}{\rho_G}} \quad , \tag{3-8}$$

as also shown in **Fig. 3-3**. The form of this new correlation is also identical to that of **Equation (1-1)**, though the coefficient C = 0.3 is smaller than that of the Mishima-Ishii model or the Wallis-Dobson model. This means that the SW-to-SL flow regime transition in the present large-height duct experiments occurred at systematically lower normalized liquid level than in the lower-height ducts.

However, it appears that the constant value for C represents well slugging in rectangular ducts where interfacial waves grow two-dimensionally.

3. 2. 3 Analysis of TPTF Steam/Water Experiments

The results from the TPTF 8- and 4-inch pipe experiments performed at 3 MPa are compared also in two different ways to study the influence of pipe diameter on transition conditions. The TPTF transition boundary data is first compared in Mandhane-type flow regime maps in **Fig. 3-4**, where non-dimensional density-modified Froude numbers [Wallis 1969]

$$J_k^* = J_k \sqrt{\rho_k / \left[\left(\rho_L - \rho_G \right) g D \right]} \tag{3-9}$$

are used in place of dimensional superficial velocities. The influences of pipe diameter are thus presented in terms of $\sqrt{D}$ when pressure is the same, and appear separately on liquid and gas flow rates.

The values of J_L^* at the transition for 4-inch pipe were almost equal to those for 8-inch pipe, indicating that the influence of the pipe diameter on the liquid flow rate at the transition is well represented by the term $\sqrt{D}$. This result may support a scaling method to simulate flow regime transitions in horizontal piping using Froude number [Zuber 1980]. In the large scale test facility (LSTF) in JAERI, for example, a parameter $L/\sqrt{D}$ is used to scale the size of the horizontal legs to simulate integral thermal-hydraulic responses of the reference PWR during LOCAs and transients [The ROSA-IV Group 1990]. In the parameter $L/\sqrt{D}$, the Froude number $u_L/\sqrt{D}$ to simulate flow regime transitions is used being multiplied by a parameter L/u_L to conserve the time for flow that goes through the horizontal legs.

The TPTF 4- and 8-inch pipe results at pressure of 3 MPa are compared in **Fig. 3-5** in terms of J_{GL}^* and α. The modified Taitel-Dukler (T-D) model

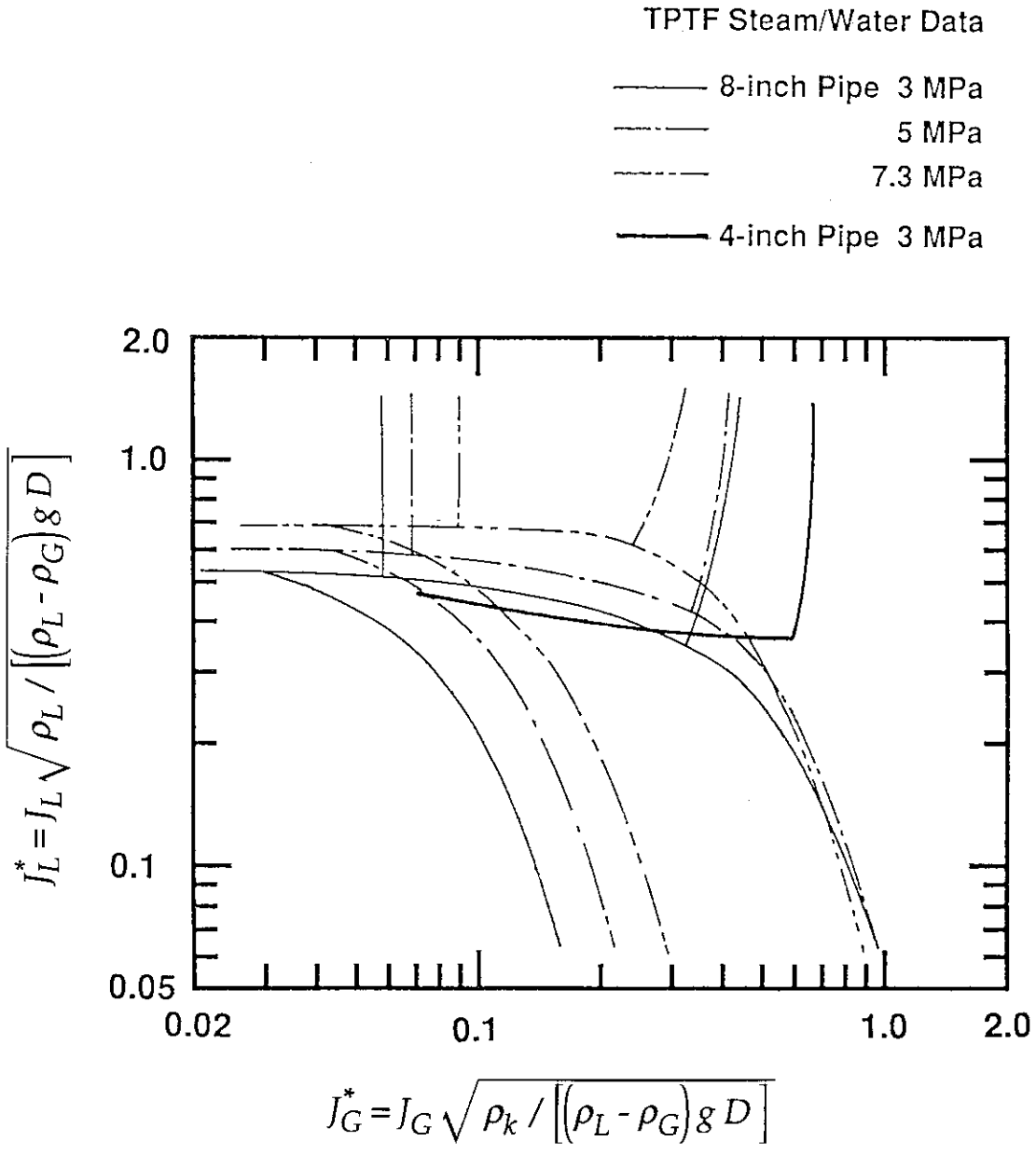

Fig. 3-4 Comparison of TPTF Flow Regime Maps in terms of Density-modified Froude Numbers (4 and 8-inch pipes, 3 to 7.3 MPa)

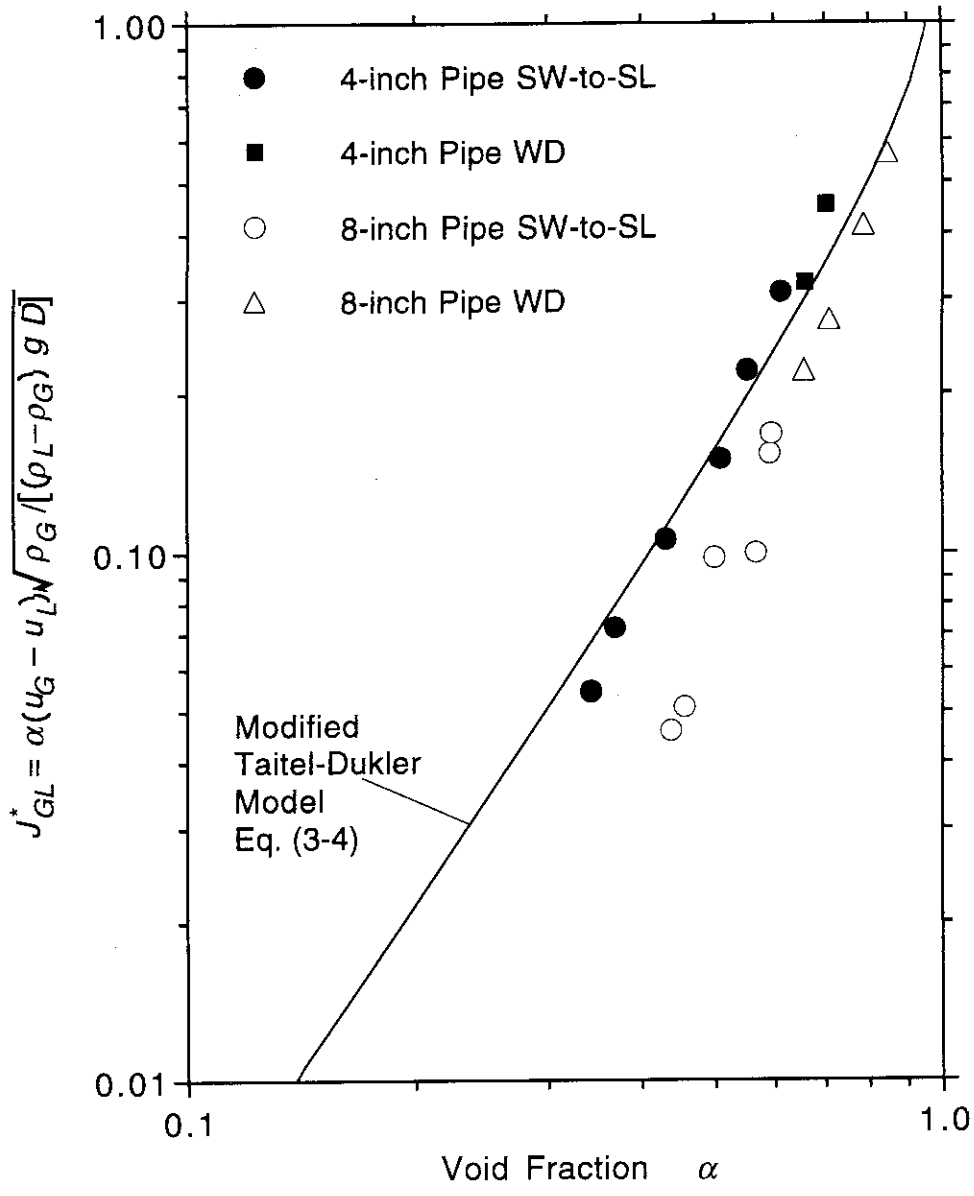

Fig. 3-5 Comparison of TPTF Data with Modified Taitel Dukler Model (4 and 8-inch pipe, 3 MPa data)

(**Equation (3-4)**) is also compared in **Fig. 3-5**. The 4-inch pipe data agreed well with the modified T-D model. However, the 8-inch pipe data indicated a systematic deviation from the T-D model towards higher void fractions. This result indicates that the SW-to-SL flow regime transition in a larger-diameter pipe takes place at lower normalized liquid levels, for a given value of J_{GL}^{*} , than in a smaller-diameter pipe. The same tendency has been found for the large-height duct experiments in **Section 3. 2. 2**. This result suggests that the influence of the channel height cannot be fully accounted for only by non-dimensionalizing the velocities using a parameter $\sqrt{D}$ of the Froude number. Further discussion concerning this point will be made in **Section 3. 4**.

3. 3 Influence of System Pressure

Influence of system pressure on the flow regime transition to slug flow regime is investigated based on the TPTF steam/water two-phase flow data for the 8-inch pipe test section at pressures ranging from 3 to 12 MPa. The fluid physical properties such as densities ρ_k, viscosities μ_k and liquid surface tension T are all in terms of system pressure. These properties have certain influences on the flow regime transition. The influence of densities, for example, has already appeared in **Section 3. 2**.

Flow regime maps obtained for different pressures are compared in **Fig. 3-4** in terms of density-modified Froude numbers J_k^{*} . This comparison shows that the value of J_L^{*} at the SW-to-SL flow regime transition increased with system pressure. Furthermore, it shows that both the SW-to-WD and SL-to-WD transition boundaries moved towards lower value of J_G^{*} as the pressure was raised, making the region of slug flow regime small in the flow regime map. The slug flow regime finally disappeared when the pressure was raised to about 8.6 MPa in the present TPTF experiments. This phenomena was found similarly in the 4-inch diameter pipe experiments, and will be discussed in **Chapter 6**.

To study further the influence of system pressure on the SW-to-SL flow regime transition, the TPTF results are compared with the modified T-D model (**Equation (3-4)**) in **Fig. 3-6**. The modified model predicted well the 8-inch pipe, 5 and 7.3 MPa data. However, the 8-inch 3 MPa data did not agree well with this model as has been shown in **Fig. 3-5**.

In **Fig. 3-7**, the same TPTF data are compared with the original T-D model, using J_G^* as a ordinate parameter. Note that the data value of J_G^* was larger than that of J_{GL}^* , while both the original and modified T-D models draw the same curve in terms of α. The original model predicted the 8-inch 3 MPa data better than the modified model. However, as system pressure was raised, the deviation of the data from the model became significant for the original model.

The systematic deviation of the data from the original T-D model obviously resulted from neglect of the influence of liquid flow rate. Note that the superficial liquid velocity for the transition boundary increased with pressure as shown in **Fig. 3-4**. A good agreement of the data with the modified T-D model indicates that the increase in the transitional gas-liquid relative velocity with system pressure is compensated well by decrease in the term $\sqrt{\rho_G / (\rho_L - \rho_G)}$ of J_{GL}^* except for the 8-inch 3 MPa case shown in **Figs. 3-5** and **3-6**. Therefore, it appears that the deviation of the 8-inch 3 MPa data from the modified T-D model is peculiar to relatively-low pressure flows in large-diameter pipes.

Figure 3-6 shows further that the empirical correlations for air/water two-phase flow experiments by Koizumi et al. (1990 a) using a 0.21-m-i.d., 30.5-m-long horizontal pipe,

$$J_{GL}^* = 0.5\,\alpha^{2.5}\,, \tag{3-10}$$

and Hori et al. (1985) using a 0.2-m-i.d., 8.2-m-long horizontal pipe,

$$J_{GL}^* = 0.75\,\alpha^{3}\,, \tag{3-11}$$

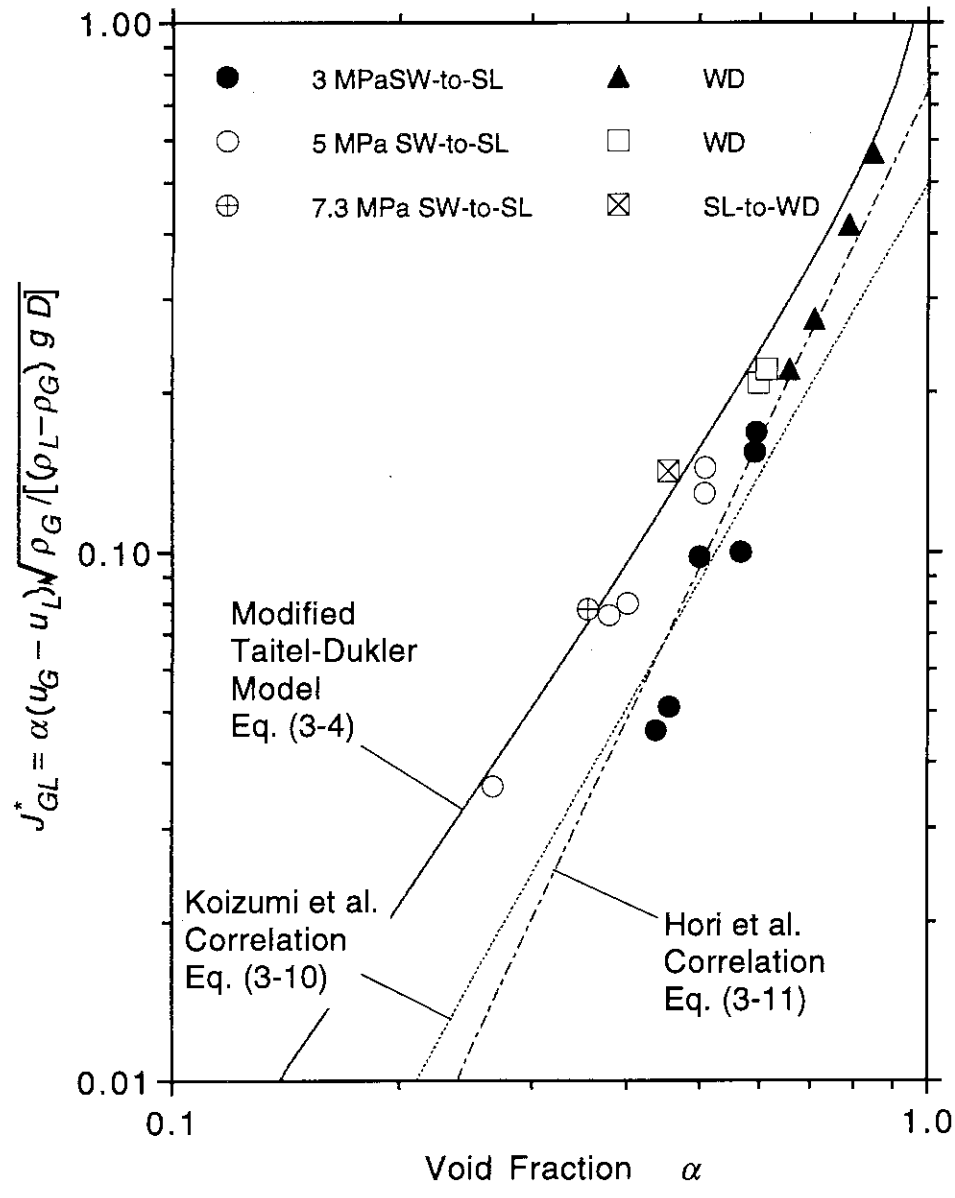

Fig. 3-6 Comparison of TPTF Data with Modified Taitel-Dukler Model and Empirical Correlations by Koizumi et al. and Hori et al. (8-inch pipe, 3, 5 and 7.3 MPa data)

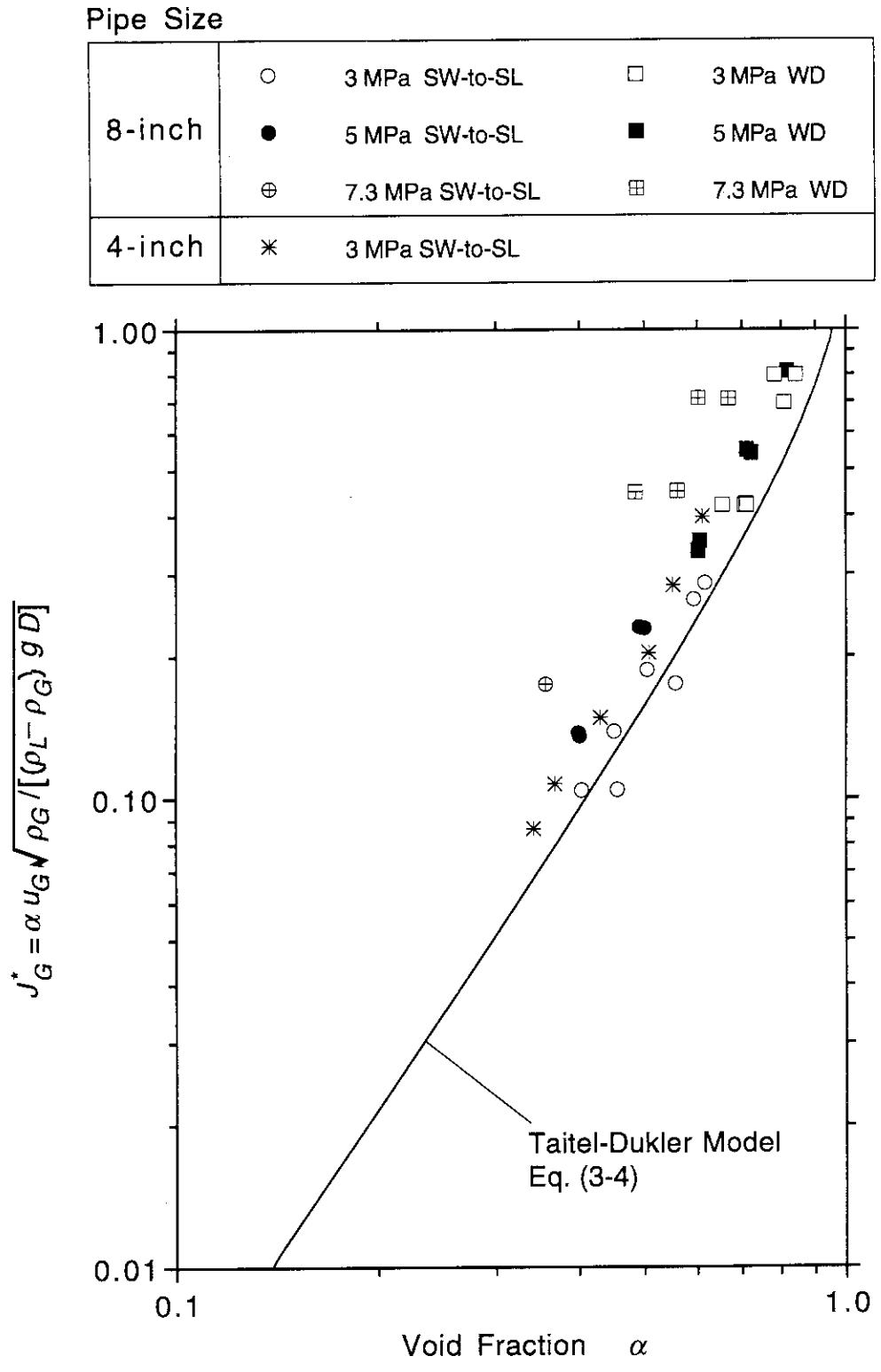

Fig. 3-7 Comparison of TPTF Data with Original Taitel-Dukler Model (4 and 8-inch pipe, 3, 5 and 7.3 MPa data)

agree well with the 8-inch 3 MPa data. This agreement is another evidence that the influences of system pressure can be represented by non-dimensionalizing the velocity using the densities.

3.4 Influence of Channel Height on Interfacial Wave Height

Many investigators have considered that the wave height of interfacial waves is one of the key parameters that influence the transitional gas-liquid relative velocity. However, the influences of the wave height have not been studied systematically, partly because it is difficult to experimentally define the critical instance when the wave starts to grow into a liquid slug. The dependence of wave height on various parameters including the channel height has not been studied systematically either. This section discusses the dependence of the wave height on the channel height and the role of the wave height on the mechanism of slugging by referring to the method used to prepare the Taitel-Dukler model.

Taitel and Dukler (1976) obtained the coefficient C of **Equation (1-1)** based on a simple assumption that static force balance on the wave crest describes a trigger point for the wave growth into a slug. Combination of a gas phase one-dimensional Bernoulli pressure equation, and a balance equation between lift force by the Bernoulli pressure drop at the wave crest and the restoration force by gravity acceleration due to the wave height give

$$C = \sqrt{2 / X(X+1)} \tag{3-12}$$

where $X = h_G / h_G'$, with h_G' and h_G being the gas channel height at the wave crest and trough, respectively. Wave height is then given by $h_G - h_G'$.

The value of the obtained coefficient C as **Equation (3-12)** depends on the expected critical wave height with which slugging starts. For an infinitesimally small wave height, for example, X -> 1.0, and C -> 1.0. Taitel and Dukler replaced X

with $X = A_G / A_G^{'}$ for pipe flows, and obtained a modified form of **Equation (1-1)** assuming small wave heights as,

$$u_G - u_L \geq C \sqrt{\frac{(\rho_L - \rho_G) g \cos\theta A_G}{\rho_G dA_L / dh_L}} \quad . \tag{3-13}$$

Taitel and Dukler assumed further that C is given approximately by

$$C = \left(1 - \frac{h_L}{D}\right), \tag{3-14}$$

based on their experimental observation [Taitel and Dukler 1977]. This defines the wave height ratio X in terms of the liquid level h_L, with no dependence on the channel height.

For rectangular duct flows, a constant value of 0.5 for C gives the Wallis-Dobson model (**Equation (3-3)**), and 0.3 to the fit to the present large-height duct data (**Equation (3-8)**). Difference in these values for C for different height channels implies, however, that the wave height ratio X depends on the channel height.

Therefore, normalized wave heights $\left(h_G - h_G^{'}\right)/D$ were calculated, in terms of liquid level at the wave trough, by using **Equations (3-12)** and **(3-14)** for pipe flows, and **Equation (3-12)** and constant values of C for duct flows. A relation of gas phase cross-section in a pipe in terms of liquid level, shown below, was used.

$$A_G = \frac{D^2}{4}\left(\cos^{-1} Y - Y\sqrt{1 - Y^2}\right) \ , \tag{3-15}$$

where $Y = \left(\frac{2h_L}{D} - 1\right)$. Obtained results are compared in **Fig. 3-8**. This figure shows that the dependence of C on the channel height can be explained consistently when the normalized critical wave height at a given normalized liquid level increases with the channel height.

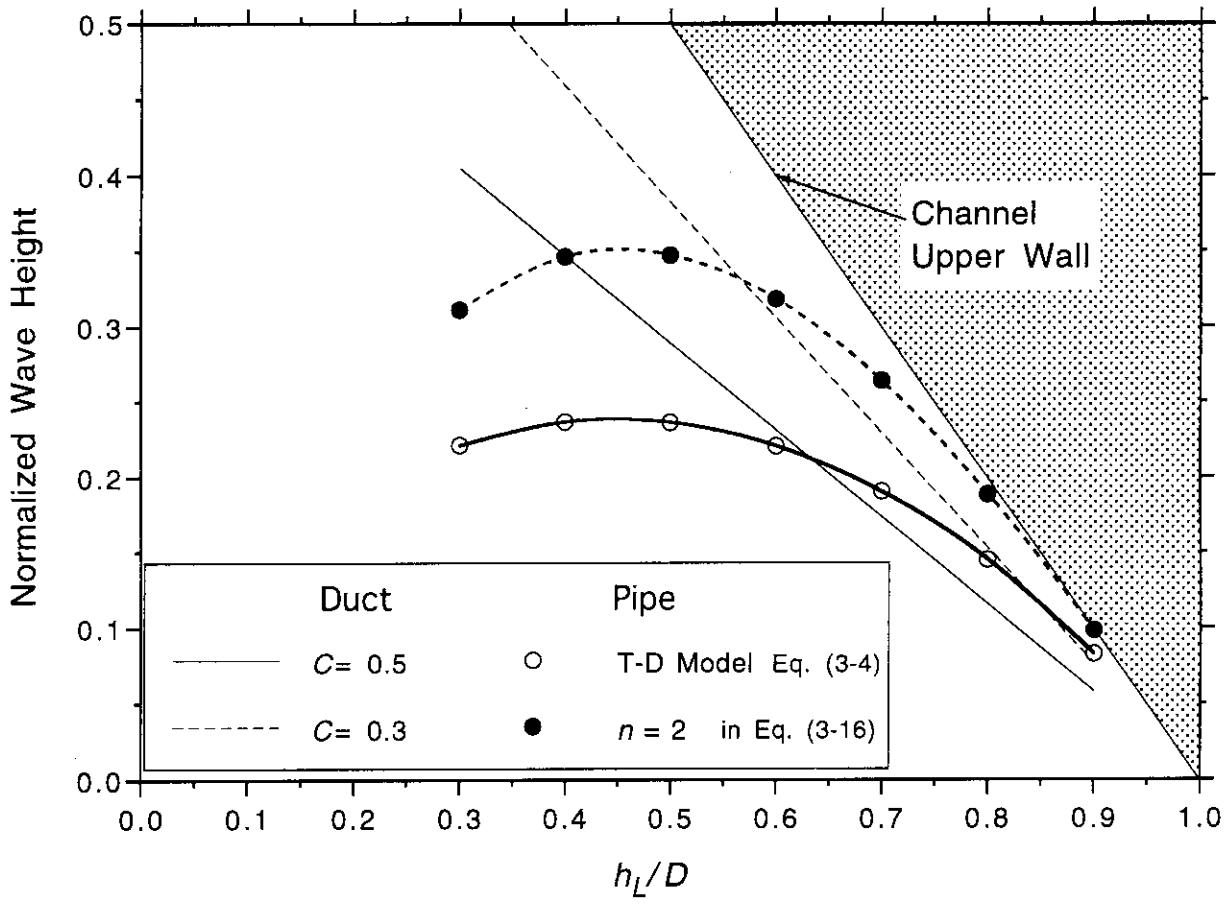

Fig. 3-8 Normalized Wave Height for Several Coefficients C of Equation (1-1)

The T-D model has shown a good predictability for small-diameter pipe flows as well as for high-pressure steam-water flows. However, the predictability of the modified T-D model for large-diameter pipe flows under relatively low system pressures was poor as has been shown in **Fig. 3-6**. However, the predictability of the modified T-D model can be greatly improved when the value of the original coefficient $\left(1 - \frac{h_L}{D}\right)$ for **Equation (3-13)** is decreased, for example, by replacing it with $\left(1 - \frac{h_L}{D}\right)^n$ as

$$u_G - u_L \geq \left(1 - \frac{h_L}{D}\right)^n \sqrt{\frac{\left(\rho_L - \rho_G\right) g \cos\theta A_G}{\rho_G dA_L / dh_L}} \quad . \tag{3-16}$$

This correlation predicts the 8-inch 3 MPa data very well when n = 2 is applied as shown in **Fig. 3-9**. The wave height in terms of the liquid level for this value of n is compared in **Fig. 3-8**. The new correlation **(3-16)** with n = 2 agrees well with the empirical correlations by Koizumi et al. (1990 a) and Hori et al. (1985) for air/water two-phase flows as shown in **Fig. 3-9**.

The influence of wave height has been discussed in this section as one of the critical parameters that control the SW-to-SL flow regime transition. However, interfacial gas-liquid interactions during the wave growth include complicated process and require further clarification. For example, the contraction of gas phase channel would cause kinematic energy loss, when the wave crest of high-height waves comes close to the channel upper wall, due to separation of the gas flow from the liquid surface. In this case, it is difficult to predict the entire gas phase pressure profile along the length of the wave using the simple Bernoulli pressure equation. The role of such parameters as gas-phase pressure and velocity and wave height are thus further investigated in **Chapter 5**.

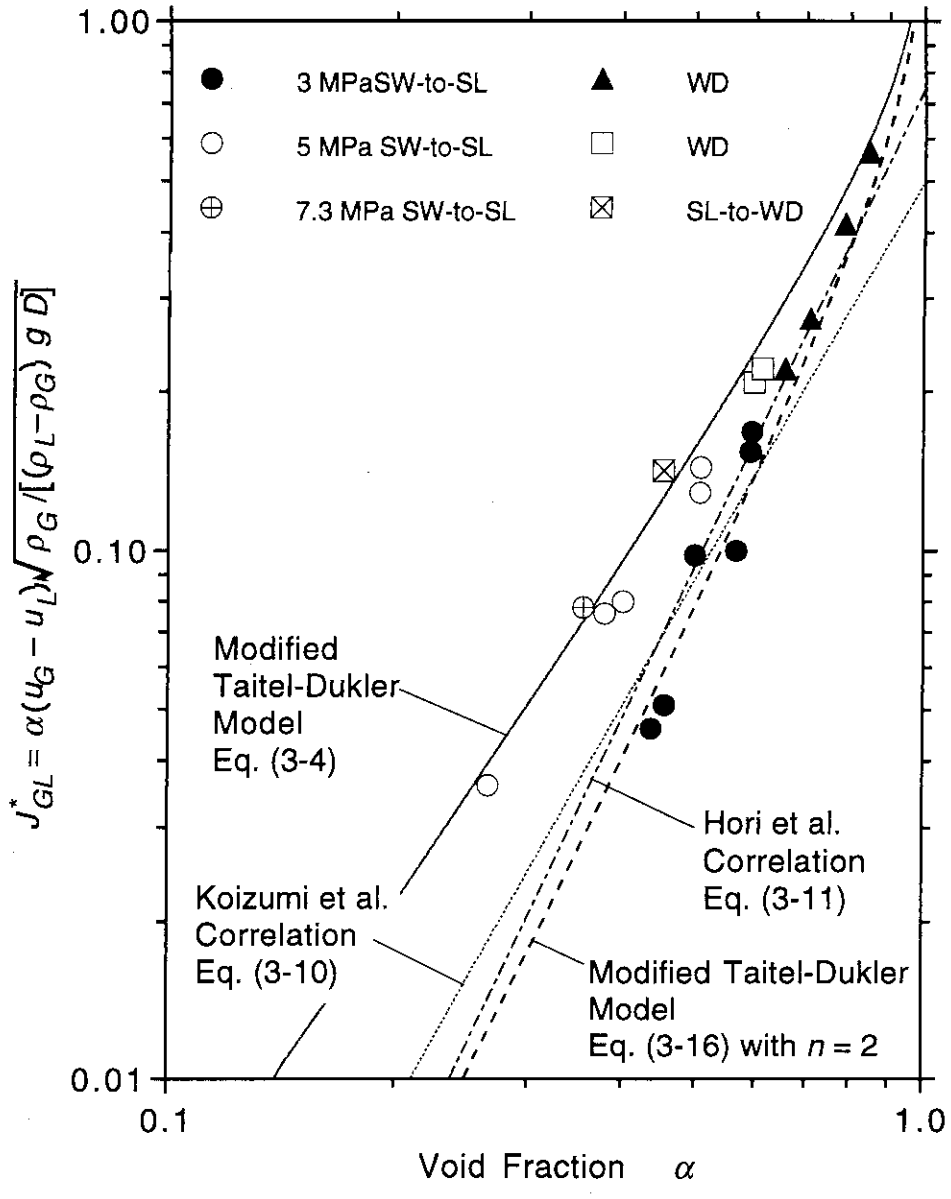

Fig. 3-9 Comparison of TPTF Data with
Modified Taitel-Dukler Model with New Coefficient and
Empirical Correlations by Koizumi et al. and Hori et al.
(8-inch pipe, 3, 5 and 7.3 MPa data)

3. 5 Conclusions

The dependence of the SW-to-SL flow regime transition on channel height (i.e., pipe diameter) and system pressure was investigated experimentally. Steam/water experiments were conducted in two (180 and 87 mm i.d.) horizontal pipe test sections of the TPTF for pressures up to 12 MPa, and air/water experiments were conducted in a large-height (0.7 m) duct test section under atmospheric pressure. The obtained conclusions are as follows.

(1) A tendency was found for both duct and pipe flows that the SW-to-SL flow regime transition occurs at lower non-dimensional gas-liquid relative velocity J^*_{GL} or at lower normalized liquid level h_L/D when the channel height is increased at system pressures ≤ 3 MPa. This tendency can be explained consistently if the normalized critical wave height is assumed to increase with channel height. Based on this tendency, a new correlation to predict the transition for the relatively-low pressure flows in large-diameter pipes (**Equation (3-16)**) was obtained by modifying the coefficient of the Taitel-Dukler model to predict the transition.

(2) An empirical correlation to predict the transition in a rectangular duct (**Equation (3-8)**) was obtained from the large-height duct air/water experiments. Liquid flow rates at the transition boundary for the steam/water pipe flows were well scaled by the density-modified Froude number J^*_k with a parameter of $\sqrt{D}$.

(3) The influence of system pressure on the transition for steam/water flows under the pressures ≥ 5 MPa was well represented by J^*_{GL} using fluid densities.

(4) The gas-liquid relative velocity u_G - u_L correlated the transition better than the gas velocity u_G alone, in particular for steam/water two-phase flows at system pressures ≥ 5 MPa.

4. Interfacial Friction Factor for Stratified-Wavy Flows in the Vicinity of Transition Boundary from Stratified-Wavy to Slug Flow

4. 1 Introduction

An empirical correlation for interfacial friction factor f_i in the SW flow and the stratified-wavy to slug (SW-to-SL) flow regime transition boundary is developed in this section, based on the TPTF data for pressures of 3 to 9 MPa using 4- and 8-inch pipe test sections. The correlation is based on two non-dimensional parameters: the ratio of the gas-phase hydraulic diameter to the critical wave length, and the ratio of the gas-liquid relative velocity to the limiting velocity. Both parameters are based on the Kelvin-Helmholtz instability theory. The correlation succeeds to represent the dependence of f_i on pressure and pipe diameter within the above experimental ranges. The flow and interfacial wave conditions are examined further by means of flow criticality and r.m.s. amplitude (standard deviation) of the liquid holdup signals.

4. 2 Characterization of Interfacial Waves

Typical densitometer signals, measured at L/D = 48 and converted into liquid holdup (1-α) , are shown in **Fig. 4-1** for the three 8-inch pipe 3 MPa experiments. The superficial gas and liquid velocities, J_G, and J_L, the standard deviation (i.e., the r.m.s. amplitude of interfacial waves) σ and the averaged void fraction α are indited. The liquid level in the test section was obtained from the γ-ray densitometer signal. The liquid level was converted into liquid holdup assuming a flat interface in the pipe cross-section [Kawaji et al. 1987]. **Figure 4-1** shows that both the liquid level and interfacial wave amplitude increased with the liquid flow rate around the SW-to-SL flow regime transition boundary.

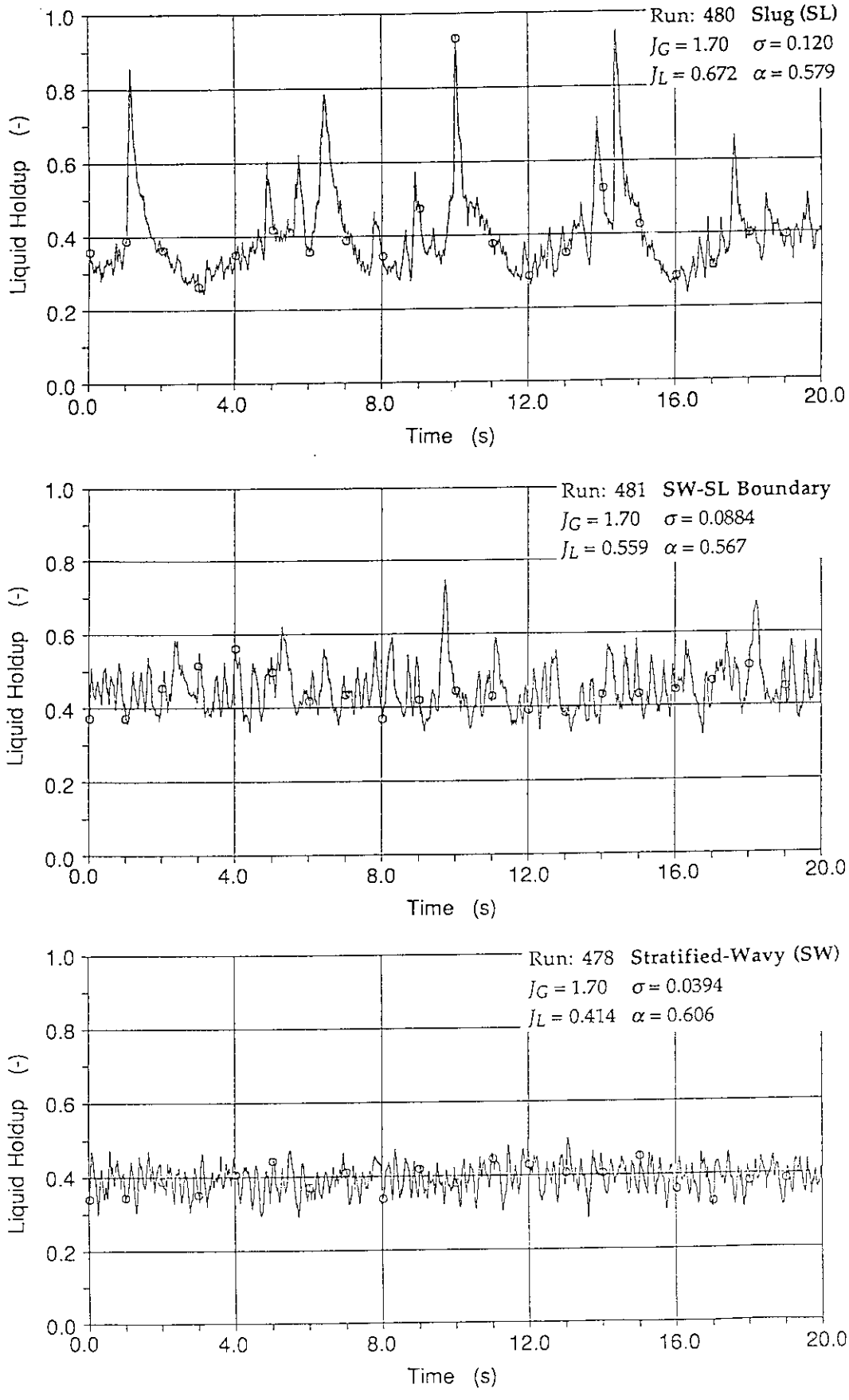

Fig. 4-1 Typical γ-ray Densitometer Signals as Liquid Holdup (8-inch Pipe, L/D = 48, 3 MPa, Recording Rate = 50 Hz)

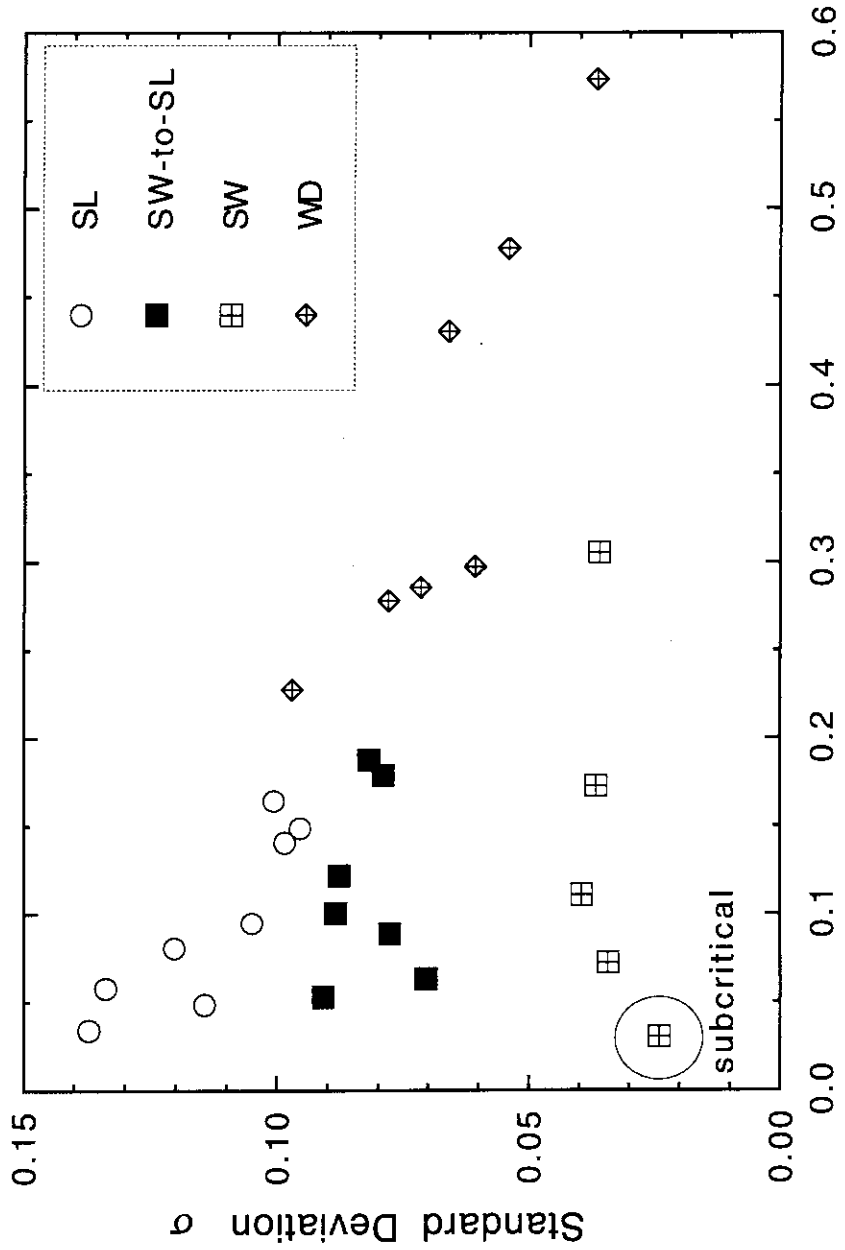

Fig. 4-2 (a) Standard Deviation of Interfacial Level Fluctuation vs. Non-Dimensional Gas-Liquid Relative Velocity (8-inch Pipe, L/D = 48, 3 MPa)

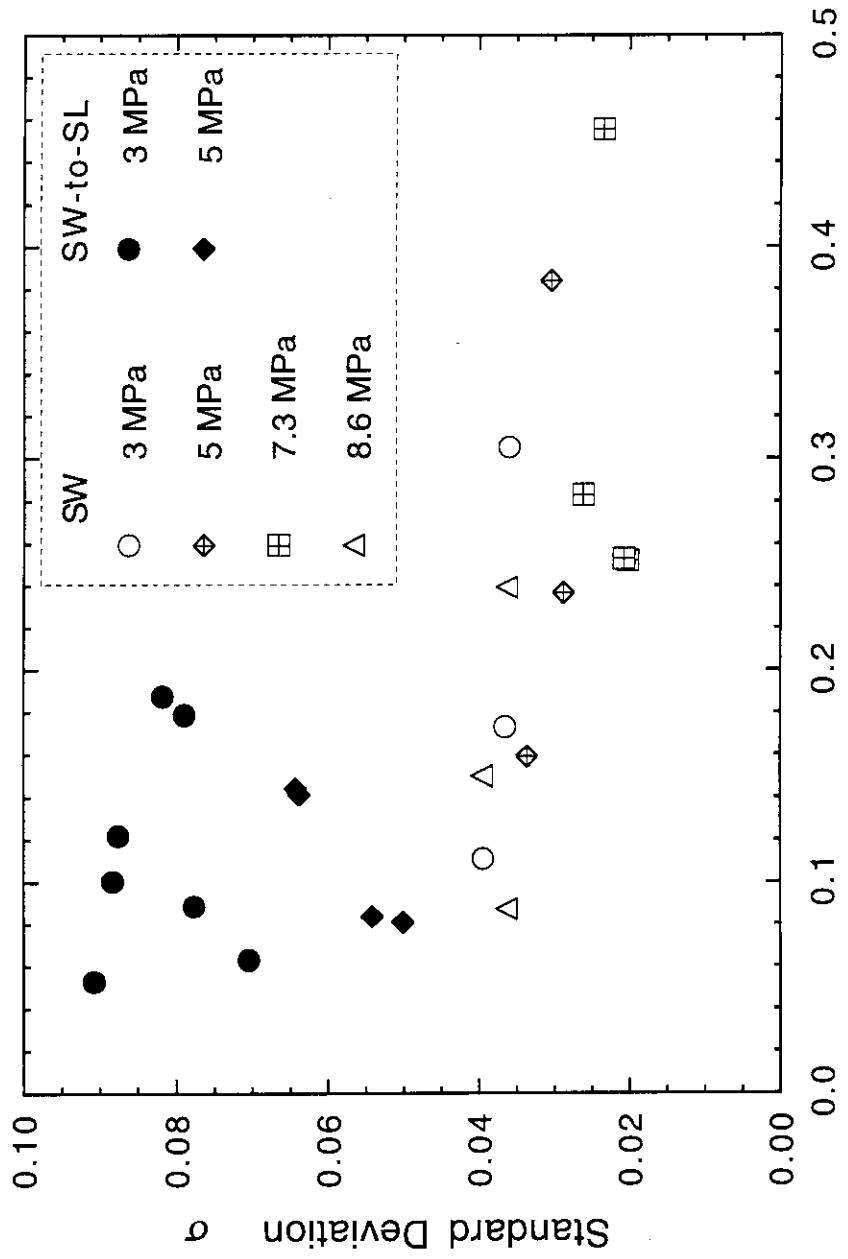

Fig. 4-2 (b) Standard Deviation of Interfacial Level Fluctuation vs. Non-Dimensional Gas-Liquid Relative Velocity (8-inch Pipe, L/D = 48, 3, 5, 7.3 and 8.6 MPa)

Figure 4-2 (a) compares the standard deviation $\sigma(\alpha)$ of the liquid holdup signals for the 8-inch pipe experiments against the non-dimensional gas-liquid relative velocity J_{GL}^{*} . The standard deviation was obtained from

$$\sigma(\alpha) = \sigma(1 - \alpha) = \sqrt{\sum_{n=1}^{m} (\alpha - \alpha_n)^2 / m} \quad , \tag{4-1}$$

where α is the averaged void fraction for m (= 8000) data points. The phase average velocities were obtained from the measured values of flow rate and α using relationships of $u_L = J_L / (1 - \alpha)$ and $u_G = J_G / \alpha$. The data for the SW flow regime and the SW-to-SL flow regime transition boundary were obtained with the constant liquid flow rates, and showed small change in $\sigma(\alpha)$ against change in the gas-liquid relative velocity. For the SL and wavy-dispersed (WD) flow regimes, however, $\sigma(\alpha)$ decreased considerably when the gas-liquid relative velocity was increased even for the cases with the same liquid flow rate. The result for a higher pressure (5 MPa) was similar to this 3 MPa case. However, $\sigma(\alpha)$ at the SW-to-SL flow regime transition boundary decreased as the system pressure was increased as shown in **Fig. 4-2 (b)**.

4. 3 Evaluation of Interfacial Friction Factor for Stratified-Wavy Flow

4. 3. 1 Interfacial Friction Factor

For a steady fully-developed stratified two-phase flow with no interfacial gradient in a horizontal pipe, the interfacial friction factor was obtained from the one-dimensional momentum equations for gas and liquid phases as shown in **Appendix 3**. The obtained interfacial friction factor is

$$f_i = 2 \frac{S_L \tau_L \alpha - S_G \tau_G (1 - \alpha)}{S_i \rho_G (u_G - u_L)^2} . \tag{4-2}$$

In evaluating f_i using **Equation (4-2)**, the Blasius empirical correlation $f_k = 0.079 / Re_k^{0.25}$ was used to define the wall friction coefficient for both gas and

liquid phases, where $Re_k = \frac{D_k u_k}{\nu_k}$ is the Reynolds number. The hydraulic diameters D_k were defined as $D_L = 4A_L / S_L$ and $D_G = 4A_G / (S_G + S_i)$ for liquid and gas phases, respectively, following Govier and Aziz (1972).

Figure 4-3 presents the obtained interfacial friction factor against the non-dimensional gas-liquid relative velocity j^*_{GL} for the SW regime and SW-to-SL transition boundary in both the 8 and 4-inch pipe experiments. The flow condition covered wide ranges in void fractions of $0.34 < \alpha < 0.75$, and in gas and liquid Reynolds numbers of $6.33\text{x}10^4 < Re_G < 1.02\text{x}10^6$ and $4.36\text{x}10^5 < Re_L < 1.94\text{x}10^6$, respectively. It was found that f_i for the SW flow was not so much different from that for the SW-SL boundary, and gradually decreased as j^*_{GL} was increased. Furthermore, the value of f_i decreased when system pressure was increased.

The dependence of f_i on j^*_{GL} was similar to that of the r.m.s. amplitude of the liquid holdup signal, $\sigma(\alpha)$, shown in **Fig. 4-2(a)**. However, the difference in f_i between the SW regime and the SW-to-SL transition boundary was not so marked as that for the wave amplitude presented as $\sigma(\alpha)$. This result is different from what Andritsos and Hanratty (1987) observed in their air/water experiments for liquid film flows; they found that f_i increases almost linearly with the wave steepness, the ratio of the wave height to length, in particular for the 2-D waves with periodic and regular wave profiles. Contrary to this, the interfacial waves in the TPTF experiments were irregular in both the wave height and wave length as shown in **Fig. 4-1**. This irregularity probably caused f_i not necessarily to increase linearly with $\sigma(\alpha)$, unlike the Andritsos and Hanratty observation.

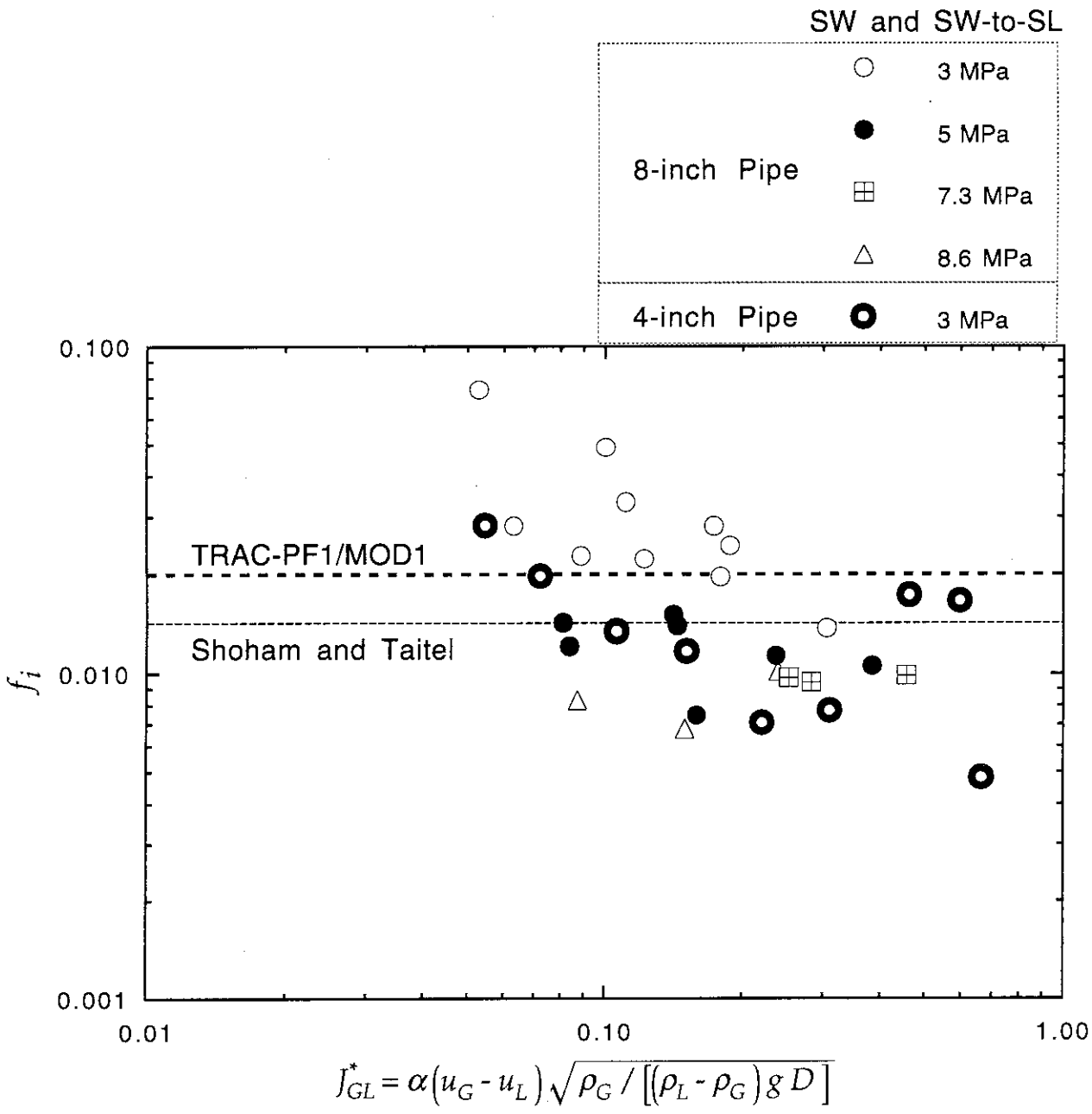

Fig. 4-3 Interfacial Friction Factors vs.
Non-Dimensional Gas-Liquid Relative Velocity

4. 3. 2 Evaluation of Current Interfacial Friction Models and Correlations

Many researchers have studied interfacial friction factors and proposed empirical correlations as noted in **Chapter 1**. Major correlations are listed in **Table 4-1** including those currently used in the LOCA analysis computer codes. Their applicability to the TPTF data is examined in the following.

Two dotted lines in **Fig. 4-3** are the constant-f_i correlations of the TRAC-PF1/MOD1 code [Safety Code Development Group 1984] and Shoham and Taitel (1984). These are based on the film flow experiments data by Lee and Bankoff (1983) and Cohen and Hanratty (1965), respectively. The TPTF f_i data, taken for various system pressures and pipe diameters, scattered widely around these constant values. The data further indicated an overall tendency to decrease as the gas-liquid relative velocity was increased. The constant-f_i correlation thus fails to represent the effects of system pressure, pipe diameter and gas-liquid relative velocity.

In **Fig. 4-4**, the f_i data for the SW flow and the SW-to-SL flow regime boundary under system pressures of 3 to 9 MPa in 8-inch pipe are compared with the Kowalski correlation (1987) for shallow water flow with $\alpha > 0.737$. This correlation predicts f_i as a function of the gas and liquid Reynolds numbers, and highly overestimates f_i for the TPTF experiments, probably because the range of the liquid Reynolds number $8.80\text{x}10^3 < Re_L^* < 4.78\text{x}10^5$ for this correlation is far lower than $6.92\text{x}10^5 < Re_L^* < 3.42\text{x}10^6$ for the TPTF experiments.

Compared also in **Fig. 4-4** is the correlation by Ohnuki et al. (1988) which is based on their air/water counter-current experiments simulating flooding in PWR hot leg, and is used in the TRAC-PF1/MOD2 code. This correlation predicts f_i by applying a constant multiplier to f_G calculated from the Blasius correlation, and highly underpredicts the TPTF data, especially for low pressures.

Table 4-1 Major Interfacial Friction Factor Models and Correlations

RELAP5/MOD2 [Ranson et al. 1987]	$f_i = \frac{16}{Re_i}$ $(Re_i \le 1187)$ $f_i = 0.0135$ $(1187 < Re_i \le 4000)$ $f_i = \frac{0.0786}{Re_i^{0.25}}$ $(4000 < Re_i = \frac{D_G \lvert u_G - u_L \rvert}{\nu_G})$	
TRAC-PF1/MOD1 [Safety Code Devl. Group 1984]	$f_i = 0.02$	based on steam/water counter-current flow experiments by Lee and Bankoff (1983)
Ohnuki et al. (1988) (TRAC-PF1/MOD2)	$f_i = 1.84\, f_G$, $f_G = \frac{16}{Re_G}$ (laminar) $f_G = \frac{0.0791}{Re_G^{0.25}}$ $(Re_G \le 10^5)$ $f_G = 0.0008 + \frac{0.05525}{Re_G^{0.237}}$ $(Re_G > 10^5)$	air-water counter-current flow
Kowalski (1987)	$f_i = 7.5 \times 10^{-5} \frac{Re_L^{*0.83}}{(1-\alpha) Re_G^{*0.3}}$, $Re_k^* = \frac{D u_k}{\nu_k}$	air/water and Freon-gas/water co-current shallow-water flow ($\alpha > 0.737$) $2.26\times10^4 \le Re_G^* \le 4.31\times10^6$ $8.80\times10^3 \le Re_L^* \le 4.78\times10^5$
Andritsos and Hanratty (1987)	$f_i / f_G = 1 + 15\left(\frac{j_G}{j_{G,t}} - 1\right)\sqrt{\frac{h_l}{D}}$ $(j_G > j_{G,t})$ $f_i / f_G = 1$ $(j_G \le j_{G,t} = 5\sqrt{\rho_{G0} / \rho_G})$	air/water co-current film-flow
Lee and Bankoff (1983)	$f_i = 0.012 + 2.694\times10^{-4}\left(\frac{Re_L}{1000}\right)^{1.534}\left(\frac{Re_G - Re_G^+}{1000}\right)$, $Re_G^+ = \frac{1.837\times10^5}{Re_L^{0.184}}$	steam/water counter-current film-flow $2.35\times10^4 \le Re_G \le 5.10\times10^4$ $2.00\times10^3 \le Re_L \le 1.20\times10^4$
Shoham and Taitel (1984)	$f_i = 0.0142$	based on air/water film-flow experiments by Cohen and Hanratty (1965)
1: Kim (1983) 2: Cheremisinoff and Davis (1979)	$f_i = a\, Re_L + b$, 1: $a = 0.14 \times 10^{-5}$, $b = 0.021$ 2: $a = 2.0 \times 10^{-5}$, $b = 0.008$	1: nearly horizontal steam/water counter-current film-flow 2: based on air/water film-flow experiments by Cohen and Hanratty (1965) $1.0\times10^2 \le Re_L \le 1.7\times10^3$

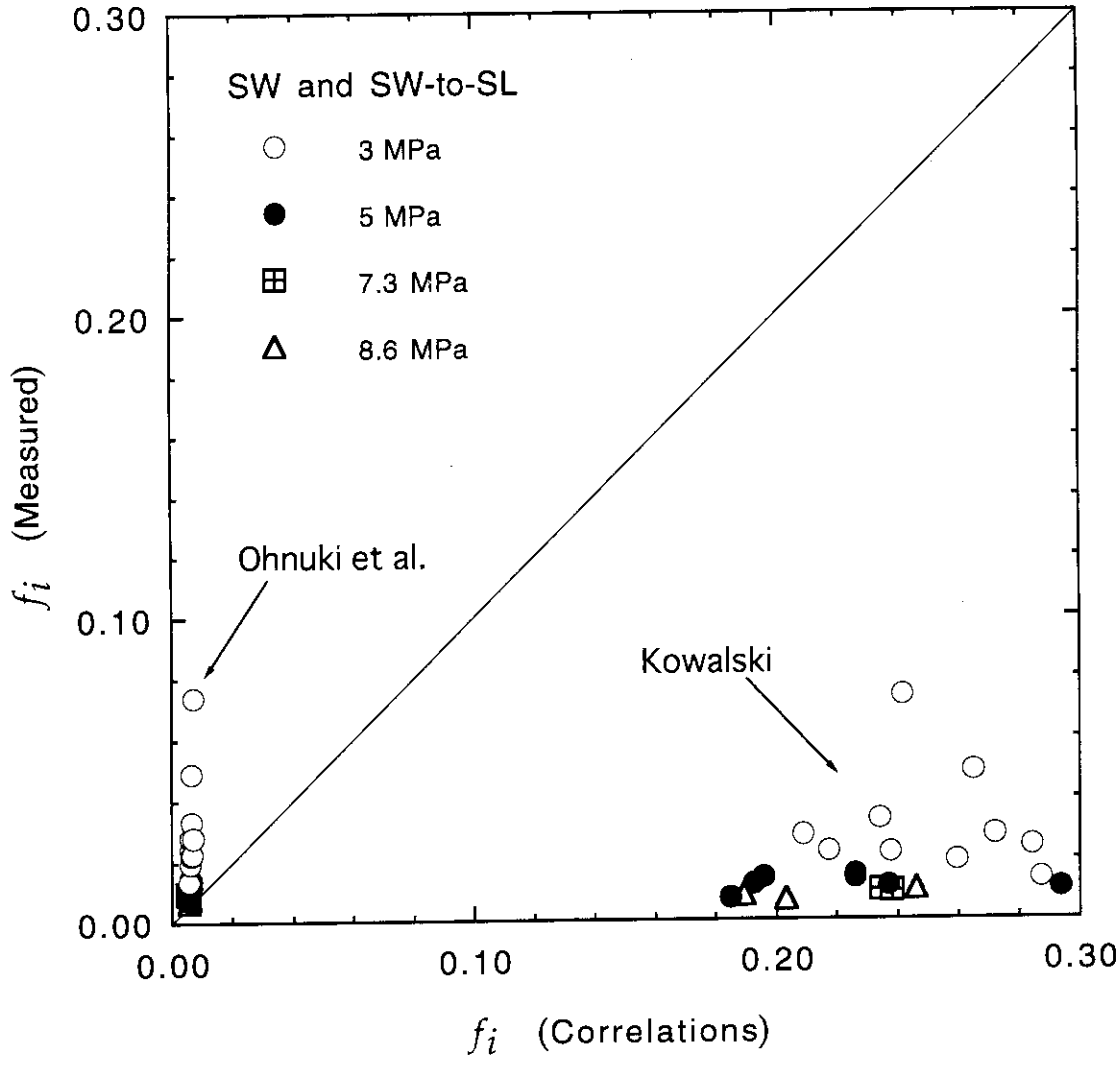

Fig. 4-4 Comparison of Interfacial Friction Factors with Ohnuki et al. Correlation used in TRAC-PF1/MOD2 Code and Kowalski Correlation (8-inch Pipe)

The RELAP5/MOD2 code [Ranson et al. 1987] applies the Blasius correlation to f_i with with no multiplier, and thus underpredicts the TPTF data more significantly than the TRAC-PF1/MOD2 code.

Three other correlations in **Table 4-1** of Lee and Bankoff (1983), Kim (1983) and Cheremisinoff and Davis (1979) are based on the film flow experiments with low liquid Reynolds number. These correlations present f_i as a function of the liquid Reynolds number and obviously highly overestimate the TPTF data.

These comparisons so far indicate that the available f_i correlations are not applicable to the TPTF experiments which were conducted at high Reynolds number for both liquid and gas phases, than the experiments on which these correlations are based.

4. 3. 3 New Empirical Correlation for Interfacial Friction Factor

In this section, a new empirical correlation for f_i is developed for the SW flow in the vicinity of the flow regime transition boundary to the SL flow. The parameters in this correlation are selected considering mechanisms that generate deep-water waves. The work of Andritsos and Hanratty (1987) for shallow water waves gives the starting point for the present study.

Andritsos and Hanratty observed in their air/water experiments that f_i starts to increase at a certain threshold gas velocity where the interfacial waves begin to grow, and that f_i increases with the wave steepness, while the wave length remains almost constant. Based on these observation, they obtained a correlation (**Table 4-1**) by relating the steepness of waves with a constant wave length to f_i / f_G . The correlation is presented in a function of the length and velocity parameters selected to characterize the interfacial waves. The average liquid depth h_L is chosen as a characteristic length to represent the wave celerity

and the influence of liquid viscosity, both of which are important in film flows. This correlation overestimates the TPTF data for 8-inch pipe experiments, as shown in **Fig. 4-5**, alike the other correlations based on film flow experiments. However, the basic idea used in this correlation, representing f_i / f_G by a function of the length and velocity parameters characterizing interfacial waves, appears to be suitable to describe the dependence of f_i on pipe diameter and system pressure.

For deep-water flows, Plate (1977) observed wave growth in his air-water separated flow experiments in a large horizontal rectangular duct, and broke down the wave growth process into three steps. In the first step, interfacial waves begin to grow, but only in the wave amplitude, exponentially with fetch (wave travel distance), and the wave length remains constant as observed by Andritsos and Hanratty for film flows. In the second step, wave trains appear, and both the wave length and amplitude increase, though slowly, with fetch. In the third step, these two processes mix until the wave growth saturates and wave breaking occurs.

In the present TPTF experiments, the observed interfacial waves have various length and amplitudes as shown in **Fig. 4-1**, and are similar to those in the third step observed by Plate (1977) above. The wave length, estimated from liquid level data under an assumption that wave velocity is represented by the sum of average liquid velocity and the wave celerity on stationary liquid for deep-water waves, ranged from ~0.3 to ~0.6 m. These values lie between the deep- and shallow-water wave lengths. Based on the small-amplitude (linear) surface wave theory, however, the deviation in the wave celerity due to the change in the wave length is small; ~1.5 to ~12% for the wave length of 0.3 to 0.6 m in the liquid depth of 0.09 m. Therefore, an attempt is made to correlate f_i using the

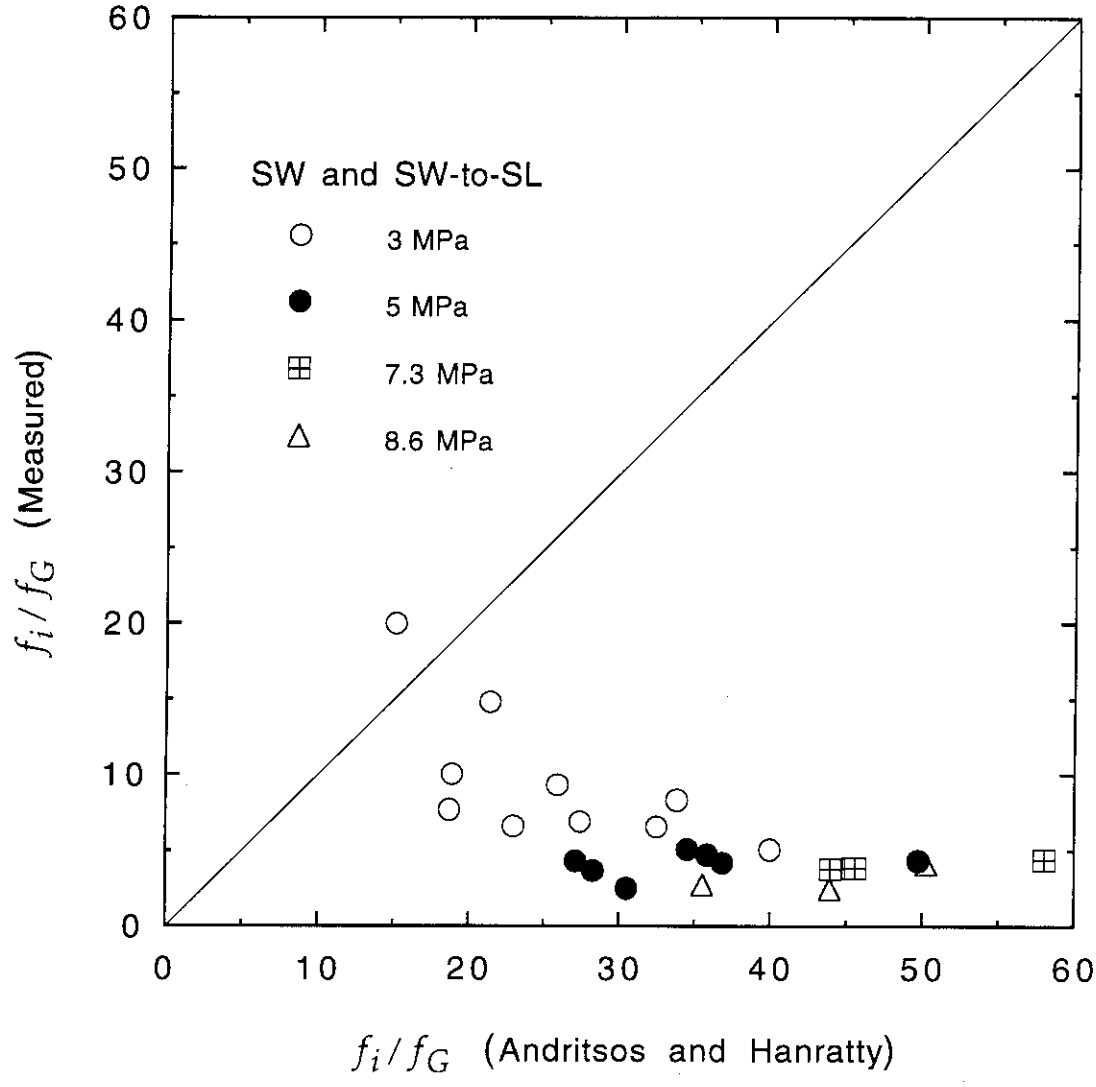

Fig. 4-5 Comparison of Interfacial Friction Factors with Andritsos and Hanratty Correlation (8-inch Pipe)

parameters characteristic of deep-water waves as a first approximation, assuming the interfacial waves are generated and grown because of the Kelvin-Helmholtz (K-H) instability.

The K-H instability theory including an effect of the surface tension T shows that the interfacial instability takes place when the gas-liquid relative velocity for the deep-water waves between thick layers of gas and liquid flows is presented as

$$(u_G - u_L)^2 \geq (1/\rho_L + 1/\rho_G)\left[kT + \frac{g}{k}(\rho_L - \rho_G)\right] = \Delta u_{\min}{}^2 \quad . \tag{4-3}$$

where $k = 2\pi/\lambda$ is the wave number and λ the wave length. This equation is derived in **Appendix-2**. The wave length of the incipient instability that occurs when $u_G - u_L = \Delta u_{\min}$ is

$$\lambda_0 = 2\pi\sqrt{T/[g(\rho_L - \rho_G)]} \quad . \tag{4-4}$$

These critical wave length λ_0 and the corresponding minimum relative velocity $\Delta u_{\min}$ are property group, and are chosen as the length and velocity scales for the interfacial friction factor f_i . The influences of fluid properties, thus the dependence on system pressure, are represented by both parameters of λ_0 and $\Delta u_{\min}$.

The hydraulic diameter of the gas channel, D_G, is the length scale to characterize the gas-phase turbulence, and the value of which is close to the gas channel height which poses the maximum wave height. The interfacial waves in the present SW flows are saturated in their growth with random wave length and wave height, as noted before. Therefore, D_G is selected as a parameter representing the wave height that is limited by the gas channel height. If the wave profile in different-diameter pipes is similar, D_G represents the dependence of wave height on the pipe diameter.

In summary, the parameters chosen to correlate f_i are

$$\frac{f_i}{f_G} = F\left[\lambda_0,\ \Delta u_{\min},\ D_G,\ (u_G - u_L)\right]. \tag{4-5}$$

From these parameters, two non-dimensional parameters $\frac{u_G - u_L}{\Delta u_{\min}}$ and $\frac{D_G}{\lambda_0}$ are further formed. The former is considered to represent the strength of the interfacial instability, and the latter to represent the interfacial roughness in the form similar to the wave steepness. Using these parameters, an empirical correlation is obtained for the TPTF data for both the SW flow regime and SW-SL flow regime boundary as

$$\frac{f_i}{f_G} = \left(\sqrt{3}\,\frac{\lambda_0}{D_G}\cdot\frac{u_G - u_L}{\Delta u_{\min}}\right)^{-8/5}. \tag{4-6}$$

Equation (4-6) correlates the TPTF data for various pipe diameters and system pressures well as shown in **Fig. 4-6**, within an accuracy of about ±50%. This correlation is applicable to flows with gas-liquid relative velocities greater than $\Delta u_{\min}$. It is interesting to note that the term $\sqrt{3}\,\lambda_0$ in the correlation is the wave length of the most-rapidly growing wave according to the inviscid Rayleigh-Taylor instability theory [Chandrasekhar (1961)].

When the gas-liquid relative velocity increases, f_i / f_G decreases as shown in **Fig. 4-6**, and approaches to 1.0. However, f_i / f_G begins to increase before it reaches 1.0 as shown in **Fig. 4-7**, since transition to wavy-dispersed (WD) flow occurs. In the WD flow regime, liquid entrainment effectively causes an increase in the density of gas phase with the entrained droplets. The average gas velocity also effectively increases as the gas flow area decreases by the liquid droplets if the liquid level is unchanged. In the present method to obtain f_i using **Equation (4-2)**, these effects are not taken into account. Because of these effects, however, the liquid level decreases since τ_i increases, and the obtained f_i increases.

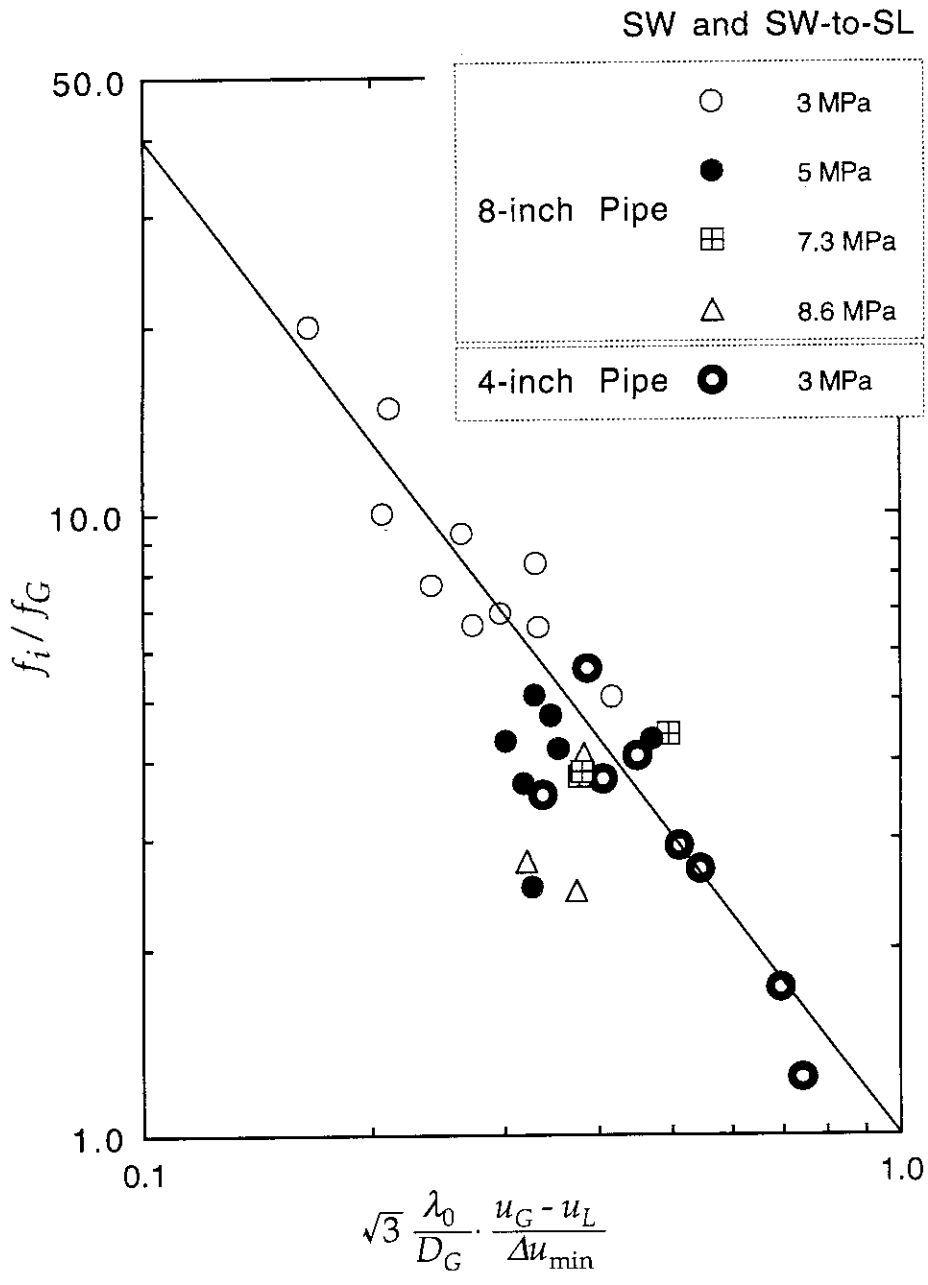

Fig. 4-6 Comparison of Interfacial Friction Factors with New Empirical Correlation (SW flow regime and SW-SL flow regime boundary)

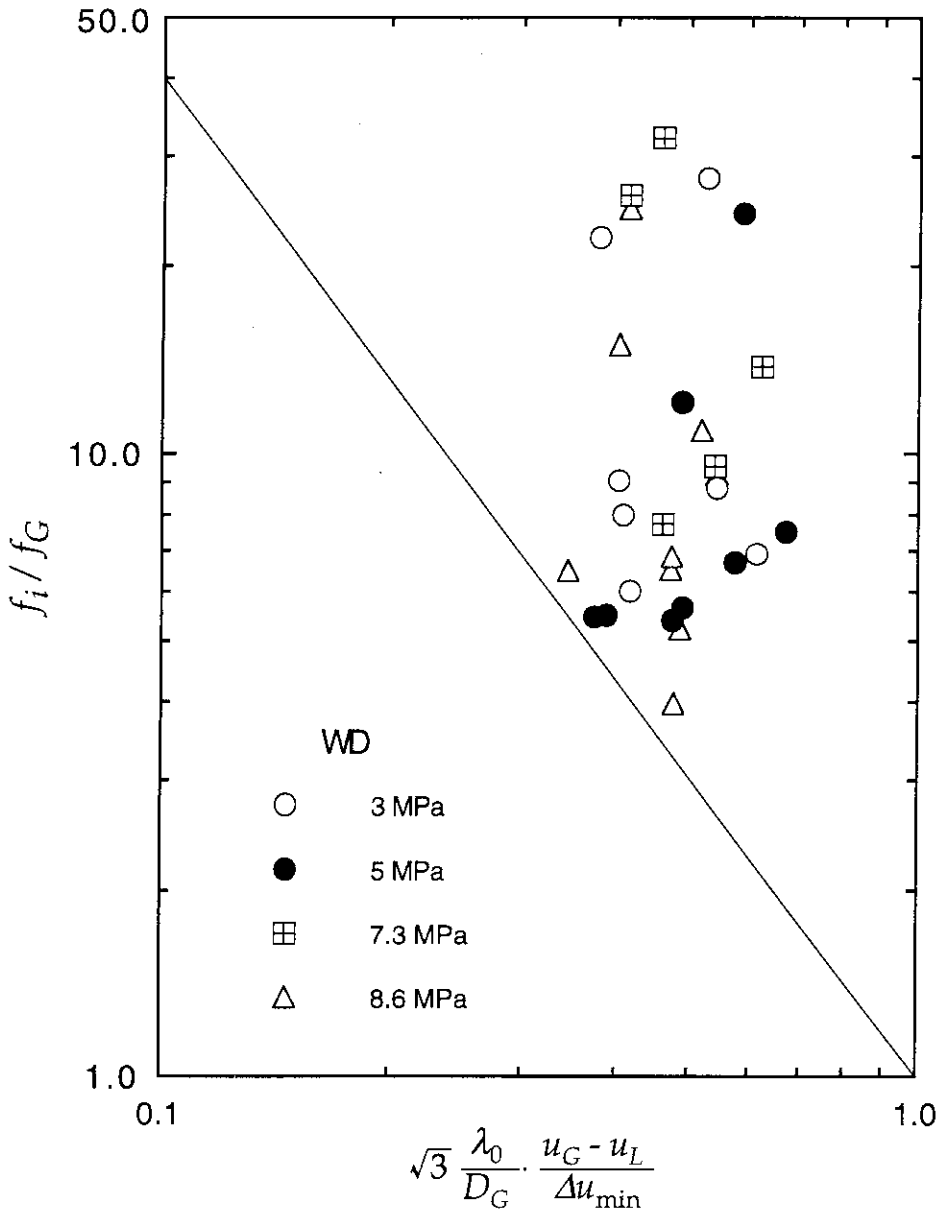

Fig. 4-7 Comparison of Interfacial Friction Factors with New Empirical Correlation (wavy-dispersed flow regime)

4.4 Conclusions

The interfacial friction was investigated for high-pressure (3 to 9 MPa) steam/water SW flow regime, in the vicinity of the transition boundary to SL flow, using the TPTF experimental data for 4 and 8-inch diameter horizontal pipe test sections. The flow condition covered wide ranges of void fractions of $0.342 < \alpha < 0.753$, and gas and liquid Reynolds numbers of $6.33 \times 10^4 < Re_G < 1.02 \times 10^6$ and $4.36 \times 10^5 < Re_L < 1.94 \times 10^6$, respectively. The obtained conclusions are as follows.

(1) Interfacial waves observed in the SW flow regime became larger in r.m.s. amplitude, and became more irregular in both amplitude and wave length, as the transition boundary to SL flow regime was approached.

(2) Currently available correlations to predict f_i for the horizontal stratified two-phase flow (**Table 4-1**) are based mostly on liquid film flow experiments with relatively small liquid Re number. These correlations use liquid Re number or film thickness as the controlling parameter, or multiply the wall friction factor by a constant factor. These correlations were inapplicable to the present data.

(3) A new empirical correlation **Equation (4-6)** was developed for the interfacial friction factor f_i for the SW flow regime, in the vicinity of the transition boundary to the SL flow regime. The correlation is based on two non-dimensional parameters: the ratio of the gas-phase hydraulic diameter to the critical wave length, and the ratio of the gas-liquid relative velocity to the limiting velocity for the interfacial instability in deep-water flow. The correlation successfully represents the dependence of f_i on pressure and pipe diameter within the present experimental ranges for the SW flow and SW-to-SL transition boundary.

5. Influence of Gas-Phase Bernoulli Pressure Drop on Slugging

5.1 Introduction

This section summarizes the measurement of the gas phase pressure in the large-height duct experiments to clarify the role of the gas phase pressure during evolution of interfacial waves into a liquid slug (slugging). An analysis of the measured pressure is performed further making reference to the one-dimensional Bernoulli prediction of the local static pressure. The effect of liquid entrainment at the wave crest on the wave growth is also discussed.

5.2 Experiments

In the large-height duct test section, the air static pressure was measured on the channel top wall at five locations. The measurement locations were selected so as to cover various stages of wave growth in slugging, including complete blockage of the air flow by a liquid slug. The measurement was performed for the slugging at the SW-to-SL transition boundary. The instrument setup is shown in **Fig. 2-6 (c)**. Liquid level and gas pressure were measured at the same location by placing each sensor on the same vertical plane normal to the flow axis.

The conditions for flow regime transition depend on the geometrical scale as well as fluid physical properties. The test section has a height close to the diameter of the PWR primary horizontal leg. The experimental results from this test section, therefore, are more representative of flow in the PWR legs from the scaling point of view. The effects of the fluid physical properties and the differences in flow between duct and pipe, however, should be considered separately to apply the present results to reactor analyses.

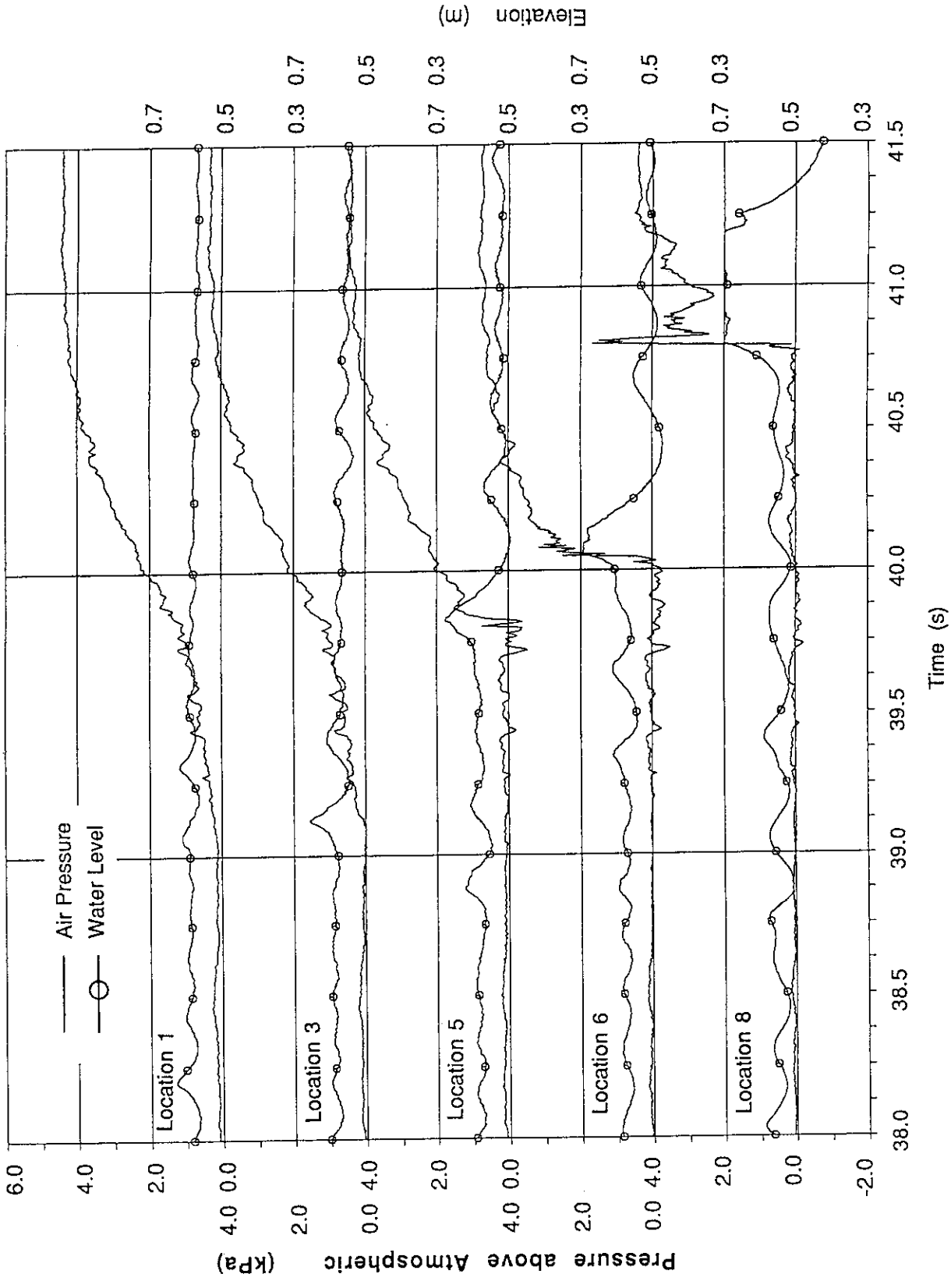

Fig. 5-1 Pressure and Water Level Data

(J_L = 0.89 m/s, J_G = 1.49 m/s)

5. 3 Water Level Signals

Typical liquid level signals obtained at eight stations along the test section for slugging (J_L = 0.89 m/s, J_G = 1.49 m/s) have been shown in **Fig. 3-1**. The slugging occurred between liquid level sensor locations Nos. 3 and 6. In this section, this slugging is examined in detail, as a typical example.

Prior to slugging, wave trains appeared on the water surface. The amplitude of waves increased as the waves traveled downstream. One of the waves began to grow faster than the others, around location 3 (4.5 m from the test section inlet) in this case. The wave finally hit the top wall of the test section, around location 6 (7.5 m from the inlet), forming a liquid slug. A fairly long distance (~3 m) was necessary for the wave to travel before it grew into a slug.

This observation is a contrast to that in smaller-height (diameter) channels where slugging occurs due to an almost sudden growth of slugging waves. Waves interact each other during the growth, since the growing waves travel faster than the downstream waves and catch them up. It should be noted that the level signals obtained at fixed locations, shown in **Fig. 3-1**, do not directly represent the instantaneous wave form since both the amplitude and velocity of waves vary with time.

5. 4 Pressure Signals

Figure 5-1 presents air pressure and water level signals obtained at the same locations. The pressure at location 1 shows a gradual increase after about 39 s (the origin of the time scale is arbitrary). This increase in the pressure resulted from a rapid growth of the slugging wave on the downstream side, around location 3. This growing wave throttled and limited the air flow over its crest. The pressure downstream this high wave, e.g., at location 5 (6.5 m from the

inlet) and further downstream, was nearly atmospheric. The upstream pressurization rate increased after 39.8 s as this wave grew into a liquid slug around location 6.

At locations 6 through 8, the pressure indicated a sudden increase when the slug (or pseudo-slug) passed across the transducer location. This pressure difference across the slug accelerated the slug towards the channel downstream end. The slug upstream pressure continued to increase until the slug traveled to around location 8 (40.8 s), where the pressure reached a plateau of about 4.4 kPa above the atmospheric pressure. The slug, having been accelerated by the upstream pressure, no longer limited the air flow through the channel. The slug tail velocity at this time was about 4.6 m/s, which was close to the air velocity of about 5 m/s corresponding to the inlet flow rate. After the slug left the test section exit, the pressure throughout the test section dropped to nearly atmospheric pressure. When the slug or pseudo-slug reached a pressure transducer, the pressure signals often exhibited spikes because of impingement of water droplets onto the transducer diaphragm.

5. 5 Bernoulli Effect

The measured pressures were compared with the static pressure drop calculated by the Bernoulli equation, by taking into account of the transient nature of the phenomena. When a high-amplitude wave appears, the wave upstream pressure increases with time as has been noted in **Section 5. 4**, because the air flow rate over the wave crest becomes lower than the test section inlet flow rate. That is, the air flow rate varies along the test section as well as with time. This important observation makes a contrast to existing models where the gas and liquid flow rates are assumed constant.

In **Fig. 5-2**, the flow condition at slugging is schematically presented. For simplicity, the air flow is assumed to be one-dimensional on the upstream side of a wave crest. The air flow rate varies along the test section, as found above. However, it is assumed here to be quasi-steady over a short time period which covers the axial distance that a wave travels across the probes for the pressure and level measurement at one location. The flow rate is assumed further to be locally constant over the corresponding distance across the wave crest. The velocity is inversely proportional to the air flow area that can be obtained from the measured water level. The air static pressure on the upstream-side of the wave crest, $p(z, t)$, can be obtained from the Bernoulli equation with respect to the air velocities,

$$p(z, t) = p_u(t) + \frac{1}{2}\rho_G\left[u_{G,u}(t)^2 - u_G(z, t)^2\right] , \qquad (5\text{-}1)$$

where, $p_u(t)$ and $u_{G,u}(t)$ are the pressure and air velocity measured well upstream the wave and $u_G(z, t)$ is the air velocity on the upstream-side of the wave crest. In the present study, $p_u(t)$ is represented by the static pressure measured 1 or 2 m upstream the location where the wave is passing.

If the Bernoulli equation is applicable over a whole wave, the static pressure should recover on the wave downstream side. The measured pressure,

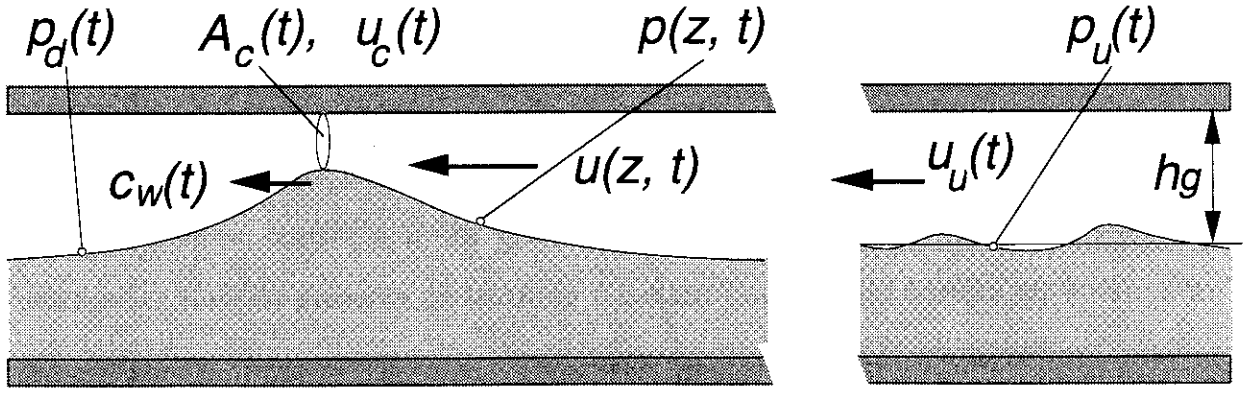

Fig. 5-2 Schematic of Flow Condition at Slugging

however, indicates a stepwise change across the wave crest. This suggests that loss of kinetic energy occurs due probably to separation of air flow at or downstream the wave crest. The water entrainment by air flow may also contribute to the energy loss.

The local air flow rate at the wave crest is

$$Q(t) = A_{G\ c}(t)\left[u_{G\ c}(t) + c_w(t)\right], \tag{5-2}$$

where,

$$u_{G,c}(t) = C_d\sqrt{\frac{2}{\rho_G K}\left[p_u(t) - p_d(t)\right]}, \tag{5-3}$$

$c_w(t)$ is the velocity of the wave crest, and $p_d(t)$ is the pressure measured downstream the wave crest at a location where the air velocity is much smaller than the air velocity at the wave crest $u_{G,c}(t)$. For the present case, $c_w(t)$ was about 2 to 4 m/s and was much lower than $u_G(z, t)$. The air flow area $A_{G,c}(t)$ is obtained using the measured water level at the wave crest. The coefficient C_d is to account for the non-uniformity of air velocity distribution, and it is 1.0 for a one-dimensional flow. The coefficient K is the energy loss coefficient. The observed configuration of high-amplitude waves and pseudo-slugs, with an abrupt increase in air flow area on the downstream side of the crest, suggests $K \approx 1.0$. In this study, therefore, the value of K was assumed to be 1.0 for simplicity. The calculated air flow rate over a high wave crest is always smaller than the test section inlet flow rate.

The calculated air velocity and air static pressure near the wave crest are shown in **Figs. 5-3 (a)** through **(c)** in comparison with the measured pressure and liquid level at three different measurement locations. The comparison is given for a time period of 0.35 s centered at the time when the wave crest passes the measuring locations. The data shown in **Figs. 5-3 (a)** through **(c)** are the pressure differences between the pressures along the wave and at 1 or 2 m upstream location, $\left[p(z, t) - p_u(t)\right]$.

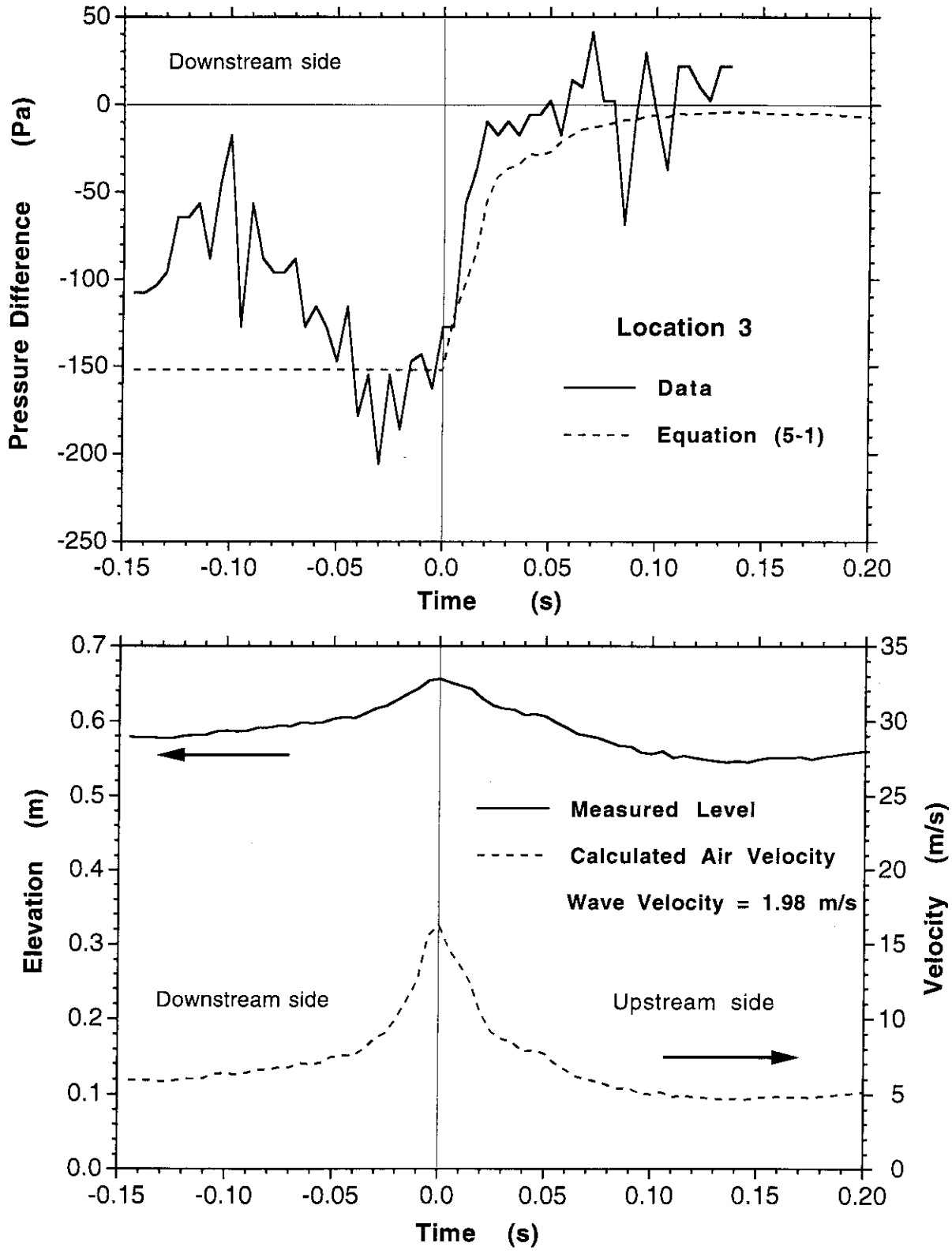

Fig. 5-3 Comparison of Bernoulli Pressure Drop with Data
(J_L = 0.89 m/s, J_G = 1.49 m/s)
(a) Location 3 (4.5 m from test section inlet)

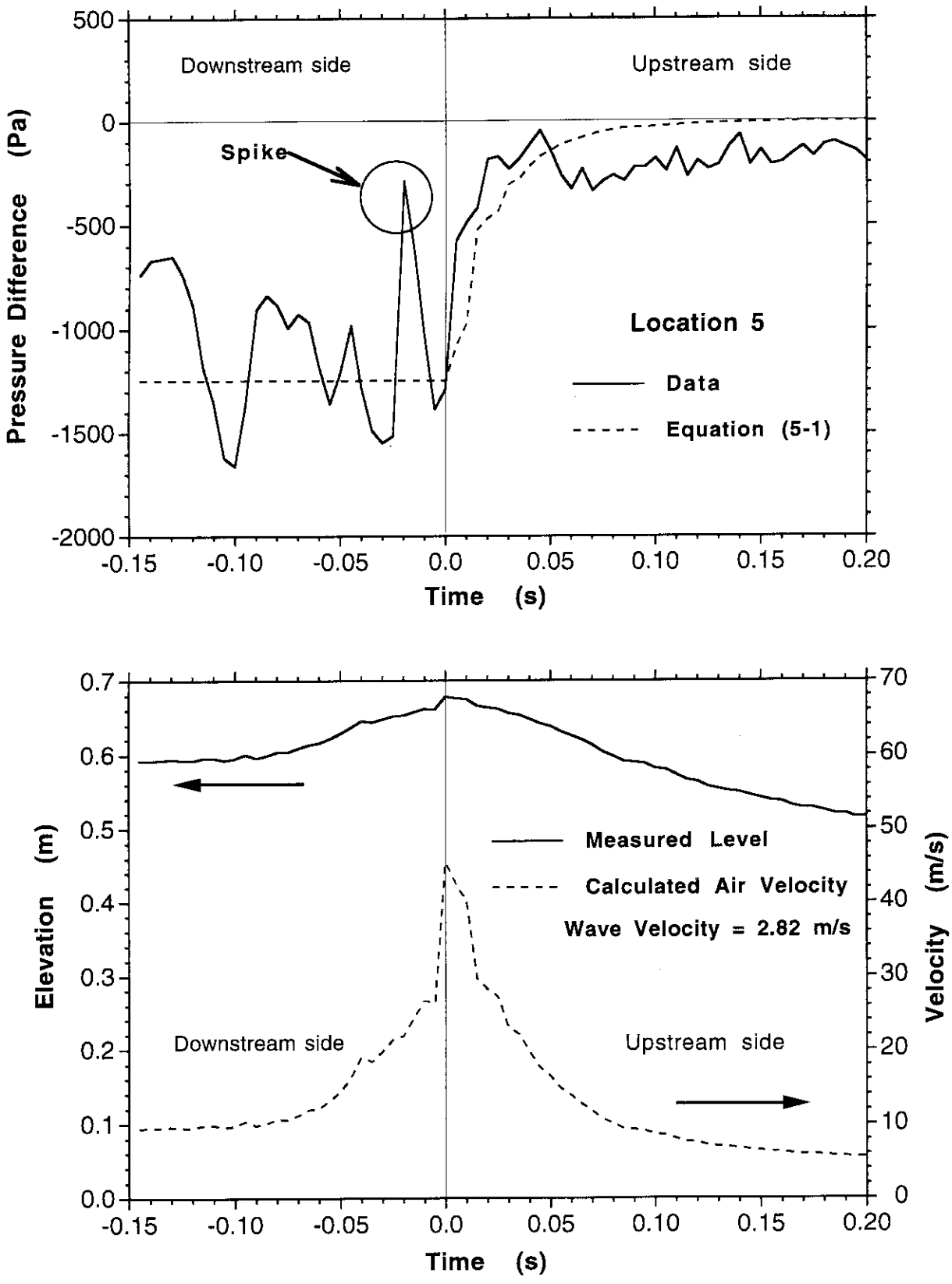

Fig. 5-3 Comparison of Bernoulli Pressure Drop with Data
($J_L = 0.89$ m/s, $J_G = 1.49$ m/s)
(b) Location 5 (6.5 m from test section inlet)

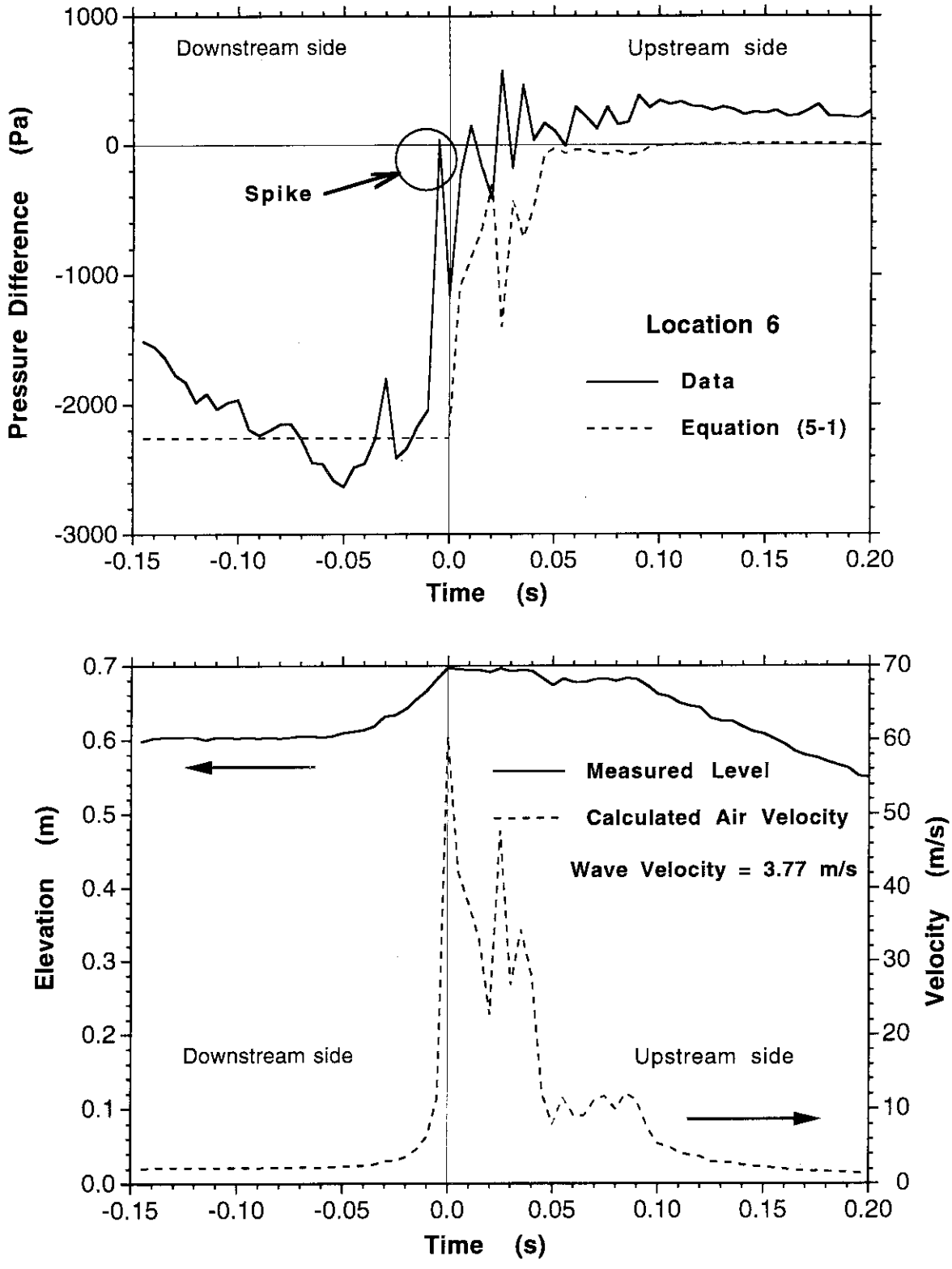

Fig. 5-3 Comparison of Bernoulli Pressure Drop with Data
($J_L = 0.89$ m/s, $J_G = 1.49$ m/s)
(c) Location 6 (7.5 m from test section inlet)

For the wave recorded at location 3 (4.5 m from the inlet), the calculated pressure drop agreed well with the data as shown in **Fig. 5-3 (a)**. The measured pressure drop of 0.12 kPa at the wave crest corresponds to a water head of about 0.012 m. This is far smaller than the wave height of about 0.1 m. In the experiment, the pressure is measured on the channel top wall. Therefore, the measured value may show a smaller static pressure drop than on the water surface, especially for low-height waves of which the wave crests are apart from the channel top. For this case, furthermore, the static pressure recovers considerably in the downstream side of the wave, though not completely. This suggests that $K < 1.0$ for this particular case where the wave crest is less steep than the other two cases below. The present calculation with an assumption of $K = 1.0$ tends to underestimate the air flow rate. Even with the inlet air flow rate, however, the expected pressure drop is 0.33 kPa. The data anyhow showed that the Bernoulli pressure drop is limited to the very vicinity of the wave crest and is small in the incipient growth of slugging waves.

When the wave reached location 5 (6.5 m from the inlet), the measured pressure agreed well with the result calculated with $K = 1.0$ as shown in **Fig. 5-3 (b)**. The low pressure region was limited again to the vicinity of the wave crest in the upstream side. In this stage of slugging, the upstream liquid level decreased considerably causing the wave height effectively increased. The pressure drop was thus still a little smaller than the static water head corresponding to the wave height in the wave upstream side. In the wave downstream side, however, the pressure did not recover. The pressure drop in reference to the wave upstream had a similar magnitude to the wave static head. The wave velocity was increased to 2.82 m/s, because of the acceleration by the pressure difference across the wave. These results showed that the pressure drop over the wave is effective in developing the wave primarily in the wave downstream side.

Even for the case at location 6 (7.5 m from the inlet) where a liquid slug had almost completed to form, the comparison was favorable as shown in **Fig. 5-3 (c)**. The air flow path in this case was almost blocked and the air flow rate was small, though the calculated air velocity was high in the vicinity of the wave crest.

Note that the pressure for the wave recorded at location 5 (**Fig. 5-3 (b)**) did not recover in the downstream side of the wave. This suggests the separation of air flow from the interface, resulting in a free turbulent flow of air bounded by three walls; upper ceiling and two side walls. For the present case, the interface on the wave and the upper ceiling formed a convergent-divergent nozzle for the air flow with relatively large converging and diverging angles of 18.0° and 19.5° respectively. The convergence of the air flow in the wave upstream may have had an influence to cause the separation of air flow around the wave crest in the wave downstream.

Provided that the wave crest was covered by a laminar boundary layer, the separation may be simulated by flows in a two-dimensional diffuser bounded by flat walls. The approximate method by von Kármán and Pohlhausen [Pohlhausen 1921, Schlichting 1968] gives the separation point, being independent of the angle of divergence. The distance of the separation point from the wave crest, under an assumption that the boundary layer begins to develop at the wave crest, is about $0.21L_n$, where L_n is the length between the wave crest and the intersection of an extrapolation of the wave downstream interface to the upper ceiling. The obtained distance for the wave at location 5 is about 0.0128 m. (The angle of 19.5° is used to obtain L_n.) The non-recovery of pressure shown in **Fig. 5-3 (b)** supports this results, though this distance is too small to confirm, since the minimum measurement segment is 0.0141 m; wave velocity = 2.82 m/s, recording frequency = 200 Hz.

From the comparisons above, it is clear that the Bernoulli pressure drop contributes to the wave growth even at the very final stage of slugging. The pressure drop is notable only in the vicinity of the wave crest at the upstream of the wave. It is not likely that the Bernoulli lift force alone can form a large liquid slug, when the pressure drop only in the wave upstream side is considered. However, the pressure drop across the wave accelerates the wave, because the pressure does not recover at the downstream side of the wave at the very final stage of slugging in particular, and can contribute to the wave growth. Video pictures further suggest that the interaction of a high-amplitude wave, which is accelerated by the pressure difference across it, with the foregoing waves is an important mechanism for the formation of a slug.

5. 6 Entrainment near the Wave Crest

The air flow rates in this study are much higher than those in previous studies conducted with smaller-height conduits. For high waves, therefore, air speed at the wave crest can exceed a criterion for onset of liquid entrainment. The critical air velocity for the incipience of liquid entrainment predicted by the Ishii and Grolmes model (1975) for liquid film flows is about 17 m/s for the present duct experiments. The calculated air velocities shown in **Figs. 5-3 (a)** and **(b)** are much higher than this criterion at locations 5 and 6, respectively. The pictures taken at location 3 also exhibited liquid entrainment at the wave crest as shown in **Fig. 5-4**, where the calculated peak air velocity was nearly equal to the critical value.

From the visual observation, the entrained liquid droplets seemed to impinge the channel top a little downstream the wave crest. As noted in **Figs. 5-3 (b)** and **(c)**, the pressure measured downstream the wave crest included spiky noises for the locations 5 and 6. This is probably due to impingement of the liquid droplets onto the pressure transducer diaphragm.

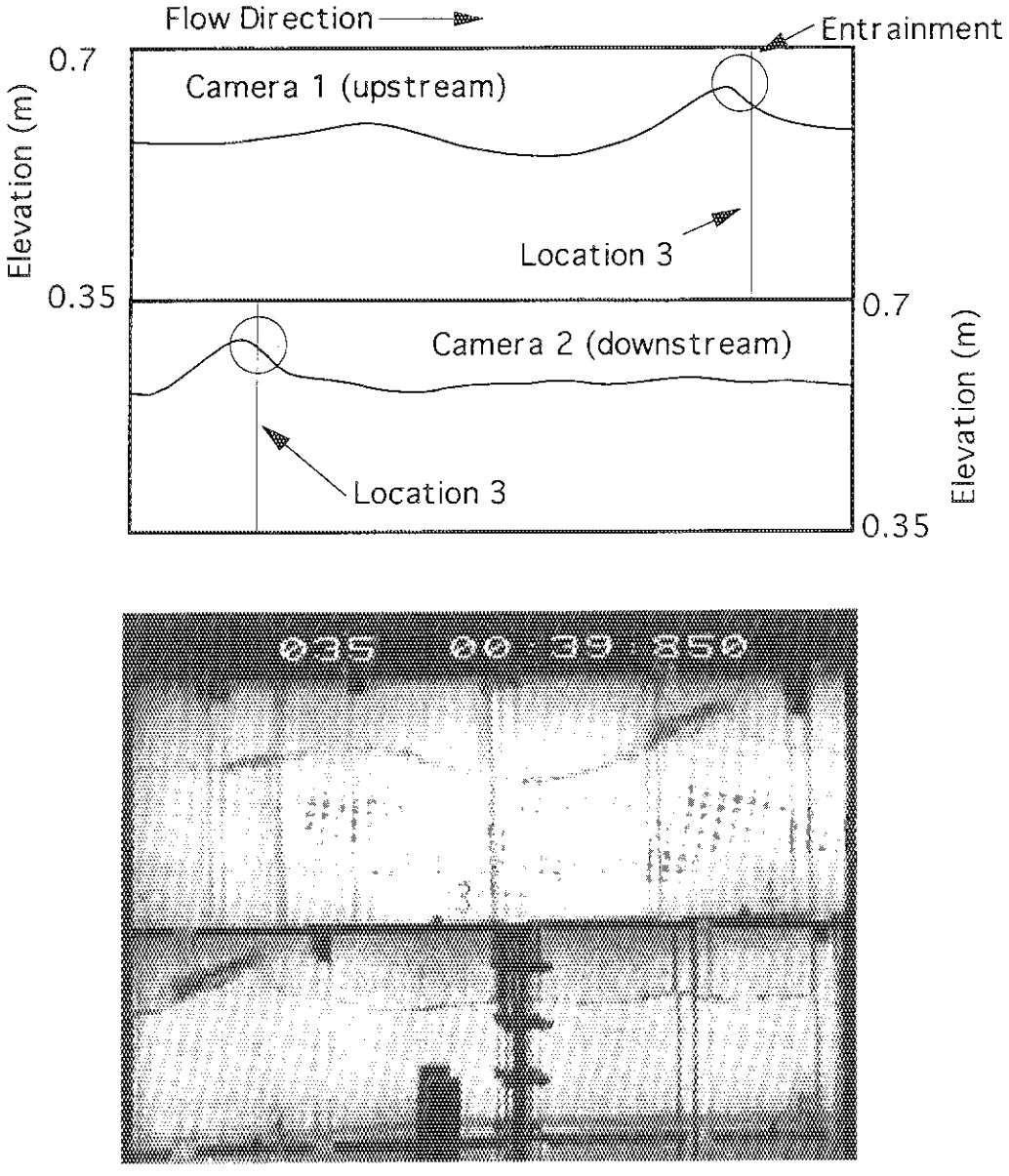

Fig. 5-4 Typical Slugging Wave (High-Speed Video Picture)
(J_L = 0.89 m/s, J_G = 1.49 m/s, Location 3)

From the measurement of static pressures, the Bernoulli effect is confirmed to be significant in the vicinity of the wave crest. However, liquid entrainment at the wave crest deteriorates the wave growth by cutting off high waves at their crest. That is, a lift force needs to overcome the "entrainment effect" so that the wave crest can reach the channel top wall, for slugging to occur in a large-height channel. The upward velocity of the wave crest development was obtained from the video pictures to be about 0.09 m/s at the final stage for slugging.

5.7 Conclusion

The flow regime transition between the stratified-wavy and slug flows in a large-height (0.7 m) long (28.3 m) horizontal duct was studied for an air-water co-current two-phase flow under atmospheric pressure. The pressure drop over a wave growing into a liquid slug in a closed channel, referred to as the Bernoulli effect on the slugging process, was evaluated from measurement of air static pressure profile. The obtained conclusions are as follows.

(1) The pressure measured on the channel top wall agreed with the prediction by the Bernoulli equation fairly well on the upstream side of the crest. The measured maximum pressure drop was smaller than the water static head corresponding to the wave height for a smaller wave which just began to grow, but became comparable to the water static head with the wave growth. The pressure drop, however, occurred only in the vicinity of the wave crest in the wave upstream side.

(2) The pressure drop in the wave downstream side did not recover, and a considerable pressure drop developed across the crest due to loss of air kinetic energy. Meanwhile, the significant liquid entrainment occurred in the vicinity of the wave crest and had a tendency to prevent the wave growth into a slug.

(3) In summary, the slugging results from the competition of the promoting effects of lift force due to the Bernoulli effect and wave acceleration due to the axial pressure gradient for the wave growth, and the impeding effects of the liquid entrainment by the high-velocity air flow. All these effects arise as the wave crest comes close to the channel top wall.

6. Flow Regime Transition to Wavy Dispersed Flow in High-Pressure Steam/Water Two-Phase Flows

6.1 Introduction

In the TPTF experiments, the measured steam superficial velocity for the flow regime transition from slug (SL) to wavy-dispersed (WD) flow decreased considerably as system pressure was increased as shown in **Fig. 6-1**, while the liquid superficial velocity increased little by little. The slug flow regime finally became non-observable when the pressure reached about 8.6 MPa [Anoda et al. 1989, Nakamura et al. 1991 a]. In this section, the onset of liquid entrainment from the wavy interface is investigated as a primary cause for the SL-to-WD flow regime transition in the steam/water flows under pressures up to 12 MPa. The range of Reynolds numbers for liquid and gas phases in the TPTF experiments was $1.3\text{x}10^6 < Re_L < 6.3\text{x}10^6$ and $3.7\text{x}10^5 < Re_G < 2.8\text{x}10^6$, respectively. The interfacial wave form and onset of liquid entrainment were visually observed by the video probe.

6.2 Experimental Results

6.2.1 Visual Observation of Slug to Wavy-Dispersed Flow Regime Transition

The gas-liquid interface was visually observed using a side-view type video probe [Nakamura et al. 1992] inserted into the gas stream. The video probe viewed the horizontal upstream direction so that the observed flow was free from the perturbation by the probe.

In the slug flow, stratified-wavy (SW) flow appears between liquid slugs as shown in **Fig. 1-1.** At pressure of 3 MPa, the stratified-wavy flow included large-amplitude two-dimensional (2-D) interfacial waves with the wave crest spanning

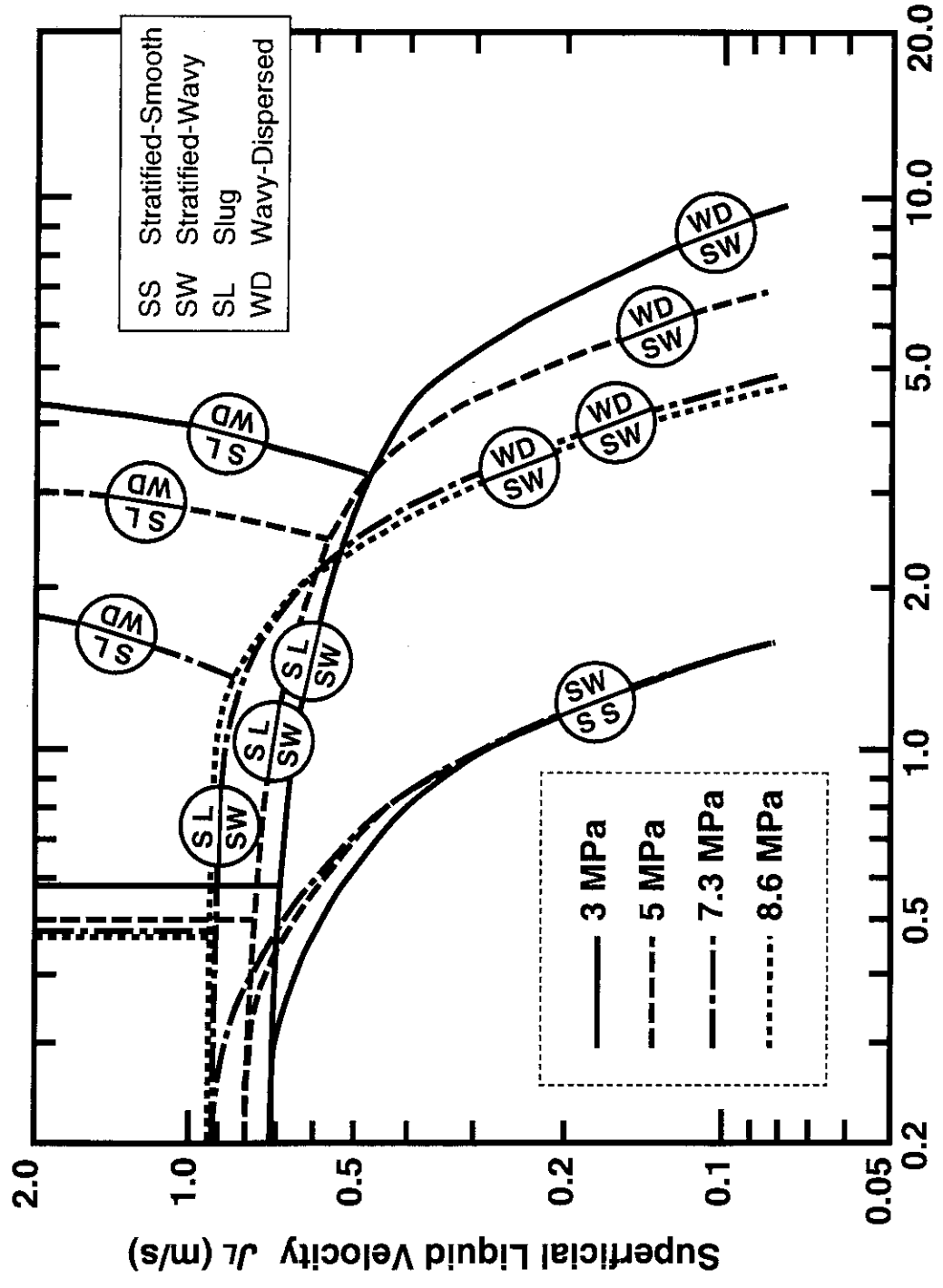

Fig. 6-1 Flow Regime Map (TPTF 8-inch pipe, 3 to 9 MPa, Anoda et al. 1989)

almost the entire width of interface. The liquid entrainment began at these crests, as the gas flow rate was increased, while the liquid flow rate was kept constant. With further increase in the gas flow rate, pebbly three-dimensional (3-D) interfacial waves began to appear randomly among the 2-D waves. Liquid entrainment occurred also from these 3-D waves. Even after a large amount of entrained liquid droplets has been formed, pseudo slugs still appeared occasionally. These pseudo slugs had a frothy front and did not necessarily block the entire pipe cross-section. Similar flow has been observed and designated to be "developing-slug" flow by Nydal et al. (1992) or the "disturbance-wave" in air-water annular flow by Fukano and Ousaka (1989).

When the gas flow rate was increased further, the liquid droplets covered the interface completely, and, then, the liquid droplets became to impinge the video probe window continuously making the visual observation difficult. This last flow condition may be annular-dispersed (AD) flow shown in **Fig. 1-1**, while the measurement was insufficient to confirm the existence of a continuous liquid film on the pipe inner wall.

As system pressure was raised, the liquid entrainment and 3-D waves became to initiate at smaller gas flow rates. The frequency of liquid slugs and the wave amplitudes of the 2-D waves decreased. At system pressures of ~8.6 MPa and above, the 2-D waves always ejected droplets from the wave crest and their amplitudes were much smaller than those at lower pressures. Then, no transition to SL flow regime was observed.

Based on the visual observation above, the onset of liquid entrainment appears to be a sign for the flow regime transition to wavy-dispersed (WD) flow. The wavy-dispersed (WD) flow is treated as a distinct flow regime between SL and AD flow regimes, while WD flow regime still retains slug-like intermittent

nature at pressures around 3 MPa. When there is no liquid entrainment from the interfacial waves between liquid slugs, the flow regime was judged to be SL.

Note that the amplitude of interfacial waves for WD flow regime decreased as system pressure was raised. The onset of liquid entrainment obviously has an effect to decrease the wave amplitude by blowing the wave crest off as found in **Chapter 5**.

6. 2. 2 Critical Parameters for Slug to Wavy-Dispersed Flow Regime Transition

Figure 6-2 shows the TPTF data obtained at pressures of 3 to 12 MPa in terms of void fraction α and non-dimensional gas-liquid relative velocity J^*_{GL}. Compared in **Fig. 6-2** are the data for flows at the SW-to-SL and SL-to-WD flow regime transitions, and WD flows. Compared also in **Fig. 6-2** is the modified Taitel and Dukler model (1976) for the SW-to-SL transition (**Equation (3-4)**). The TPTF data for the SW-to-SL flow regime transition agree well with the modified Taitel-Dukler model for pressures ≥ ~5 MPa as found in **Chapter 3**.

Taitel and Dukler have suggested that the model predicts also the transition to annular flow when $\alpha > 0.5$. As shown in **Fig. 6-2**, data measured for different flow regimes actually fell on a single line by the modified Taitel-Dukler model, for each system pressure, while the line shifted a little with the pressure. The void fraction α for the SL-to-WD flow regime transition boundary, however, decreased significantly from ~0.6 to ~0.15 as pressure was increased from 3 to 12 MPa. The gas-liquid relative velocity Δu around this transition also decreased significantly from ~3 to ~0.5 m/s, as shown in **Fig. 6-3**. Note that Δu of ~0.5 m/s at system pressure of 12 MPa was even smaller than the liquid absolute velocity.

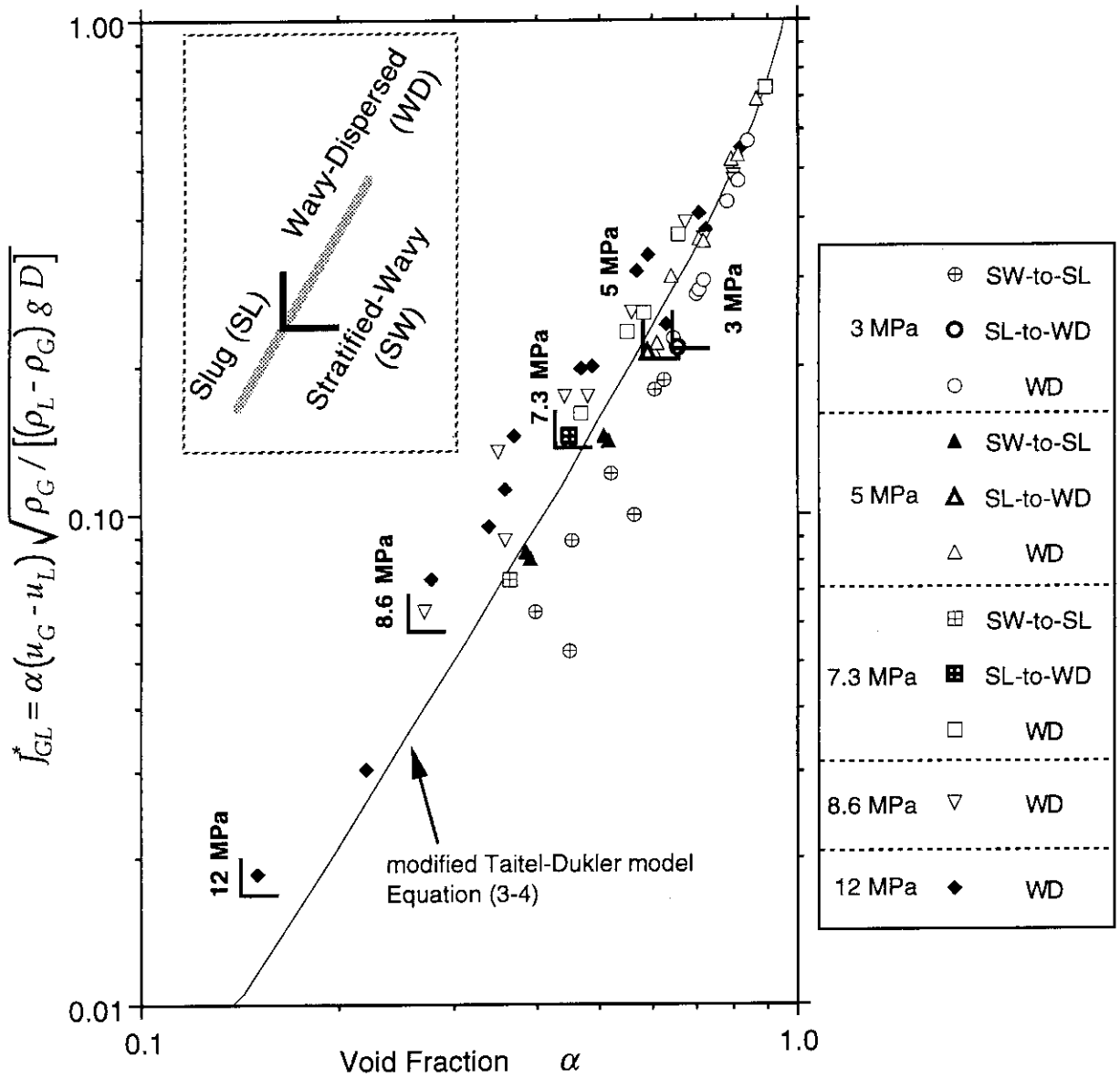

Fig. 6-2 TPTF Data for Transition Boundaries around Slug Flow and Wavy-Dispersed Flow (3, 5, 7.3, 8.6, 12 MPa)

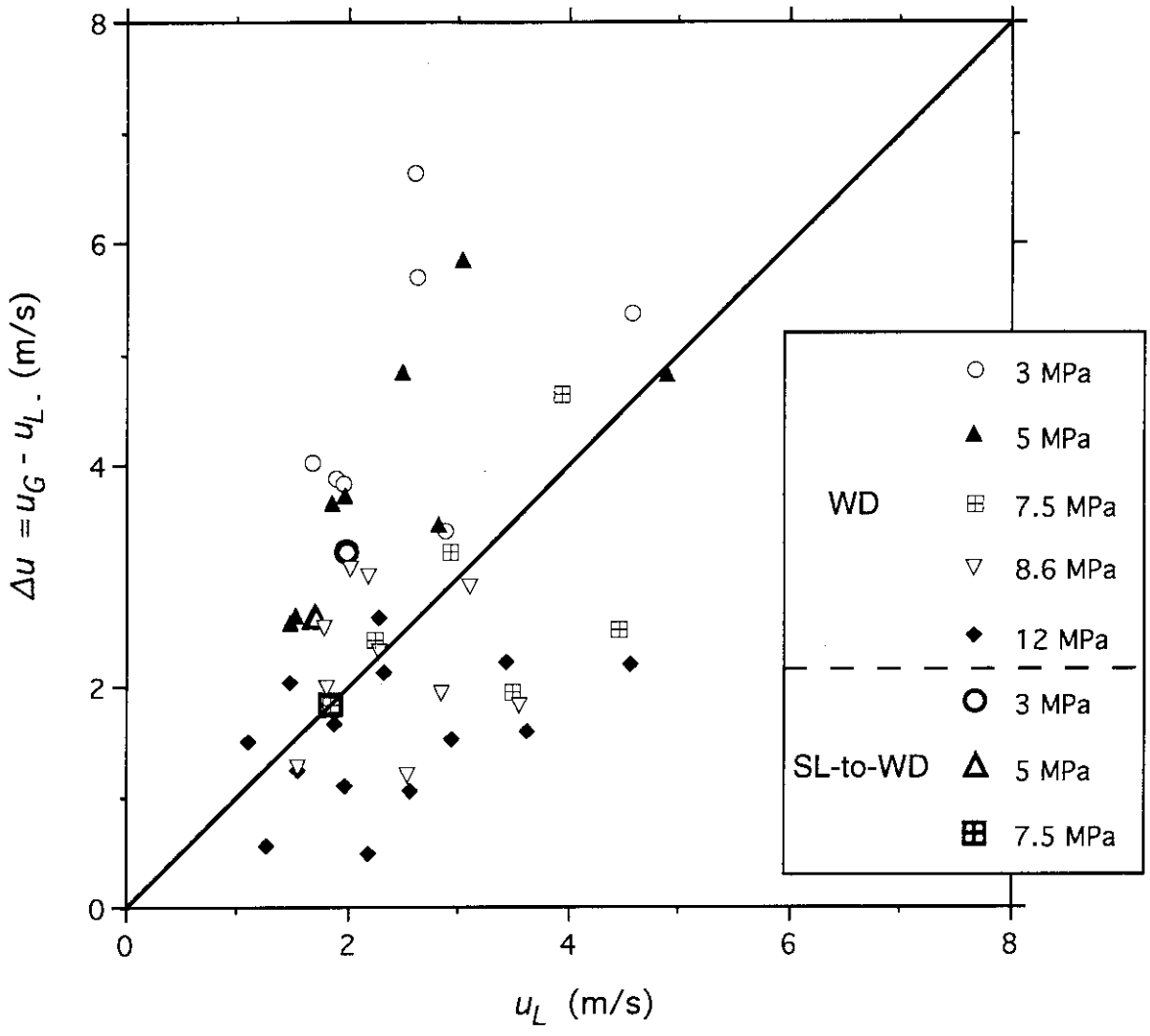

Fig. 6-3 Comparison of Gas-Liquid Relative Velocity (3, 5, 7.3, 8.6 and 12 MPa)

The Kelvin-Helmholtz (K-H) instability plays an important role in the formation and growth of interfacial waves as shown in **Chapters 1** and **3**, and the SW-to-SL flow regime transition condition is presented by an equation

$$\Delta u \geq C \sqrt{\frac{(\rho_L - \rho_G) g h_G}{\rho_G}} \quad . \tag{6-1}$$

The modified Taitel-Dukler model can be reduced to this form with $C \approx \alpha$. Given a certain liquid level, SL flow regime develops when Δu satisfies the **inequality (6-1)**. Based on observation and discussion above, the SL-to-WD flow regime transition is considered to take place at a value of Δu where the liquid entrainment occurs. Therefore, the critical value of Δu for the onset of liquid entrainment is larger than the critical value for slugging.

Barnea and Taitel (1993) recently showed that the K-H interfacial instability results in liquid slugs or roll waves depending on the void fraction. This work supports the idea of Taitel and Dukler that their model to predict the transition to SL flow regime also predicts the transition to annular flow. The good agreement of the TPTF data with the Taitel-Dukler model in **Fig. 6-2** suggests that the wave generation by the K-H instability is a necessary step for the onset of liquid entrainment. However, the pressure-dependence of the minimum void fraction for the onset of liquid entrainment suggests the existence of some additional mechanisms that induce the liquid entrainment.

6. 3 Applicability of Models and Correlations for Onset of Entrainment

The onset of liquid entrainment was observed at the wave crest of interfacial waves in the TPTF experiments. Ishii and Grolme (1975) predicted the onset of liquid entrainment in thin liquid film flows assuming that shearing-off of roll waves is the dominant mechanism. Because of this assumption, the Ishii-Grolme model has the gas-liquid relative velocity Δu in the velocity term and

includes liquid phase dynamic viscosity μ_L. The criterion obtained for rough turbulent film flows (Re_L > 1500-1750) is,

$$\frac{\mu_L \Delta u}{\sigma}\sqrt{\frac{\rho_G}{\rho_L}} = \sqrt{1+300\frac{\delta}{D}}\ N_\mu^{0.8}, \tag{6-2}$$

$$N_\mu = \frac{\mu_L}{\sqrt{\rho_L T\sqrt{\frac{T}{g(\rho_L-\rho_G)}}}}, \tag{6-3}$$

where T is the surface tension and δ is the film thickness [McCarthy et al. 1979]. The parameter N_μ is the viscosity number and is obtained by replacing droplet diameter d in the Ohnesorge number $On = \frac{\mu_L}{\sqrt{\rho_L T d}}$ with the Laplace coefficient $La = \sqrt{\frac{T}{g(\rho_L-\rho_G)}}$. The Ohnesorge number has been used to describe breakup of liquid droplets by surrounding gas stream [Miesse 1955, Tanrnogrodzki 1993]. The Laplace coefficient is based on the critical wave length for the Taylor instability. The viscosity number N_μ is a property group. Its value for the TPTF experiments, however, is far smaller than those for the experiments on which the Ishii-Grolme model is based as shown in **Fig. 6-4**.

The term $\sqrt{1+300\frac{\delta}{D}}$ in **Equation (6-2)** came from the Wallis correlation for interfacial friction factor for rough wavy film flow [Wallis 1969],

$$f_i = 0.005\sqrt{1+300\frac{\delta}{D}}. \tag{6-4}$$

This correlation, however, does not fit to the deep-water flow in the TPTF experiments. **Equation (6-2)** was thus modified as follows, by deleting this term and adjusting the exponent of the viscosity number to obtain the best fit to the TPTF data as shown in **Fig. 6-4**,

$$\frac{\mu_L \Delta u}{T}\sqrt{\frac{\rho_G}{\rho_L}} = N_\mu^{0.85}. \tag{6-5}$$

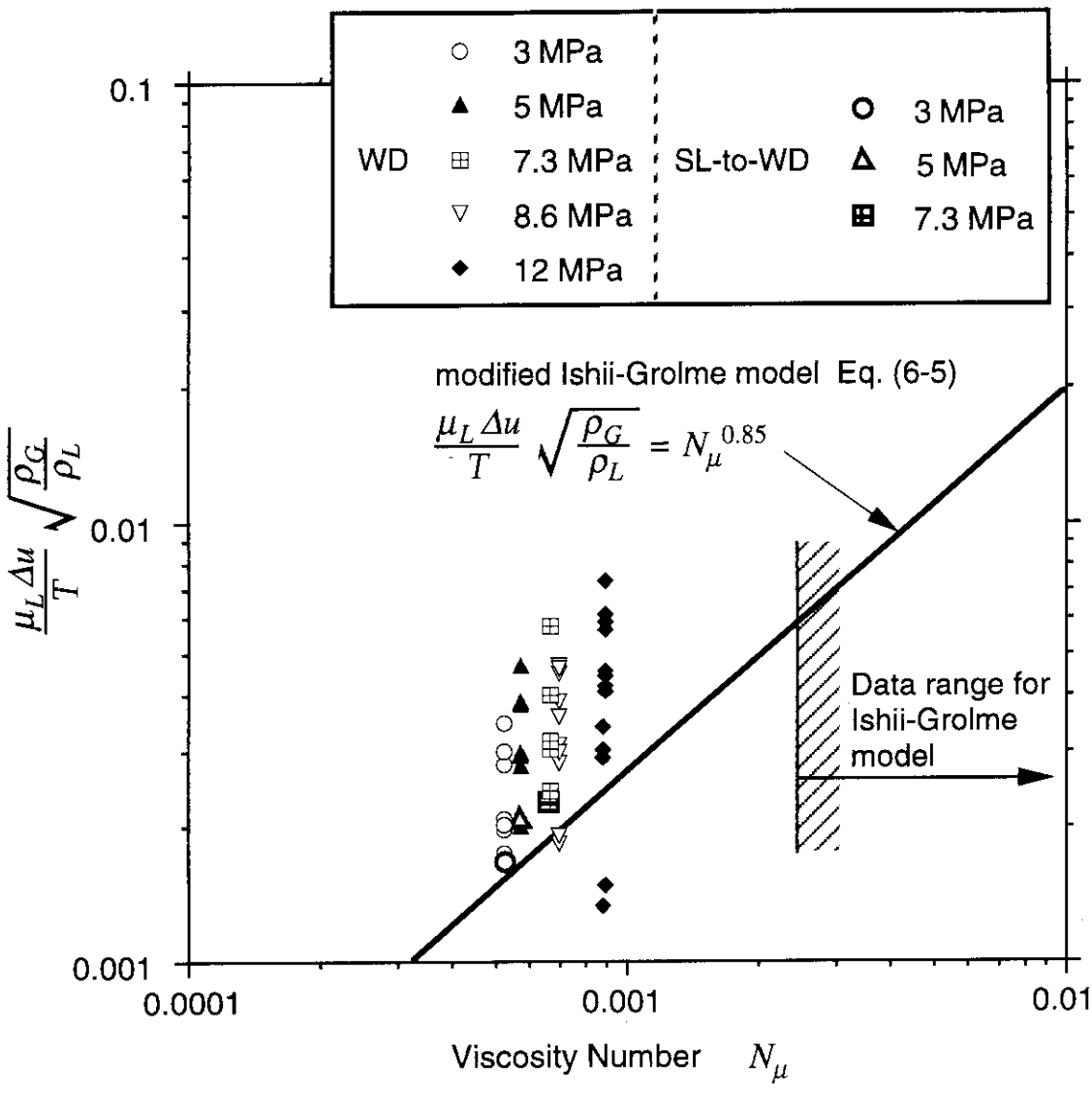

Fig. 6-4 Comparison of TPTF Data with modified Ishii-Grolme Model for Onset of Entrainment

The modified Ishii-Grolme model overestimated the critical value of Δu for pressures > 8.6 MPa, and was inconsistent to the pressure dependence of the TPTF data. As has been pointed out by Wallis (1969), furthermore, the influence of μ_L on the liquid entrainment, which is important for film flows, should be negligible for deep-water flow. Note that the increased exponent on N_μ in the modified Ishii-Grolme model means smaller influence of μ_L on Δu than the original Ishii-Grolme model.

Steen and Wallis (1964) proposed an empirical correlation based on their vertical annular flow experiments, which includes the gas phase dynamic viscosity μ_G, rather than μ_L;

$$\frac{\mu_G J_G}{T}\sqrt{\frac{\rho_G}{\rho_L}} = 0.000246. \tag{6-6}$$

They claimed that the effect of μ_L becomes unimportant when the liquid flow rate exceeded a certain critical value. The correlation gave the critical value of the superficial gas velocity J_G. The correlation, however, underestimated the critical value of J_G for the TPTF experiments as shown in **Fig. 6-5**. In the TPTF experiments, the high liquid level caused the gas velocity u_G to be much larger than J_G unlike the Steen-Wallis annular flow experiments. The Steen-Wallis parameter (l.h.s. of **Equation (6-6)**) was thus modified by replacing J_G with Δu;

$$\frac{\mu_G \Delta u}{T}\sqrt{\frac{\rho_G}{\rho_L}} \quad . \tag{6-7}$$

The modified parameter correlates the TPTF data well with a critical value of 0.0004 as shown in **Fig. 6-6**,

$$\frac{\mu_G \Delta u}{T}\sqrt{\frac{\rho_G}{\rho_L}} = 0.0004. \tag{6-8}$$

The obtained correlation underestimates the critical Δu for the low-pressure (3 MPa) cases. This trend, however, is consistent with the observation that the wave amplitude of interfacial waves increased as the system pressure was decreased. The larger wave amplitudes effectively decreases the critical values of

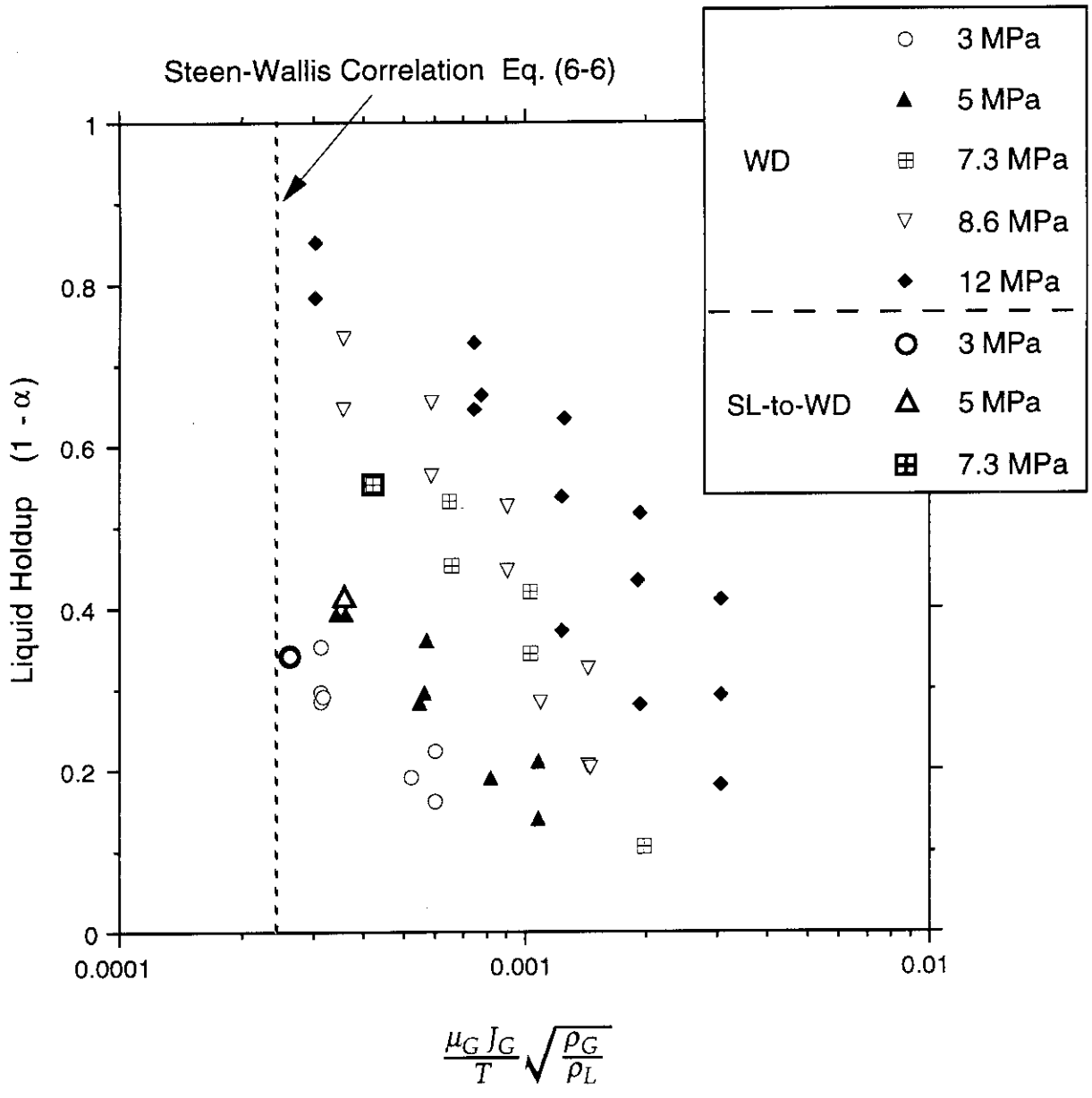

Fig. 6-5 Comparison of TPTF data with
Steen-Wallis Correlation for Onset of Entrainment

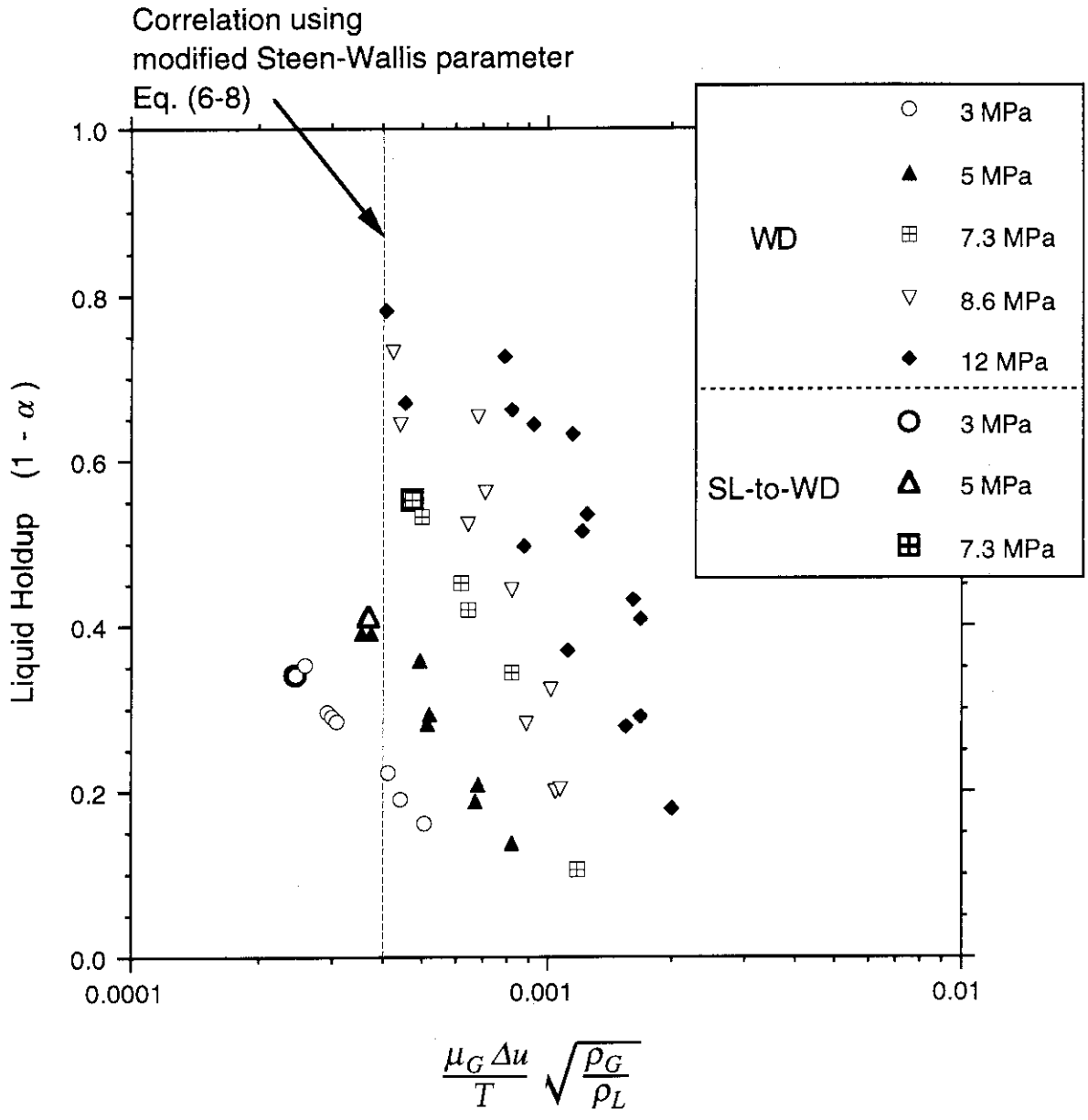

Fig. 6-6 Comparison of TPTF data with modified Steen-Wallis Parameter for Onset of Entrainment

Δu at the wave crests. The influences of the interfacial wave amplitudes are thus necessary to be taken into account for the better prediction.

Recently Liebert et al. (1993) developed a correlation based on the data from the UPTF and IVO experiments which are full-scale models of a U-shaped loop seal piping of the PWR primary loop. The UPTF and IVO experiments simulated steam/water flows at system pressures < 1.5 MPa and atmospheric air/water flows, respectively. The critical conditions for the onset of liquid entrainment was obtained from the measurement of the gas flow rate and the residual liquid level in the loop seal horizontal section. The liquid was stagnant in the bottom of the section. The modified gas-phase Kutateladze number,

$$Ku_{mod} = u_G \sqrt{\frac{\rho_G}{\sqrt{T\, g\,(\rho_L - \rho_G)}}} \sqrt{\frac{\mu_L}{\mu_G}} = Ku_G \sqrt{\frac{\mu_L}{\mu_G}}\ , \tag{6-9}$$

was found to correlate both steam/water and air/water data. This Liebert correlation; Ku_{mod} = ~20, is compared with the TPTF data in **Fig. 6-7**. The deviation of the UPTF/IVO data towards lower u_G for liquid holdup > ~0.5 is said to be because of the de-entrainment of liquid droplets in the upward vertical piping part. As shown in **Fig. 6-7**, the liquid entrainment occurred at Ku_{mod} < 20 in the TPTF experiments that were conducted at much higher pressures than in the UPTF/IVO experiments.

The correlation ignored the influence of liquid velocity u_L because the correlation is based on the experiments conducted with stagnant liquid phase. Since u_L was even larger than Δu in the TPTF experiments as shown in **Fig. 6-3**, the correlation was modified by replacing u_G with Δu, for comparison with the TPTF data in **Fig. 6-8**,

$$Ku_{mod,\ \Delta u} = \Delta u \sqrt{\frac{\rho_G}{\sqrt{T\, g\,(\rho_L - \rho_G)}}} \sqrt{\frac{\mu_L}{\mu_G}}\ . \tag{6-10}$$

The bounding value is $Ku_{mod,\ \Delta u}$ = ~8 for system pressures ≤ 5 MPa and tends to decrease down to ~5, as the system pressure is increased to 12 MPa. **Figure 6-8**

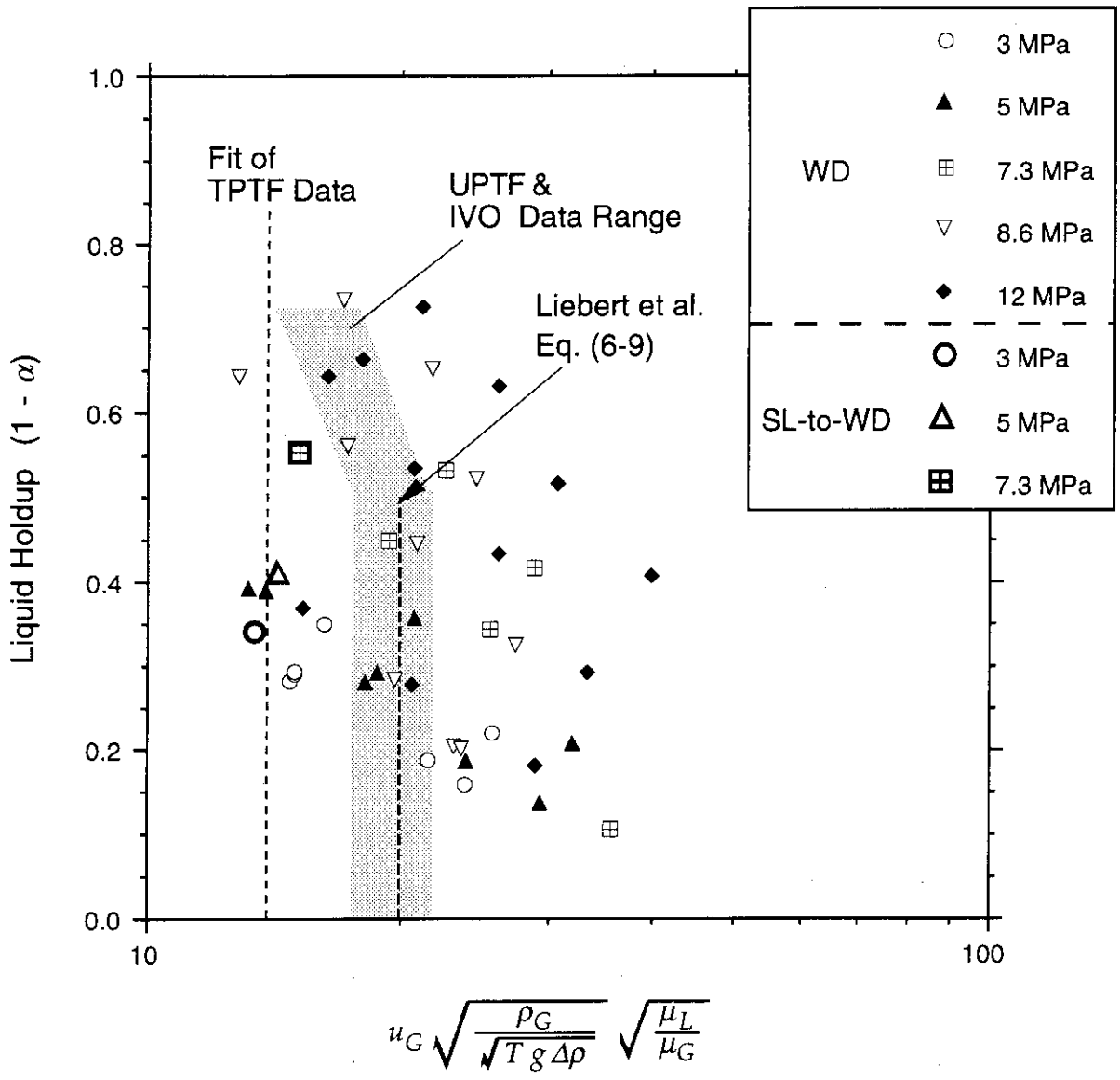

Fig. 6-7 Comparison of TPTF data with
Liebert et al. Correlation for Onset of Entrainment

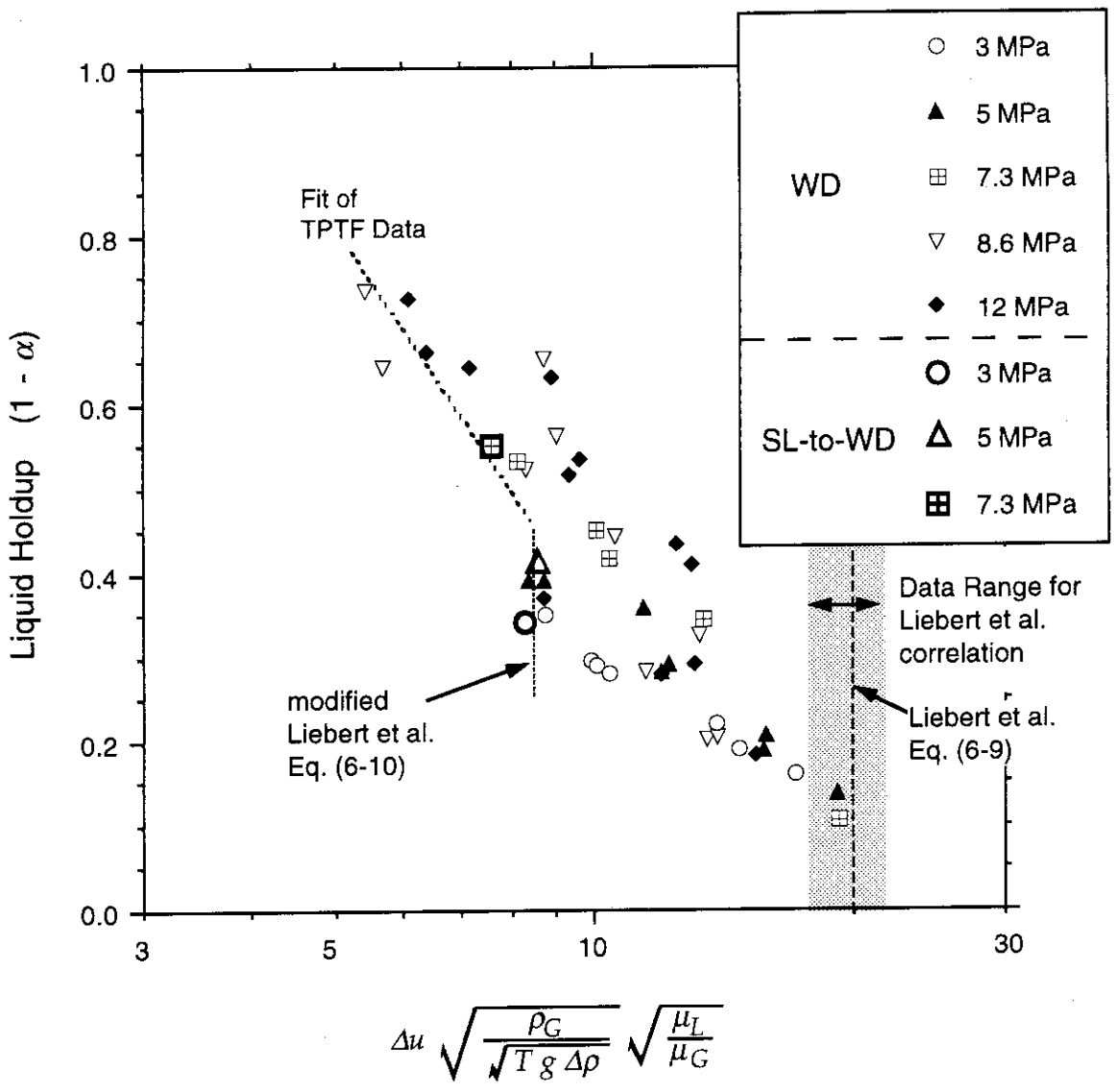

Fig. 6-8 Comparison of TPTF data with
Modified Liebert et al. Correlation for Onset of Entrainment

shows that the modified parameter does not well correlate the TPTF data. Furthermore, the incorporation of the gas and liquid viscosities into the correlation does not seem to have physical meaning in the context of the discussion above.

6.4 Predictive Capability of the Correlations Obtained in the Present Study

The correlations and modified-models that have been obtained in the present study can provide the SW-to-SL and SL-to-WD transition boundaries for fully-developed steam/water two-phase flows in a horizontal pipe at a given system pressure. The transition boundaries are obtained by combining the newly obtained correlations and modified-models, through an iterative procedure as follows. The predictive capability of the newly obtained correlations and modified-models is evaluated by comparing them with the present TPTF data.

1) Specify the flow conditions such as the system pressure P, the gas superficial velocity J_G and the pipe diameter D. Obtain the physical properties of the saturated fluid from the steam table, such as the densities ρ_k, the viscosities μ_k and the liquid surface tension T, based on P.

2) Assume the normalized liquid level h_L/D, and obtain the interfacial width S_i, the phase perimeters S_k, the phase cross section A_k, the phase hydraulic diameters D_k, the void fraction α and the gas-phase average velocity u_G, and Reynolds number Re_G.

3) Calculate the gas-liquid relative velocity Δu using **Equation (3-16)** for the SW-to-SL flow regime transition, or **Equation (6-8)** for the SL-to-WD flow regime transition, and obtain the average velocity u_L and the Reynolds number Re_L of the liquid flow. The exponent for the coefficient of **Equation (3-16)** is applied as $n = 1$, except for 8-inch flows at system pressures ≤ 3 MPa where $n = 2$.

4) Obtain the interfacial friction factor f_i from **Equation (4-2)** using the phase wall friction factor f_k calculated from the Blasius correlation and the phase wall

shear stress τ_k calculated from **Equation (A2-3)**.

5) Calculate the interfacial friction factor f_i for SW flow regime in the vicinity of the SW-to-SL flow regime transition using **Equation (4-6)**. If the obtained value is different from that obtained in step (4), iterate the procedure from step (2) with a new value of h_L/D until f_i by **Equation (4-6)** agrees with that by **Equation (4-2)** within a tolerable limit.

6) Calculate the superficial velocities J_k, using the obtained value of h_L/D.

Figures 6-9 (a) and **(b)** compare the present TPTF data with the calculated flow regime transition boundaries in terms of J_k, for system pressures of 3 and 8.6 MPa, respectively. Note that the calculated J_L for the SL-to-WD flow regime transition boundary might be underestimated, since **Equation (4-6)** underestimates f_i for WD flow regimes.

As shown in **Fig. 6-9 (a)**, the SW-to-SL transition data for both 4- and 8-inch pipes agree well with the calculated transition boundary for flows at 3 MPa. The agreement between the data and the prediction for the SL-to-WD transition is also good, considering that the newly obtained correlation (**Equation (6-8)**) overestimates the transition boundary data as previously shown in **Fig. 6-6**. The predictions agree well with the present data also for flows at system pressure of 8.6 MPa as shown in **Fig. 6-9 (b)**. The SW flow data (J_G = 2.10 m/s) close to the SW-to-SL boundary confirms that the wave generation by the K-H instability is a necessary step for the onset of liquid entrainment as found in **Section 6. 2. 2**.

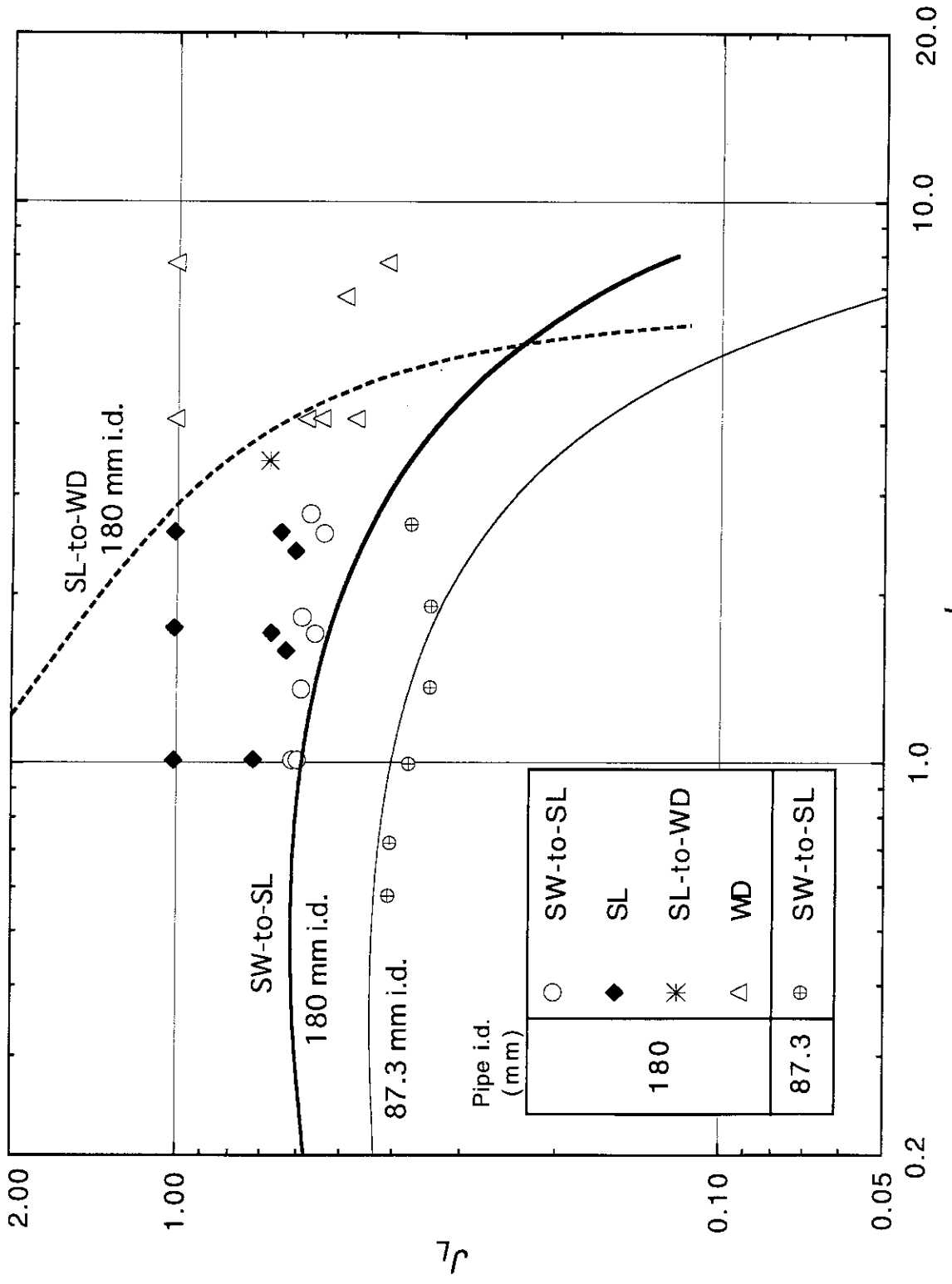

Fig. 6-9 (a) Comparison of TPTF Data with Predictions (3 MPa)

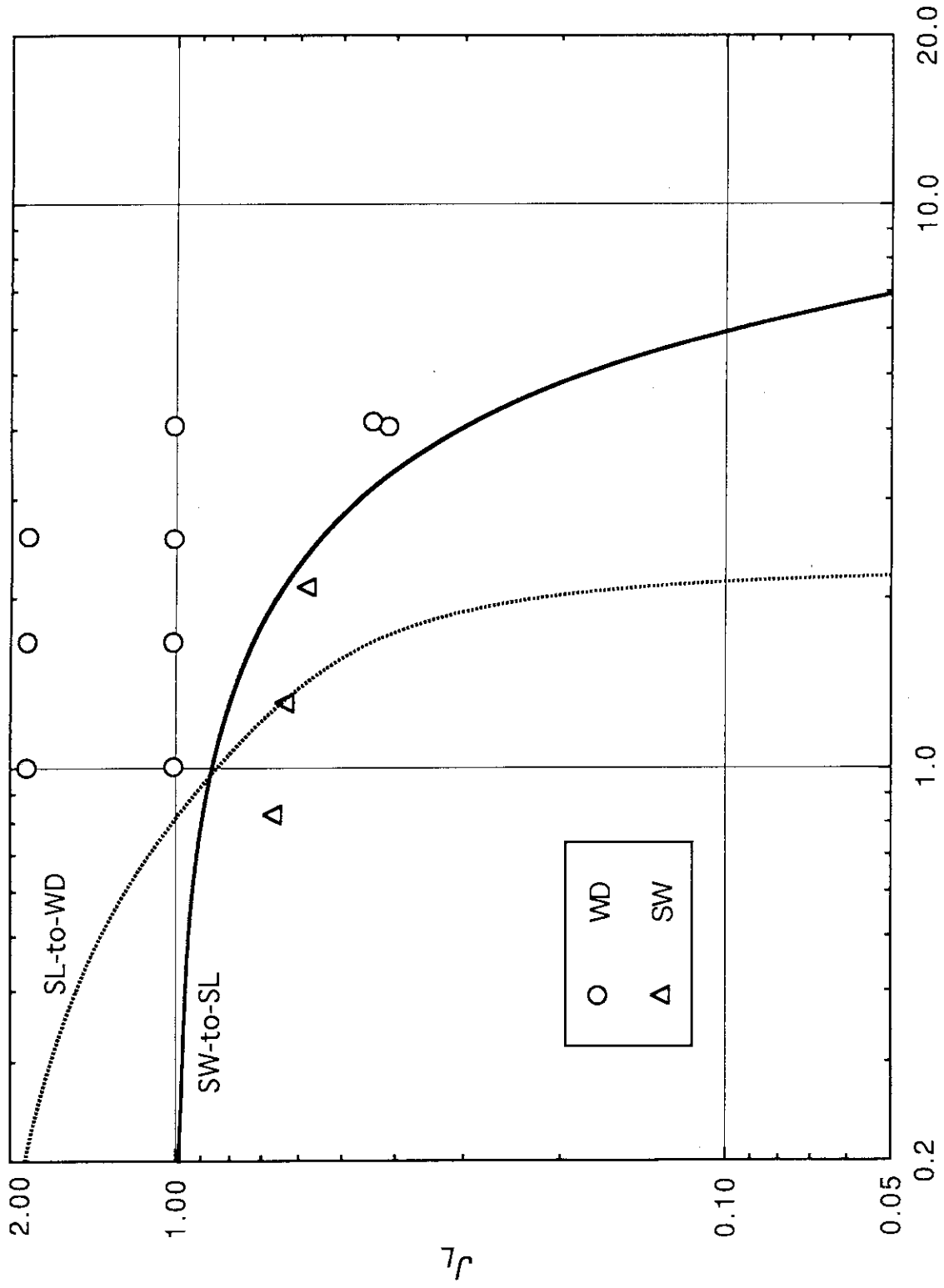

Fig. 6-9 (b) Comparison of TPTF Data with Predictions (180 mm i.d., 8.6 MPa)

6. 5 Conclusions

The pressure dependence of the flow regime transition from SL to WD flow regime was investigated in the TPTF steam/water flow experiments for system pressures up to 12 MPa, based on the video probe visual observation. The previous models and correlations to predict the onset of liquid entrainment were examined against the TPTF data. The obtained conclusions are as follows.

(1) The gas-liquid relative velocity $\Delta u = u_G - u_L$ is the controlling parameter to predict the onset of liquid entrainment. The critical value of Δu for the onset of liquid entrainment decreases significantly when the system pressure is increased. This same parameter Δu also controls the occurrence of the SW-to-SL flow regime transition (i.e., slugging), and its critical value decreases with the increase in the system pressure, but increases with the void fraction. At a given system pressure, therefore, the liquid entrainment may initiate with Δu lower than that for slugging when the void fraction is high enough. The liquid entrainment suppresses the interfacial wave growth into liquid slugs. As the system pressure is raised, the liquid entrainment predominates even at low void fractions since the critical value of Δu to start liquid entrainment decreases with the system pressure more significantly than that for slugging. This explains the TPTF experimental results that the slug flow regime becomes non-observable for the system pressure above about 8.6 MPa.

(2) The Steen-Wallis parameter correlates the TPTF data for the onset of liquid entrainment well when the gas-phase superficial velocity J_G is replaced with Δu (**Equation (6-8)**). The influences of the interfacial wave amplitudes are necessary to be taken into account for the better prediction.

(3) The obtained correlations and modified-models in the present study show good predictive capability for both the SW-to-SL and SL-to-WD flow regime transition boundaries within the test condition ranges of the present experiments.

7. Conclusions

The present thesis has described the results of an experimental study on the mechanisms of the stratified-wavy to slug (SW-to-SL) flow regime transition[1)] and the related phenomena in gas/liquid two-phase flows through horizontal channels.

The SW-to-SL flow regime transition causes significant increase in pressure drop along the channel and interphase heat exchange. The flow intermittency of the resulting slug flow causes large fluctuation in gas and liquid flow rates and system pressure around the channel. The prediction of this flow regime transition was thus considered important for engineering applications and safety analysis for nuclear water reactors in connection with LOCAs and transients. This was the motivation of the present study.

In the present study, the dependence of this transition on channel height (pipe diameter) and system pressure was investigated. Fluid physical properties such as density, viscosity and surface tension change significantly depending on system pressure for steam/water two-phase flows. A wide range of these parameters was covered, far beyond the previous studies, to improve the predictive capabilities under flow conditions typical of nuclear reactors. For this purpose, experiments for high-pressure (up to 12 MPa) steam/water flows were performed in the TPTF large-diameter (up to 180 mm) pipe test sections, and air/water flow experiments were performed in a large-height (0.7 m) duct test section. The primary conclusions obtained from the present study are as follows. Labels S and A for the number of conclusions denote the conclusions from steam/water and air/water experiments, respectively.

---

1) This flow regime transition occurs when necessary conditions are satisfied for interfacial waves to grow into liquid slugs that block the entire flow cross-section. This process is termed "slugging".

(1) S, A The condition for the SW-to-SL flow regime transition was represented approximately by a general correlation in terms of non-dimensional time-averaged gas-liquid relative velocity J_{GL}^* and time-averaged void fraction α (or liquid height). Slugging occurred when J_{GL}^* became equal to or larger than a specified critical value presented as a function of α.

(2) S, A There was a tendency for the SW-to-SL flow regime transition at system pressures ≤ 3 MPa that J_{GL}^* with a fixed void fraction α decreased with channel height. This tendency can be explained consistently if the normalized critical wave height is assumed to increase with channel height for a given value of J_{GL}^* and α. Based on this tendency, a new correlation to predict the transition for relatively-low pressure flows in large-diameter pipes was obtained as

$$u_G - u_L \geq \left(1 - \frac{h_L}{D}\right)^n \sqrt{\frac{\left(\rho_L - \rho_G\right) g \cos\theta A_G}{\rho_G dA_L / dh_L}} \quad , \tag{3-16}$$

modifying the coefficient of the Taitel-Dukler model.

(3) S, A The SW-to-SL flow regime transition in the present experiments conducted in large-height channels occurred at much higher liquid superficial velocity J_L than in smaller-scale experiments conducted by previous investigators. For a systematic interpretation of such tendency, the use of non-dimensional fluid velocity J_L^* with a parameter $\sqrt{D}$ accounted well not only for the influences of the channel height (scale effects), but also of the system pressure.

(4) S The gas-liquid relative velocity $\Delta u = u_G - u_L$ correlates the transition condition much better than the gas velocity u_G by itself. Such use of u_G by itself neglecting the contribution of u_L has been the convention taken by almost all the previous models and correlations. The improvement is significant for high-pressure (≥ 5 MPa) steam/water flows in a large-diameter horizontal pipe where

the liquid velocity u_L in the SW regime becomes comparable to u_G.

(5) S The relative velocity Δu and void fraction α at given flow rates depend on gas/liquid interfacial friction. The interfacial friction in SW flow is thus one of critical parameters in the prediction of the SW-to-SL flow regime transition, and is enhanced by the size of interfacial waves. A new empirical correlation,

$$\frac{f_i}{f_G} = \left(\sqrt{3}\, \frac{\lambda_0}{D_G} \cdot \frac{u_G - u_L}{\Delta u_{\min}} \right)^{-8/5}, \tag{4-6}$$

was developed for the interfacial friction factor f_i, based on the experimental observation that interfacial waves in SW flow became greater and more irregular as the transition condition was approached. The correlation includes two non-dimensional parameters: the ratio of the gas-phase hydraulic diameter to the critical wave length for the Kelvin-Helmholtz (K-H) instability, and the ratio of Δu to the critical velocity for the K-H instability. The correlation represents the dependence of f_i on system pressure and pipe diameter well within the present experimental ranges.

(6) A As wave crest of interfacial waves comes close to the channel top wall, the gas phase pressure decreased significantly around the wave crest. The pressure drop in the upstream side of the crest became comparable to the water static head after the wave had grown, causing a net lift force which would contribute to the growth of wave. The pressure drop, however, was significant only in the vicinity of the wave crest. The decreased gas phase pressure was found to be non-recoverable in the downstream side of the wave crest, in particular for large-height waves. This occurred probably because of the separation of gas phase flow from the wave surface. The irreversible pressure drop resulted in an axial pressure difference across the wave crest. This may have contributed to wave growth further by thrusting the wave.

(7) S, A Significant liquid entrainment was observed to occur at wave crests at high gas flow rates. The occurrence of such entrainment had an effect to suppress the wave growth by blowing off the wave crests. Since the gas-liquid relative velocity Δu to cause slugging increases with void fraction, the liquid entrainment started earlier than slugging at sufficiently high void fractions. Furthermore, the critical value of Δu for the onset of liquid entrainment was found to decrease more significantly than that for slugging, when system pressure was raised. As the pressure was raised, therefore, the liquid entrainment became dominant even at low void fractions, and prevented slugging from occurring. This explains the TPTF experimental result where the slug flow regime became non-observable at system pressures ≥ 8.6 MPa.

(8) S The onset of liquid entrainment in the present steam/water experiments was well predicted with the use of the Steen-Wallis parameter, when it was modified as

$$\frac{\mu_G \Delta u}{T}\sqrt{\frac{\rho_G}{\rho_L}} = 0.0004 \qquad (6\text{-}8)$$

with Δu instead of the gas superficial velocity J_G. For future refinement of this correlation, the dependence of interfacial wave height on flow parameters should be taken into account.

(9) S The obtained correlations and modified-models in the present study, noted as three equations above, showed good predictive capability for the SW-to-SL and SL-to-WD flow regime transitions. Within the present experimental ranges for steam/water two-phase flows, these correlations and models defined a region of slug flow regime consistently taking account of the influences of the system pressure and channel height on the transitions.

Acknowledgment

The author would like to express his sincere appreciation to late Professor Kanji TASAKA of the Department of Energy Engineering and Science, Nagoya University. The present study was initiated by his advice, and he spared no effort to guide and encourage the author to pursue the present study based on the experiments that required a lot of large scale fabrication and special instrumentation. Until very close to his decease on February 14, 1995, he had given critical advises towards the completion of the present thesis.

The author would like to thank Professor Kojiro NISHINA, former Professor Akira KANAGAWA and Professor Ichiro YAMAMOTO of the Department of Nuclear Engineering, Dr. Masayoshi TAMAKI of the Department of Energy Engineering and Science, and Professor Hideomi FUJITA of the Department of Mechanical Engineering, Nagoya University, for their critical reading, suggestions and comments which were indispensable to improve and complete the present thesis.

The author would like to thank Professors Kenji MORITA of the Department of Crystalline Material Engineering, Nagoya University, for his advice and encouragement.

The author is greatly indebted to Dr. Toshio FUJISHIRO, Director of the Department of Reactor Safety Research, Dr. Atsuo KOHSAKA, former Director of the Department of Reactor Safety Research and Mr. Akira MATSUMOTO, former Head of Office of Safety and Control of Japan Atomic Energy Research Institute (JAERI) for their encouragement and giving me the opportunity to apply to the doctoral course in Nagoya University.

The author wishes to extend his best gratitude to Dr. Yutaka KUKITA, Head of the Thermohydraulic Safety Engineering Laboratory in JAERI, for his guidance and supervision for the present thesis work and his continuous encouragement.

The author would like to express his gratitude to his colleagues in JAERI, including Dr. Yoshinari ANODA, Principal Research Engineer, Mr. Hideo MURATA, Deputy General Manager and Mr. Masaya KONDO, Research Engineer for their valuable discussion and encouragement, and members of Nuclear Engineering Corp. and ITJ Corp. for their great help in performing both steam/water and air/water two-phase flow experiments and processing the data.

References

Akagawa, K.: *気液二相流*, コロナ社 (1974) (in Japanese).

Andritsos, N., Bontozoglou, V. and Hanratty, T.J.: "Transition to Slug Flow in Horizontal Pipes" Chem. Eng. Comm. 118 (1992) 361-385.

Andritsos, N. and Hanratty, T.J.: "Influence of Interfacial Waves in Stratified Gas-Liquid Flows" AIChE J. 33 (1987) 444-454.

Anoda, Y., Kukita, Y., Nakamura, H. and Tasaka, K.: "Flow Regime Transition in High-Pressure Large-Diameter Horizontal Two-Phase Flow" 26th ASME/AIChE/ANS National Heat Transfer Conference, Philadelphia (1989).

Ahmed, R. and Banerjee, S.: "Finite Amplitude Waves in Stratified Two-Phase Flow: Transition to Slug Flow" AIChE J. 31 (1985) 1480-1487.

Asaka, H., Kukita, Y., Anoda, Y., Nakamura, H. and Tasaka, K.: "Improvement of TRAC-PF1 Interfacial Drag Model for Analysis of High-Pressure Horizontally-Stratified Two-phase Flow" J. Nucl. Sci. Technol. 28 (1991) 33-44.

Baker, O.: "Simultaneous Flow of Oil and Gas" Oil and Gas J. 53 (1954) 185-190.

Barnea, D. and Taitel, Y.: "Kelvin-Helmholtz Stability Criteria for Stratified Flow: Viscous versus Non-Viscous (Inviscid) Approaches" Int. J. Multiphase Flow 19 (1993) 639-649.

Benjamin, T.B.: "Gravity Currents and Related Phenomena" J. Fluid Mech. 31 (1968) 209-248.

Bird, R.B., Stewart W.E. and Lightfoot E.N.: *Transport Phenomena* John Wiley & Sons, Inc. (1960).

Chandrasekhar, S.: *Hydrodynamic and Hydromagnetic Stability* Oxford Univ. Press (1961).

Cheremisinoff, N.P. and Davis E.J.: "Stratified Turbulent-Turbulent Gas-Liquid Flow" AIChE J. 25 (1979) 48-56.

Chow, V.T.: *Open-Channel Hydraulics* McGraw-Hill (1959).

Cohen, L.S. and Hanratty, T.J.: "Effect of Waves at a Gas-Liquid Interface on a Turbulent Air Flow" AIChE J. 11 (1965) 138-144

Crowley, C.J., Wallis, G.B. and Barry, J.J.: "Validation of a One-Dimensional Wave Model for the Stratified-to-Slug Flow Regime Transition, with Consequences for Wave Growth and Slug Frequency" Int. J. Multiphase Flow 18 (1992) 249-271.

Dukler, A.E. and Taitel, Y.: "Flow Pattern Transition in Gas-Liquid Systems: Measurement and Modeling" in *Multiphase Science and Technology*, vol. 2 (ed. Hewitt, G.F., Delhaye, J.M. & Zuber, N.), Hemisphere (1986).

Ferschneider, G., Lagière, M., Bourgeois, T. and Fitremann, J.M.: "How to Calculate Two-Phase Flow of Gas and Oil in Pipe Lines" Pipe Line Industry 63 (1985) 33-39.

Fukano, T., Ito, A., Miyabe, K. and Takamatsu, Y.: "Liquid Films Flowing Concurrently with Air in Horizontal Duct (6th Report)" Trans. JSME (ser. B) 51 (1985) 503-512 (in Japanese).

Fukano, T. and Ousaka, A.: "Prediction of the Circumferential Distribution of Film Thickness in Horizontal and Near-Horizontal Gas-Liquid Annular Flows" Int. J. Multiphase Flow 15 (1989) 403-419.

Gardner, G.C.: "Onset of Slugging in Horizontal Ducts" Int. J. Multiphase Flow 5 (1979) 201-209.

Gardner, G.C.: "Co-Current Flow of Air and Water from a Reservoir into a Short Horizontal Pipe" Int. J. Multiphase Flow 14 (1988) 375-388.

Govier, G.W. and Aziz, K.: *The Flow of Complex Mixtures in Pipes*, Van Nostrand Reinhold Co. (1972).

Hanratty. T.J.: "Interfacial Instabilities caused by Air Flow over a Thin Liquid Layer" in *Waves on Fluid Interfaces*, Academic (1983) 221-259.

Hihara, E. and Saito, T.: "Slug Flow Transition in Horizontal Gas-Liquid Flow" Bull. JSME 27 (1984) 2771-2778.

Hori, K., Ueno, K. and Kawanishi K.: "大口径管内の気液二相流 (第2報: 水平並向流)" 22th National Heat Transfer Symp. of Japan C203 (1985) 356-358 (in Japanese).

Ishii, M.: *Thermo-fluid Dynamic Theory of Two-Phase Flow*, Eyrolles (1975).

Ishii, M. and Grolmes, M.A.: "Inception Criteria for Droplet Entrainment in Two-Phase Concurrent Film Flow" AIChE J. 21 (1975) 308.

Ishii, M. and Mishima, K.: "Droplet Entrainment Correlation in Annular Two-Phase Flow" Int. J. Multiphase Flow 32 (1989) 1835-1846.

Kataoka, I., Ishii, M. and Mishima, K.: "Generation and Size Distribution of Droplet in Annular Two-Phase Flow" J. Fluids Engng. 105 (1983) 230-238.

Kawaji, M., Anoda, Y., Nakamura, H. and Tasaka, K.: "Phase and Velocity Distributions and Holdup in High-Pressure Steam/Water Stratified Flow in a Large Diameter Horizontal Pipe" Int. J. Multiphase Flow 13 (1987) 145-159.

Kawaji, M., Lorencez, C., Ousaka, A. and Murao, Y.: "Evaluation of Interfacial Shear Stress in Stratified Flow in Rectangular Horizontal Duct" 30th National Heat Transfer Symp. of Japan, B123 (1993) 100-102 (in Japanese).

Kim, H.J.: "Local Properties of Countercurrent Stratified Steam-Water Flow" Ph.D. Dissertation, Dept. Mech. Engng., Northwestern Univ. IL (1983).

Kim, H.J., Lee, S.C. and Bankoff, S.G.: "Heat Transfer and Interfacial Drag in Countercurrent Steam-Water Stratified Flow" Int. J. Multiphase Flow 11 (1985) 593-606.

Koizumi, Y., Nakamura, H., Yamamoto, N. and Tasaka, K.: "Investigation of Horizontal Two-Phase Flow in Long and Large Diameter Pipe" Int. Conference on Mechanics of Two-Phase Flows, Taipei, R.O.C. (1989) 24-29.

Koizumi, Y., Yamamoto, N. and Tasaka, K.: "Air/Water Two-Phase Flow in a Horizontal Large-Diameter Pipe (1st report, Flow Regime)" Trans. JSME 56-532 (1990 a) 159-163 (in Japanese).

Koizumi, Y., Nakamura, H., Yamamoto, N. and Tasaka, K.: "Air/Water Two-Phase Flow in a Horizontal Large-Diameter Pipe (2nd report, Pressure Drop)" Trans. JSME 56-532 (1990 b) 3750-3755 (in Japanese).

Kocamustafaogullari, G., Smits, S.R. and Raji, J.: "Maximum and Mean Droplets Sizes in Annular Two-Phase Flow" Int. J. Heat Mass Transfer 37 (1994) 955-965.

Kordyban, E.S.: "Horizontal Slug Flow: A Comparison of Existing Theories" J. Fluids Engng. 112 (1990) 74-83.

Kordyban, E.S.: "Some Characteristics of High Waves in Closed Channels Approaching Kelvin-Helmholtz Instability" ASME J. Fluids Engng. 99 (1977) 339.

Kordyban, E.S.: "Experimental Study of Aerodynamic Pressure at the Wave Surface in Two-Phase Flow" in Basic Mechanisms in Two-Phase Flow and Heat Transfer, 19, ASME-Vol, November (1980).

Kordyban, E.S., and Ranov, T.: "Mechanism of Slug Formation in Horizontal Two-Phase Flow" ASME J. Basic Engng. 92 (1970) 857.

Kowalski, J.E.: "Wall and Interfacial Shear Stress in Stratified Flow in a Horizontal Pipe" AIChE J. 33 (1987) 274-281.

Kukita, Y., Anoda, Y., Nakamura, H. and Tasaka, K.: "Assessment and Improvement of RELAP5/MOD2 Code's Interphase Drag Models" 24th National Heat Transfer Conference, Pittsburgh (1987) 212-216.

Kukita, Y., Osakabe, M., Anoda, Y., Barrè, F., Nakamura, H. and Tasaka, K.: "Flooding at Steam Generator Inlet and Its Impacts on Simulated PWR Natural Circulation" ASME, FED-61/HTD-92 (1988) 111-117.

Kukita, Y., Nakamura, H., Anoda, Y. and Tasaka, K.: "Hot Leg Flow Characteristics during Two-Phase Natural Circulation in Pressurized Water Reactor" 4th Int. Topical Mtg. on Reactor Thermal Hydraulics (NURETH-4), Karlsruhe, F.R.G. (1989) 465 - 477.

Lee, S. C. and Bankoff, S. G.: "Local Heat Transfer Coefficients for Condensation in Stratified Countercurrent Steam-Water Flow" J. Heat Transfer, Trans. ASME 105 (1983) 713-718.

Liebert, J., Emmerling, R. and Weiss, P.: "Flow Phenomena during Full-Scale Loop Seal Clearing of a PWR" Proc. Euro. Two-Phase Flow Grp. Mtg., Hannover (1993).

Lin, P.Y. and Hanratty, T.J.: "Prediction of the Initiation of Slugs with Linear Stability Theory" Int. J. Multiphase Flow 12 (1986) 79-98.

Lockhart, R.W. and Martinelli, R.C.: "Proposed Correlation of Data for Isothermal Two-Phase, Two-Component Flow in Pipes" Chem. Eng. Prog. 45 (1949) 39.

Mandhane, J. M., Gregory, G. A. and Aziz, K.: "A Flow Pattern Map for Gas-Liquid Flow in Horizontal Pipes" Int. J. Multiphase Flow 1 (1974) 537.

McCarthy, G.E. and Lee, H.M.: "Review of Entrainment Phenomena and Application to Vertical Two-Phase Countercurrent Flooding" EPRI NP-1284 Project 1160-1 (1979).

Michell, J.H.: "The Heighest Waves in Water" Phil. Mag. 5 (1893) 430.

Miesse, C.C.: "Correlation of Experimental data on the Disintegration of Liquid Jets" Ind. Eng. Chem., 47 (1955) 1690-1701.

Milne-Thomson, L.M., Theoretical Hydrodynamics (5th ed.) Macmillan (1968).

Minato, A., Ikeda, T. and Naitoh, M.: "Mechanistic Model of Slugging Onset in Horizontal Circular Tubes" J. Nucl. Sci. Technol. 23 (1986) 761-768.

Mishima, K. and Ishii, M.: "Theoretical Prediction of Onset of Horizontal Slug Flow" ASME J. Fluids Engng., 102 (1980) 441.

Nakamura, H., Tanaka, M., Tasaka, K., Koizumi, Y. and Murata, H.: "System Description for ROSA-IV Two-Phase Flow Test Facility (TPTF)" JAERI-M 83-042 (1983).

Nakamura, H., Kawaji, M., Anoda, Y., Koizumi, Y. and Tasaka, K.: "Effect of Pressure on Slugging in Steam/Water Two-Phase Flow" 2nd. Int. Topical Mtg. on Nucl. Power Plant Thermal Hydraulics and Operations, Tokyo, vol. 1 (1986) 102-108.

Nakamura, H., Anoda, Y. and Kukita, Y.: "Flow Regime Transitions in High-Pressure Steam-Water Horizontal Pipe Two-Phase Flow" ANS Proc. of 1991 National Heat Transfer Conf., Minneapolis, (1991 a) 269-276.

Nakamura, H., Kondoh, M., Anoda, Y. and Kukita, Y.: "Horizontal Flow Regime Transition in a Large-Height Long Duct" Int. Conference on Multiphase Flows (ICMF) '91, Tsukuba, Japan, vol. 1 (1991 b) 11-14.

Nakamura, H., Murata, H., Itoh, H., Anoda, Y., Kumamaru, H. and Kukita, Y.: "Fiber-Optics Video Probes for Observation of High-Pressure High-Temperature Two-Phase Flow" J. Visualization Soc. Japan, 12 (1992) 47-56.

Nakamura, H., Kukita, Y. and Tasaka, K.: "An Evaluation of Bernoulli Effect on Slugging in Horizontal Two-Phase Flow" J. Nucl. Sci. Technol. 31 (1994) 113- 121.

Nakamura, H., Kukita, Y. and Tasaka, K.: "Flow Regime Transition to Wavy Dispersed Flow for High-Pressure Steam/Water Two-Phase Flow in Horizontal Pipe" J. Nucl. Sci. Technol. 32 (1995 a) 641-652.

Nakamura, H., Kukita, Y. and Tasaka, K.: "Interfacial Friction Factor for High-Pressure Steam-Water Stratified-Wavy Flow in Horizontal Pipe" J. Nucl. Sci. Technol. 32 (1995 b) 868-879.

Nydal, O.J., Pintus, S. and Andreussi, P.: "Statistical Characterization of Slug Flow in Horizontal Pipes" Int. J. Multiphase Flow 18 (1992) 439-453.

Ohnuki, A., Adachi, H. and Murao, Y.: "Scale Effects on Countercurrent Gas-Liquid Flow in a Horizontal Tube connected to an Inclined Riser" Nucl. Engng. Des. 107 (1988) 293-294.

Plate, E.J., *Turbulent Fluxes through the Sea Surface, Wave Dynamics, and Prediction* (ed. A. Favre & K. Hasselmann), Plenum (1977).

Pohlhausen, K.: "Zur Näherungsweisen Integration der Differentialgleichung der Laminaren Reibungsschicht" Zeit. Ang. Math. und Mech. 1 (1921) 252-268.

Ranson, V. H. et al.: "RELAP5/MOD2 Code Manual" NUREG/CR-4312, EGG-2396, rev. 1 (1987).

Rogovin, M. et al.: "Three Mile Island, A Report to the Comissioners and the Public" NUREG/CR-1250 (1980)

ROSA-IV Group: "ROSA-IV Large Scale Test Facility (LSTF) System Description" JAERI-M 84-237 (1984).

ROSA-IV Group: "ROSA-IV Large Scale Test Facility (LSTF) System Description for Second Simulated Fuel Assembly" JAERI-M 90-176 (1990).

Safety Code Development Group: "TRAC-PF1/MOD1 Code Manual" NUREG/CR-3567, LA-9944-MS (1984) .

Sakaguchi, T. et al.: "Transient Behavior of Flow Pattern for Air-Water Two-Phase Flow in Horizontal Tubes" Theoretical and Appl. Mech. 26 (1978) 445-459.

Scott, S.L., Shoham, O. and Brill, J.P.: "Modeling Slug Growth in Large Diameter Pipes" 3rd. Int. Conf. on Multi-phase Flow, Hague, Netherlands (1987) 55-63.

Schlichting, H.: *Boundary-Layer Theory* (sixth ed., trans. by Kestin, J.), McGraw-Hill (1968)

Shoham, O. and Taitel, Y.: "Stratified Turbulent-Turbulent Gas-Liquid Flow in Horizontal and Inclined Pipes" AIChE J. 30 (1984) 377-385.

Simpson, H.C., Roony, D.H., Grattan, E. and Al-Samarrae, F.A.A.: "Two-Phase Flow in Large Diameter Horizontal Tubes" NEL Report No. 677 (1981).

Spedding, P.L. and Spence, D.R.: "Flow Regimes in Two-Phase Gas-Liquid Flow" Int. J. Multiphase Flow 19 (1993) 245-280.

Steen, D. and Wallis, G.B.: "The Transition from Annular to Annular Mist Co-Current Two-Phase Down Flow" AEC Rept. NYO-3114-2 (1964).

Taitel, Y. and Dukler, A.E.: "A Model for Predicting Flow Regime Transitions in Horizontal and Near Horizontal Gas-Liquid Flow" AIChE J. 22 (1976) 47-55.

Taitel, Y. and Dukler, A.E.: "A Model for Slug Frequency during Gas-Liquid Flow in Horizontal and Near Horizontal Pipes" Int. J. Multiphase Flow 3 (1977) 585-596.

Tanrnogrodzki, A.: "Theoretical Prediction of the Critical Weber Number" Int. J. Multiphase Flow 19 (1993) 329-336.

Tasaka, K.: "ROSA-IV Program for the Experimental Study on Small-Break LOCA's and the Related Transients in a PWR" 10th Water Reactor Safety Res. Inf. Mtg., Gaithersburg, USA (1982).

Ueda, T.: *気液二相流 - 流れと熱伝達 -* , 養賢堂 (1981), (in Japanese).

Wallis, G.B.: *One-dimensional Two-phase Flow,* McGraw-Hill (1969).

Wallis, G.B. and Dobson, J.E.: "The Onset of Slugging in Horizontal Stratified Air-Water Flow" Int. J. Multiphase Flow 1 (1973) 173.

Weisman, J., Duncan, D., Gibson. J and Crawford, T.: "Effects of Fluid Properties and Pipe Diameter on Two-Phase Flow Patterns in Horizontal Lines" Int. J. Multiphase Flow 5 (1979) 437-462.

Wu, H.L., Pots, B.F.M., Hollenberg, J.F. and Meerhoff, R.: "Flow Pattern Transitions in a Two-Phase Gas/Condensate Flow at High Pressure in an 8-inch Horizontal Pipe" 3rd. Int. Conf. on Multi-Phase Flow, Hague, Netherland (1987) 13-21.

Zuber, N.: "Problems in Modeling Small-Break LOCA" NUREG-0724 (1980).

Appendix-1 Flow Regimes in Horizontal Two-Phase Flow

Gas/liquid two-phase flows in a closed channel show various kinds of appearances, flow patterns, depending on the channel geometry, fluid properties and flow rates. Flow condition characterized by a flow pattern is termed a flow regime. Classification of flow regimes has been based generally on visual judgment of such flow patterns by the investigators. Therefore, many flow regimes have been reported in conjunction with flow regime maps [for horizontal flows: Baker 1954, Mandhane et al. 1974, Taitel et al. 1976, Weisman et al. 1979, Simpson et al. 1981, Spedding et al. 1993]. Typical flow patterns observed in this study are indicated in **Figs. 1-1** and **1-2**. Classification into flow regimes was performed following a method by Taitel et al. (1976), though some have names different from those by Taitel et al. Brief explanations of these flow regimes are as follows.

Stratified-smooth (SS) and stratified-wavy (SW) flow regime are categorized in separated (or stratified) flows where gas phase flows over liquid phase, being completely separated by a flat or wavy interface, respectively. Interfacial waves in the SW flow regime are considered to result from interaction between high-velocity gas stream flowing over liquid phase. Contribution of interfacial waves of SW flow regime for liquid conveyance is generally negligible.

Slug (SL) and plug (or elongated bubble) (PL) flow regimes are categorized in intermittent flows where liquid phase intermittently fill the entire channel cross-section as liquid slugs and plugs. For the PL flow regime, a train of large gas bubbles propagates along the upper ceiling of the channel, being separated by liquid plugs. There is very little gas entrainment in liquid plugs. Large gas bubbles are sometimes called elongated bubbles. In the SL flow regime, liquid slugs propagate intermittently being separated by stratified-smooth or stratified-wavy flows. In liquid slugs, usually many gas bubbles are entrained. Liquid slugs and

plugs convey liquid along with the flow. In this context, SL and PL flow regimes are not firmly distinguished in this study.

Wavy-dispersed (WD) and annular-dispersed (or annular mist) (AD) flow regimes are characterized by entrained liquid droplets flowing with high-velocity gas stream. Most of liquid phase flows at the bottom of the channel, with interfacial waves on the stream surface, and gas phase flows over it. In the AD flow regime, liquid film extends the entire periphery of pipe inner wall, while no firm liquid film exists on the wall in the WD flow regime. In air/water two-phase flows, annular (AN) flow regime with no liquid entrainment may appear.

The WD flow regime was not classified by Taitel et al., but is newly defined is the present study based on the visual observation of the TPTF high-pressure steam/water two-phase flows. Taitel et al. (1976) and Weisman et al. (1979) used a term "dispersed" to deal with gas entrainment dispersed in liquid stream as gas bubbles. In this study, "dispersed" implies liquid entrainment scattered in gas stream.

Appendix-2 Kelvin-Helmholtz Instability in a Horizontal Closed Channel

The Kelvin-Helmholtz instability for gas/liquid interface in a closed channel is obtained from a linear wave theory [Milne-Thomson 1968, Ueda 1981]. For a train of irrotational interfacial waves that propagate on horizontal interface along z-axis as illustrated in **Fig. A2-1**, the interfacial profile is assumed to be presented as

$$\eta = a \sin k\,(z - ct) \tag{A2-1}$$

where a is the wave amplitude, $k = 2\pi/\lambda$ is the wave number and c is the celerity of interfacial waves on stationary liquid surface. The linear wave assumption poses a condition $ka \approx 0$. The growth of such initially-presented interfacial waves for irrotational and inviscid two-dimensional flow is considered.

A form of velocity potential is first assumed as

$$\phi = -u\,z + X(y) \cos k\,(z - ct)\ . \tag{A2-2}$$

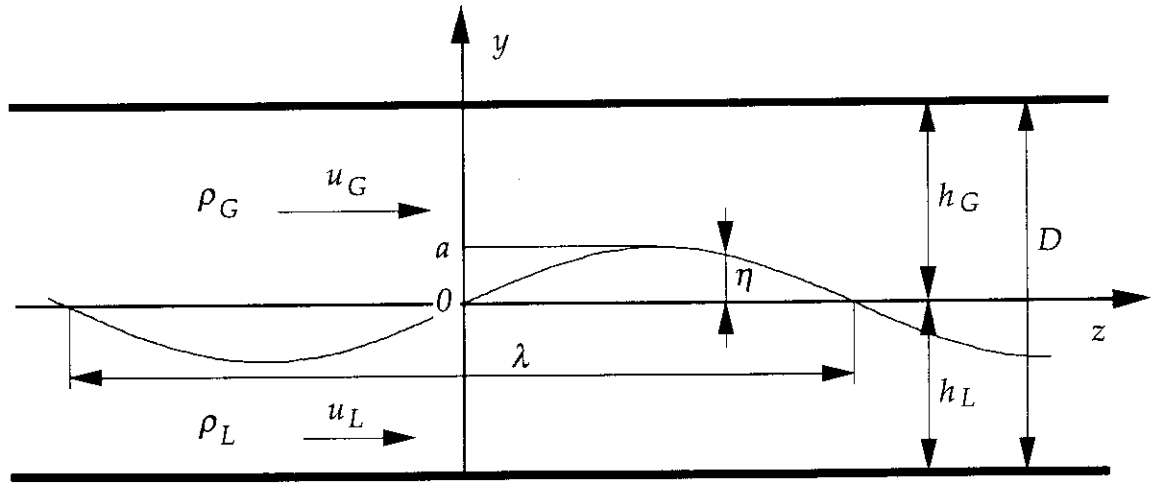

Fig. A2-1 Schematic of Interfacial Waves in Closed Channel

As a solution of Laplace equation; $\nabla^2 \phi = 0$, the velocity potential becomes

$$\phi = -u\,z + (A \cosh ky + B \sinh ky) \cos k(z - ct) \ . \qquad \text{(A2-3)}$$

For gas phase, kinematic boundary condition at the upper ceiling of the channel $-\left(\frac{\partial \phi_G}{\partial y}\right)_{y=h_G} = 0$ results in $B = 0$. Kinematic boundary condition at the gas/liquid interface is

$$-\left(\frac{\partial \phi_G}{\partial y}\right)_{y=\eta} = \frac{d\eta}{dt} = \frac{\partial \eta}{\partial t} + u_G \frac{\partial \eta}{\partial z} \ . \qquad \text{(A2-4)}$$

From **Equations A2-1, 3 and 4** and an assumption of $ka \approx 0$, velocity potential for gas phase becomes

$$\phi_G = -u_G z + a(u_G - c)\frac{\cosh k(h_G - y)}{\sinh k h_G} \cos k(z - ct) \ . \qquad \text{(A2-5)}$$

Similarly, velocity potential for liquid phase is obtained as

$$\phi_L = -u_L z - a(u_L - c)\frac{\cosh k(h_L + y)}{\sinh k h_L} \cos k(z - ct) \ . \qquad \text{(A2-6)}$$

The pressure (Bernoulli) equation for incompressive irrotational flow is

$$\frac{p}{\rho} + \frac{1}{2}\left[\left(\frac{\partial \phi}{\partial z}\right)^2 + \left(\frac{\partial \phi}{\partial y}\right)^2\right] + gy - \frac{\partial \phi}{\partial t} = C(t) \ , \qquad \text{(A2-7)}$$

where $C(t)$ is an instantaneous constant having the same value in the flow field under consideration. The phase pressures at interface are obtained by combining **Equations A2-5** or **6** with **A2-7** for gas and liquid phases respectively, as

$$p_{Gi} = -\rho_G\left[(u_G - c)^2 k \coth k h_G + g\right] a \sin k(z - ct) + p_0 \ , \qquad \text{(A2-8)}$$

$$p_{Li} = \rho_L\left[(u_L - c)^2 k \coth k h_L - g\right] a \sin k(z - ct) + p_0 \ , \qquad \text{(A2-9)}$$

where p_0 is the pressure on interface at rest. Because of surface tension T, pressure difference between gas and liquid phases at interface is

$$p_{Li} - p_{Gi} = - T \frac{\delta^2 \eta}{\delta z^2} \quad , \tag{A2-10}$$

when interface has a curvature of $- \frac{\delta^2 \eta}{\delta z^2}$. From **Equations A2-8, 9** and **10**, the equation that determines the velocity of interfacial wave propagation is obtained as

$$\rho_L (u_L - c)^2 \coth kh_L + \rho_G (u_G - c)^2 \coth kh_G = kT + \frac{g}{k}(\rho_L - \rho_G) \, , \tag{A2-11}$$

and the celerity of interfacial waves is given by

$$c = \frac{\rho_L u_L I_L + \rho_G u_G I_G}{\rho_L I_L + \rho_G I_G}$$

$$\pm \sqrt{\frac{1}{\rho_L I_L + \rho_G I_G} \left[kT + \frac{g}{k}(\rho_L - \rho_G) - \frac{\rho_L I_L \cdot \rho_G I_G}{\rho_L I_L + \rho_G I_G}(u_G - u_L)^2 \right]} \quad , \tag{A2-12}$$

where $I_L = \coth kh_L$ and $I_G = \coth kh_G$.

Interfacial waves become unstable when the root of **Equation A2-12** is negative. Stability condition for interfacial waves is thus presented by

$$(u_G - u_L)^2 \geq \frac{\rho_L I_L + \rho_G I_G}{\rho_L I_L \cdot \rho_G I_G} \left[kT + \frac{g}{k}(\rho_L - \rho_G) \right] \tag{A2-13}$$

Since deep-water waves on the interface near the middle level in a horizontal channel are concerned, $I_L , I_G \simeq 1.0$. Then, the critical gas-liquid relative velocity to cause the instability is obtained as an inequality

$$(u_G - u_L)^2 \geq (1/\rho_L + 1/\rho_G) \left[kT + \frac{g}{k}(\rho_L - \rho_G) \right] = \Delta u_{\min}{}^2 \, . \tag{A2-14}$$

For the minimum gas-liquid relative velocity; $\Delta u_{\min}{}^2$ in equation (A2-14), single value is admissible for the wave length as

$$\lambda_0 = 2\pi \sqrt{T / [g(\rho_L - \rho_G)]} \, . \tag{A2-15}$$

For an extreme case with very long wave length, $I_k = \coth kh_k \approx 1/kh_k$. Equation (A2-13) can then be simplified, by neglecting influences of surface tension, to

$$(u_G - u_L)^2 \geq \left[g(\rho_L - \rho_G) \frac{h_G}{\rho_G} \right] . \qquad \text{(A2-16)}$$

This is **Equation (1-1)** with C = 1, for the Kelvin-Helmholtz instability.

Appendix-3 Interfacial Friction Factor for Horizontal Separated Flow

The instantaneous motion of fluid in the flow can be rigorously presented using the Navier-Stokes (NS) equations for both phases. Since the instantaneous motion of fluid is fluctuational for turbulent flow, time smoothing (or averaging) over a short time period is necessary for constructing the equations of change [Bird et al. 1960]. To deal with gas/liquid two-phase flows, Ishii (1975) obtained the momentum balance equations in a time-averaged form from the NS equations, as well as mass and energy balance equations.

In this study, the high-pressure steam/water horizontal separated flow is dealt with, and is highly turbulent with very low viscosity for both phases. The flow condition is thus assumed to be inviscid, irrotational and isothermal. This assumption enables the flow being treated as one-dimensional in an inclined pipe along z axis, as shown in **Fig. A3-1**, with a flat velocity profile in each phase, and no phase change at the gas/liquid interface to occur. The drag force on the wall and interface between phases, however, is taken into account to model the momentum balance of the flow in a macroscopical manner. Then, the

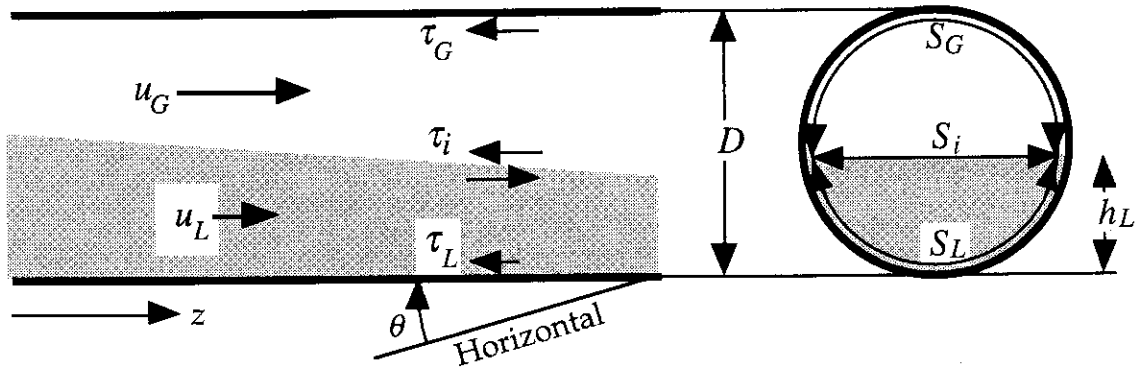

Fig. A3-1 Schematic of Horizontal Separated Flow

momentum equations obtained by Ishii are simplified, and resulted equations for liquid and gas phase respectively are as follows.

$$\frac{\partial}{\partial t}(A_L u_L) + \frac{\partial}{\partial z}(A_L u_L^2) = -\frac{S_L \tau_L}{\rho_L} + \frac{S_i \tau_i}{\rho_L}$$

$$- A_L g \cos\theta \frac{\partial h_L}{\partial z} - \frac{A_L}{\rho_L} \cdot \frac{\partial P_i}{\partial z} + A_L g \sin\theta \ , \qquad \text{(A3-1)}$$

$$\frac{\partial}{\partial t}(A_G u_G) + \frac{\partial}{\partial z}(A_G u_G^2) = -\frac{S_G \tau_G}{\rho_G} - \frac{S_i \tau_i}{\rho_G}$$

$$- A_G g \cos\theta \frac{\partial (D - h_L)}{\partial z} - \frac{A_G}{\rho_G} \cdot \frac{\partial P_i}{\partial z} + A_G g \sin\theta \ , \qquad \text{(A3-2)}$$

where the wall and interfacial shear stresses are defined respectively as

$$\tau_k = f_k \frac{\rho_k}{2} u_k^2 \ , \qquad \text{(A3-3)}$$

$$\tau_i = f_i \frac{\rho_G}{2} (u_G - u_L)^2 \ . \qquad \text{(A3-4)}$$

For a steady flow in a horizontal pipe, **Equations A3-1** and **-2** can be reduced further to

$$\frac{\partial}{\partial z}(A_L u_L^2) = -\frac{S_L \tau_L}{\rho_L} + \frac{S_i \tau_i}{\rho_L} - A_L g \frac{\partial h_L}{\partial z} - \frac{A_L}{\rho_L} \cdot \frac{\partial P_i}{\partial z} \ , \qquad \text{(A3-5)}$$

$$\frac{\partial}{\partial z}(A_G u_G^2) = -\frac{S_G \tau_G}{\rho_G} - \frac{S_i \tau_i}{\rho_G} - A_G g \frac{\partial (D - h_L)}{\partial z} - \frac{A_G}{\rho_G} \cdot \frac{\partial P_i}{\partial z} \ . \qquad \text{(A3-6)}$$

Since $u_L = J_L / (1 - \alpha)$, $u_G = J_G / \alpha$, $A_L = A(1 - \alpha)$ and $A_G = A\alpha$, l.h.s. of **Equations A3-5** and **-6** respectively become to

$$\frac{\partial}{\partial z}(A_L u_L^2) = \frac{A}{1 - \alpha} J_L^2 \frac{\partial}{\partial z}\left(\frac{1}{1 - \alpha}\right) = -\frac{A}{1 - \alpha} u_L^2 \frac{\partial (1 - \alpha)}{\partial z} \ , \qquad \text{(A3-7)}$$

$$\frac{\partial}{\partial z}(A_G u_G^2) = \frac{A}{\alpha} J_G^2 \frac{\partial}{\partial z}\left(\frac{1}{\alpha}\right) = \frac{A}{\alpha} u_G^2 \frac{\partial (1 - \alpha)}{\partial z} \ . \qquad \text{(A3-8)}$$

Elimination of the pressure term from **Equations A3-5** and **-6** and simplification of the results with **Relations A3-7** and **-8** yield

$$g\left[\rho_L \frac{\partial h_L}{\partial z} - \rho_G \frac{\partial (D - h_L)}{\partial z}\right] - \frac{\partial (1-\alpha)}{\partial z}\left(\frac{\rho_L}{1-\alpha} u_L{}^2 + \frac{\rho_G}{\alpha} u_G{}^2\right)$$

$$= \frac{1}{A}\left[-\frac{S_L \tau_L}{1-\alpha} + \frac{S_i \tau_i}{\alpha(1-\alpha)} + \frac{S_G \tau_G}{\alpha}\right] \qquad \text{(A3-9)}$$

Since $\frac{\partial (1-\alpha)}{\partial h} = \frac{S_i}{A}$, the interface level gradient to the pipe is obtained as,

$$\frac{\partial h}{\partial z} = \frac{-S_L \frac{\tau_L}{(1-\alpha)} + S_i \frac{\tau_i}{\alpha(1-\alpha)} + S_G \frac{\tau_G}{\alpha}}{g A (\rho_L + \rho_G) - S_i\left(\frac{\rho_L}{(1-\alpha)} u_L{}^2 + \frac{\rho_G}{\alpha} u_G{}^2\right)} \quad . \qquad \text{(A3-10)}$$

For a fully-developed flow with no level gradient, the numerator of **Equation A3-10** becomes to be zero and gives

$$\alpha = (S_i \tau_i + S_G \tau_G) / (S_L \tau_L + S_G \tau_G) \quad . \qquad \text{(A3-11)}$$

Using **Relations A3-3** and **-4**, **Equation A3-11** is transformed to obtain an interfacial friction factor as

$$f_i = 2 \frac{S_L \tau_L \alpha - S_G \tau_G (1-\alpha)}{S_i \rho_G (u_G - u_L)^2} \quad . \qquad \text{(A3-12)}$$